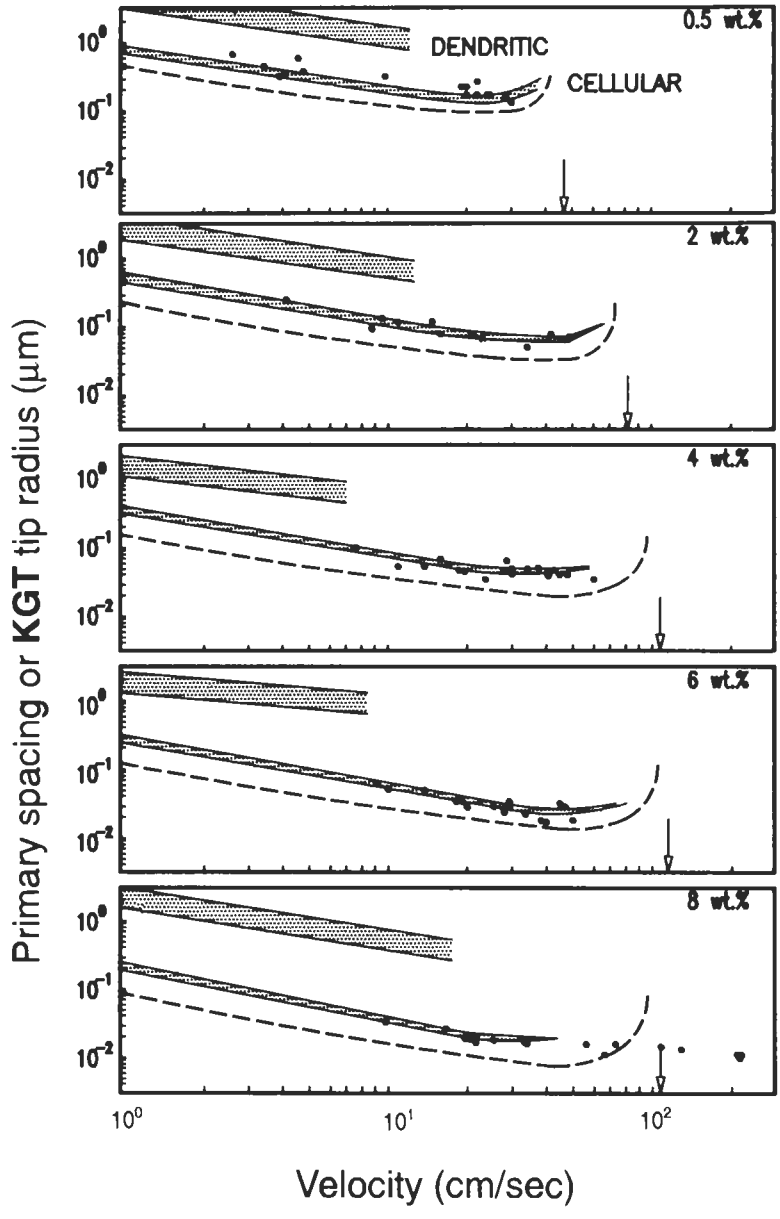

Fig. 38. Comparison of range of predicted primary spacings with experimental data for cell spacings obtained for five compositions of rapidly solidified Al–Fe alloys. The *IV/MS* tip radius is also shown dashed for comparison. LU *et al.* [1994]. The arrow shows the velocity where absolute stability is expected. Data from GREMAUD *et al.* [1991].

$$\lambda_1 = A_1 G_L^{-m} V^{-n}. \tag{93}$$

The result of the model by HUNT [1979] coincides closely with the expression derived by KURZ and FISHER [1981] using quite different assumptions about the dendrite geometry. The values $m = 0.5$ and $n = 0.25$ were obtained by both with the constant, A_1, being proportional to the fourth root of the alloy composition for dilute alloys. Thus for a given V and G_L, the primary spacing is larger for concentrated alloys than for dilute alloys. Traditionally many authors have considered that experimental values of λ_1 are better correlated to the local cooling rate, $G_L V$, such that $m = n \approx 0.5$ (FLEMINGS [1974]; OKAMOTO *et al.* [1975]; OKAMOTO and KISHITAKE [1975]; YOUNG and KIRKWOOD [1975]). On the other hand, in steels a broad discrepancy exists for the values of m and n, although many of the experimental studies have not been performed under controlled solidification conditions. JACOBI and SCHWERDTEFEGER [1976], controlling G_L and V separately, obtained values of $m = 0.25$ and $n = 0.72$. The complexity of modeling primary spacings is indicated by the fact that values of m and n fit to the numerical computations of LU and HUNT [1992] depend on the anisotropy of the surface energy.

Equation (93) is often used in conjunction with microstructural measurements to estimate the freezing conditions for various rapid solidification processing techniques. In view of the complexity of modelling λ_1 and the disparity in experimental values even at slow cooling rates, such an approach should be used with great caution.

7.2.3. Secondary dendrite arm spacing

During dendritic growth of cubic materials, the paraboloid-shape dendrite tip bulges laterally in the four {100} longitudinal planes containing the [100] growth direction. Each bulge then develops perturbations down the length of the dendrite shaft that become secondary arms as shown in fig. 39. The initial spacing of the secondary arms near the tip has been observed in transparent pure materials and alloys (HUANG and GLICKSMAN [1981], TRIVEDI and SOMBOONSUK [1984]). For both constrained and free growth, the spacing near the tip is approximately 2.5 times the tip radius over a broad range of growth conditions. Theoretical work by LANGER and MUELLER–KRUMBHAAR [1981] has also confirmed this relationship, which is related to the question of the tip stability discussed previously.

However as a result of coarsening effects during solidification, the final secondary dendrite spacing in a fully solidified casting is usually much coarser than the one formed near the tip. The observed mechanism of coarsening is the melting or dissolution of smaller arms at the expense of larger arms. Through the Gibbs–Thompson effect, local differences in curvature give rise to slight temperature and/or composition variations along the liquid solid interface. Diffusion of heat and/or solute in response to these differences cause the dissolution of small arms and the growth of others effectively increasing the average spacing of the secondary arms. For dendritic alloys, the process is practically important because it sets the length scale associated with the microsegregation. Indeed, the interplay between microsegregation and the coarsening process has only

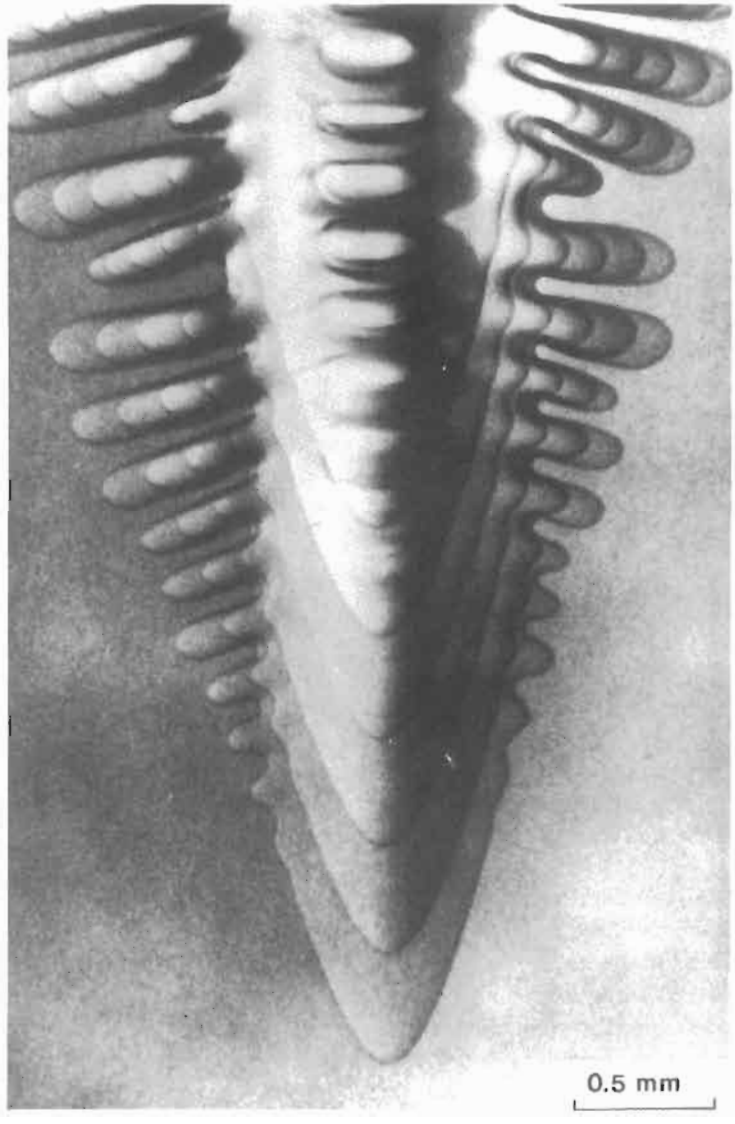

Fig. 39. Superposition of time-lapse photographs of the growth of a succinonitrile dendrite. Sidebranch evolution on the {100} branching sheets is evident. HUANG and GLICKSMAN [1981].

recently been examined (VOLLER and SUNDARRAJ [1993]). Coarsening in some alloys can be so extreme that the dendritic structure can be lost.

For all but the most dilute alloys, the rate of coarsening is determined by the diffusion of solute in the liquid (VOORHEES [1990]). Models were obtained for isothermal coarsening of the secondary arms held in the mushy zone by KATTAMIS *et al.* [1967] and

FEURER and WUNDERLIN [1977]. The latter obtained an expression for the secondary arm spacing, λ_2, given by

$$\lambda_2 = 5.5\left(M^* t_f\right)^{1/3}, \tag{94}$$

where

$$M^* = \frac{T_m \Gamma D_L \ln\left(\frac{C_b}{C_0}\right)}{m_L\left(k_0 - 1\right)\left(C_b - C_0\right)}, \tag{95}$$

where C_b is the final composition of the liquid at the base of the dendrite. When solidification is completed by a eutectic reaction, C_b is equal to the eutectic composition. The numerical factor in eq. (95) depends on the details of the geometry of the coarsening process and the dendritic structure and should be viewed as approximate. For directional solidification the local solidification time can be approximated by

$$t_f = \frac{\Delta T_f}{G_L V}, \tag{96}$$

where ΔT_f is the temperature difference between the dendrite tip and the base of the dendrite. Thus for a given growth velocity and temperature gradient λ_2 decreases with increasing composition.

KIRKWOOD [1985] obtained the above result only when the cooling rate is small compared to $m_L C_0 / t_f$. At larger cooling rates, the strict dependence, $\lambda_2 \sim t_f^{1/3}$, was not obtained and he ascribed the scatter in λ_2 vs. t_f data to this effect. In real solidification processes, coarsening takes place simultaneously with the subsequent increase in the fraction solid during cooling. MORTENSEN [1991a] presents a model that includes this effect.

7.2.4. Cell to dendrite transition

As the solidification velocity is increased for a given alloy composition and temperature gradient, one observes a transition in structure: planar, cellular, dendritic, cellular, planar. The lower and upper transitions between planar and cellular structures are given by the modified constitutional supercooling and the absolute stability criteria, respectively (§ 6.4). The transitions between cellular structures and dendritic structures at intermediate velocities are not well understood. Experimental data for the *low velocity transition* were obtained by TILLER and RUTTER [1956] and CHALMERS [1964] and were fit by the expression

$$G_L V^{1/2} \sim C_0 / k_0, \tag{97}$$

with a constant of proportionality that depends on crystallographic growth direction. Later KURZ and FISHER [1981] proposed the condition

$$G_L / V = \frac{m_L C_0\left(k_0 - 1\right)}{D_L}, \tag{98}$$

which is k_0 times the critical value of G_L/V for the plane to cell transition given by eq. (77).

In experiments by SOMBOONSUK *et al.* [1984], it became clear that cells and dendrites could coexist at the same velocity and that the conditions required for the transition were more difficult to calculate. (See BILLIA and TRIVEDI [1993]). Indeed in Hunt's calculations described above, cell and dendrite structures were found to exist at the same velocity. Hunt postulated that the cell to dendrite transition might occur when the tip temperature for the cell becomes lower than that for the dendrite (fig. 40). This postulate also predicts an upper transition velocity from dendrites back to cells with increasing solidification velocity in the rapid solidification regime. This upper transition is observed experimentally but has received no theoretical treatment.

7.3. Microsegregation

Microsegregation is the pattern of composition variation that remains in a solidified alloy. It includes the composition variation across cells or dendrites as well as the formation of other phases in the intercellular or interdendritic regions. One of the major goals of microsegregation analysis is the prediction of the volume fraction of eutectic or other secondary phases that may form between the cells and/or dendrites of the primary phase.

The simplest approximation for the prediction of microsegregation during dendritic solidification uses the Scheil equation described in § 6.2.2 where the volume under consideration is shown in fig. 41. With this approach no assumptions are necessary

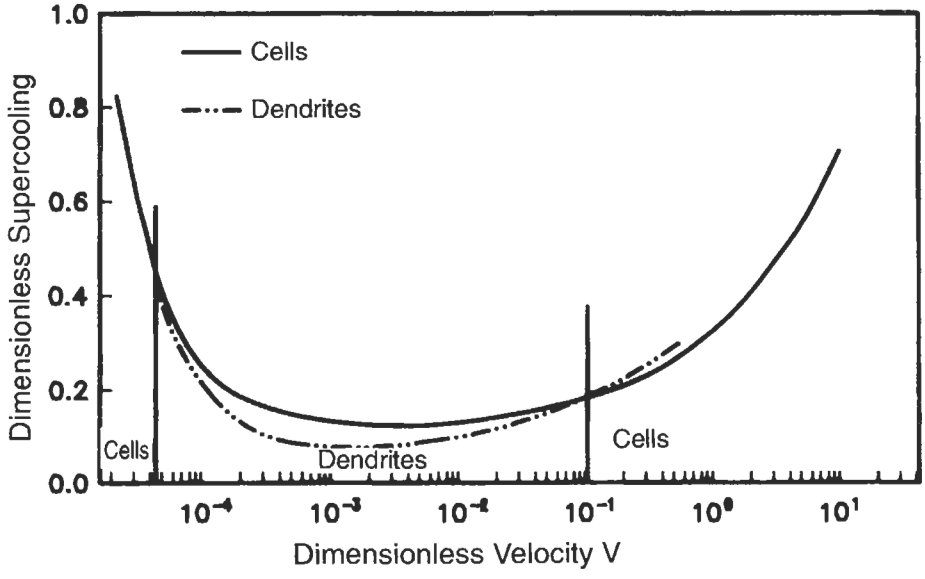

Fig. 40. Dimensionless tip supercooling vs. velocity for cells and dendrites calculated by LU *et al.* [1994]. The velocities where the curves cross define where the cell to dendrite transition is thought to take place.

References: p. 830.

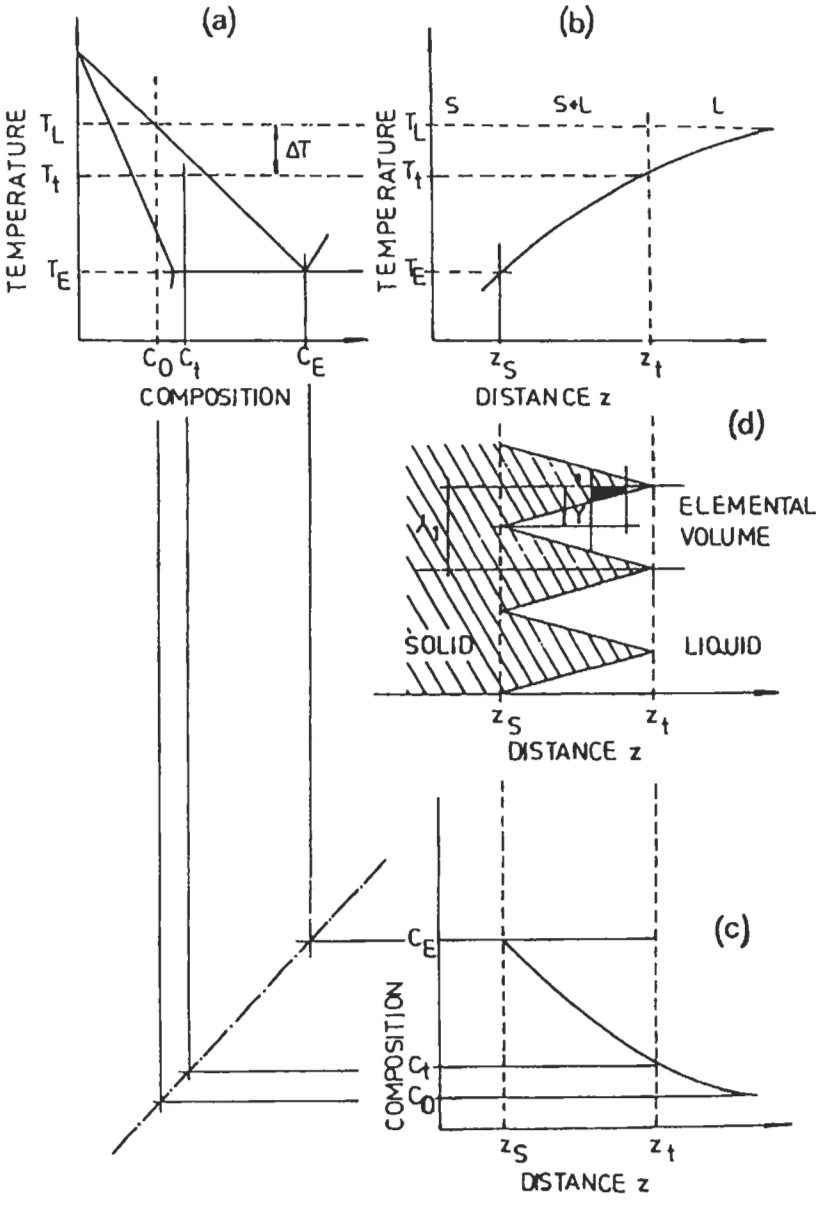

Fig. 41. Conceptual model of cellular/dendritic freezing showing: (a) portion of the phase diagram; (b) schematic temperature distribution in the melt; (c) distribution of solute within the liquid in the mushy zone; (d) representation of plate-like, unbranched dendrites showing the position of a characteristic elemental volume. (After BRODY and FLEMINGS [1966]).

concerning the geometry of the freezing solid until one desires to convert from fraction solid to distance in a cast microstructure. For example, the dependence of fraction solid on distance, r_1 from the center of a cell or dendrite with radial symmetry with a primary spacing, λ_1, can be obtained the expression,

$$f_S = 1 - \left(\frac{r_1}{\lambda_1}\right)^2. \tag{99}$$

Other geometries require other relationships between fraction solid and distance.

The predictions of the Scheil Equation establish an upper bound on the severity of microsegregation, for example, as determined by the predicted fraction of eutectic. Effects that alter the predicted microsegregation are: (a) the variation in cell or dendrite tip composition with growth conditions; (b) the degree of liquid mixing between the cells or dendrites; and (c) diffusion in the solid. All of these effects decrease the severity of microsegregation from that predicted by the Scheil Equation.

One of the first treatments of (a) and (b) was performed by BRODY and FLEMINGS [1966] and BOWER *et al.* [1966]. They assumed complete lateral mixing behind the cell tips and matched the composition gradient in the growth direction with the temperature gradient using the local equilibrium assumption (without curvature). This yields a prediction of the cell tip composition, C_L^*. A mass balance behind the tips was then used to obtain their final result which can be rewritten as

$$C_S = k_0 C_0 \left\{ \frac{1 - C_L^*/C_0}{k_0 - 1} + \left[1 - \frac{k_0\left(1 - C_L^*/C_0\right)}{k_0 - 1} \right] \left(1 - f_S\right)^{k_0 - 1} \right\}, \tag{100}$$

with $C_L^* = C_0(1 - a')$ where $a' = D_L G_L / m_L V C_0$.

Other approaches can be used to obtain the cell/dendrite tip composition along with the same mass balance. SOLARI and BILONI [1980] used the BURDEN–HUNT [1974a], [1974b] model based on the maximum growth rate hypothesis. In this work, $C_L^* = C_0(1 - a' + b')$ with $b' = [T_m \Gamma V(k_0 - 1)/m_L D_L C_0]^{1/2}$. Substitution of this value of C_L^* into eq. (100) gives the SOLARI and BILONI prediction. Use of the IV/MS dendrite model to obtain C_L^* would update this approach. The appeal of these approximate treatments is found in two limiting cases. If $C_L^* = C_0$, eq. (100) becomes the Scheil Equation. If $C_L^* = C_0/k_0$, eq. (100) becomes $C_S = C_0$ independent of f_S. This limit corresponds to planar growth where no microsegregation occurs.

GIOVANOLA and KURZ [1990] employ a method that uses the IV/MS prediction for the tip composition without assuming complete mixing between the dendrites near the tip region. They employ a polynomial to connect the tip composition to a composition well behind the tips where the complete mixing assumption is valid. The solid composition vs. fraction solid relation is determined by numerically solving algebraic equations.

The most important feature of microsegregation models that employ dendrite tip kinetics is the alteration of the composition of solid that forms at $f_S = 0$. The Scheil equation implicitly assumes that no solute is built up in front of the dendrite tip. Thus the first solid to form has composition, $k_0 C_0$. Increasing levels of solute in the liquid at the

tip correspondingly increase the amount of solute in the solid along the central dendrite trunk leaving less solute to accumulate in the interdendritic liquid regions at high fraction solid. Thus, for example, the amount of eutectic that forms will be reduced compared to the Scheil prediction.

Solid diffusion during solidification also reduces the amount of microsegregation. One approach is to apply the one-dimensional solid diffusion analysis presented in § 6.2.3 to a small volume in the mushy zone shown in fig. 41. The distance L_0 is then equated with λ_1 or λ_2 depending on whether the microstructure has fully developed secondary arms. When solid diffusion is added to the Scheil approach, one must know how the fraction solid changes with time. For a linear dependence of fraction solid on time, the term $(1-f_S)$ in eq. (100) was changed to $(1-f_S/(1+\alpha_\theta k_0))$ (see eq. 58) as was done by SOLARI and BILONI [1980]. Another approach is to numerically solve the diffusion equation in the solid and liquid (e.g. BATTLE and PEHLKE [1990]). While this approach is more accurate for the treatment of solid diffusion, it ignores the dendritic nature of cast alloys and the details of the solute profile in front of a growing dendrite. Corrections due to solid diffusion are very important for extremely slow solidification or when solid diffusion is very rapid as in the case of interstitial solutes, as for C in steels.

That the Scheil equation gives a good first approximation to dendritic microsegregation in the columnar zone of ingots has been proven, among other authors, by KATTAMIS and FLEMINGS [1965] for low alloy steels and WEINBERG and TEGHTSOONIAN [1972] for Cu-base alloys. CALVO and BILONI [1971], combining anodic oxidation techniques with electron microprobe measurements, obtained a clear map of the solute segregation together with quantitative measurements of the Cu concentration in Al-1% Cu alloys. The corrections to the Scheil approach due to solid diffusion have been tested by BOWER *et al.* [1966] and FLEMINGS *et al.* [1970]. The fraction of eutectic as well as the composition at the center of the dendrite agrees well with predictions using this approach.

In the rapid solidification regime, microsegregation profile must be measured in the TEM due to the small primary spacings. MASUR and FLEMINGS [1982] measured the composition profiles across very fine dendritic cells of Al-4.5% Cu solidified at a very high cooling rate (2×10^5 K/s) and a solidification velocity estimated to be 0.6 m/s. PALACIO *et al.* [1985] and BILONI [1983] analyzed their data using eq. (100) with values of C_L^* from the theory of BURDEN and HUNT [1974a]. Figure 42 shows the measured and *predicted* variation of solid composition as a function of f_S. The segregation profile described by this equation is in close agreement with the experimental results.

Other features of microsegregation profiles however have been noted especially in the rapid solidification regime. Flat solute profiles have been associated with cellular growth at high solute Peclet numbers by BOETTINGER *et al.* [1987]. Solute rich regions at the center of cells have been observed by KATTAMIS [1970] and by BOETTINGER *et al.* [1987]. The recent computation method of LU *et al.* [1994] may yield a better approach to understanding the details of microsegregation over a broad range of growth conditions.

7.4. Solidification of ternary alloys

Practical alloys typically contain many components and a brief discussion of

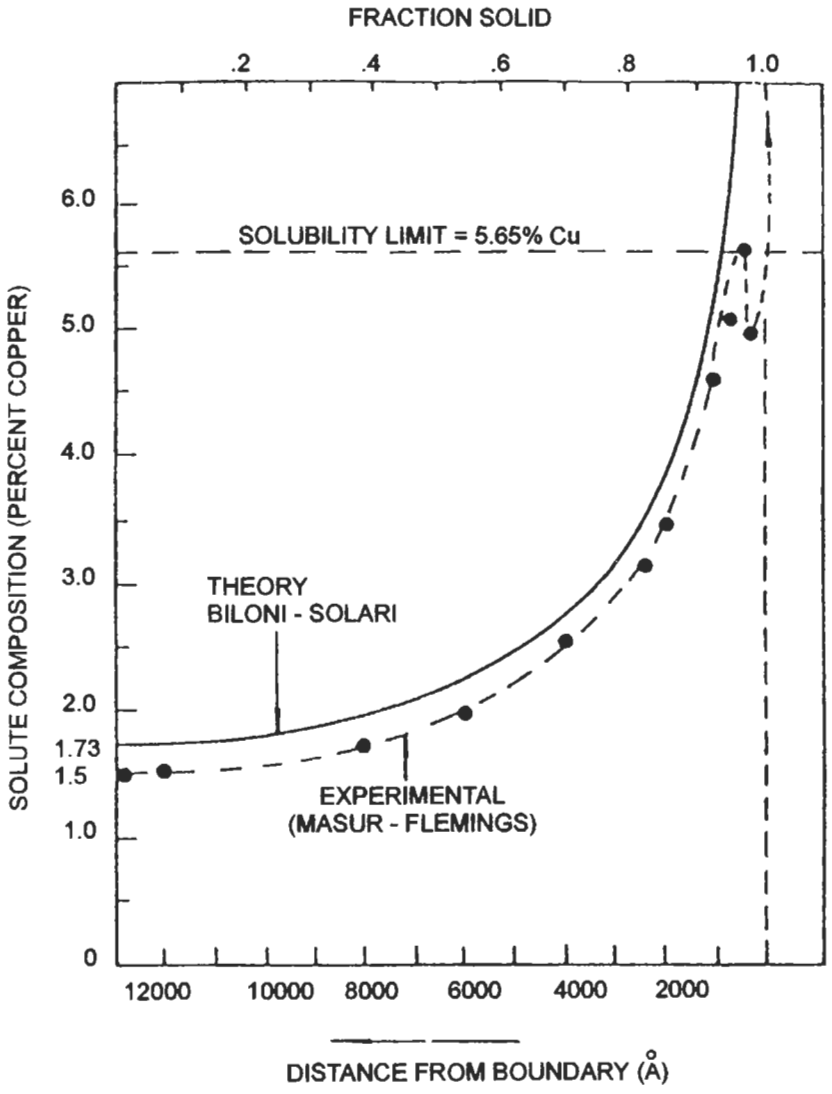

Fig. 42. Comparison between data of MASUR and FLEMINGS [1981] on the composition of a cell from center to periphery in Al-4.5 wt% Cu melt spun ribbon solidified at an estimated growth velocity of 0.6 m/s, and predictions of composition given by eq. (100) due to SOLARI and BILONI [1980].

solidification in ternary alloys is appropriate. A general view of solidification microstructures in a ternary eutectic system has been presented by MCCARTNEY *et al.* [1980a], [1980b] as shown in fig. 43. Depending on the alloy composition, various mixtures of primary phase, monovariant binary eutectic and invariant ternary eutectic can be expected. For the dendritic growth of a primary phase, the Scheil approach can be

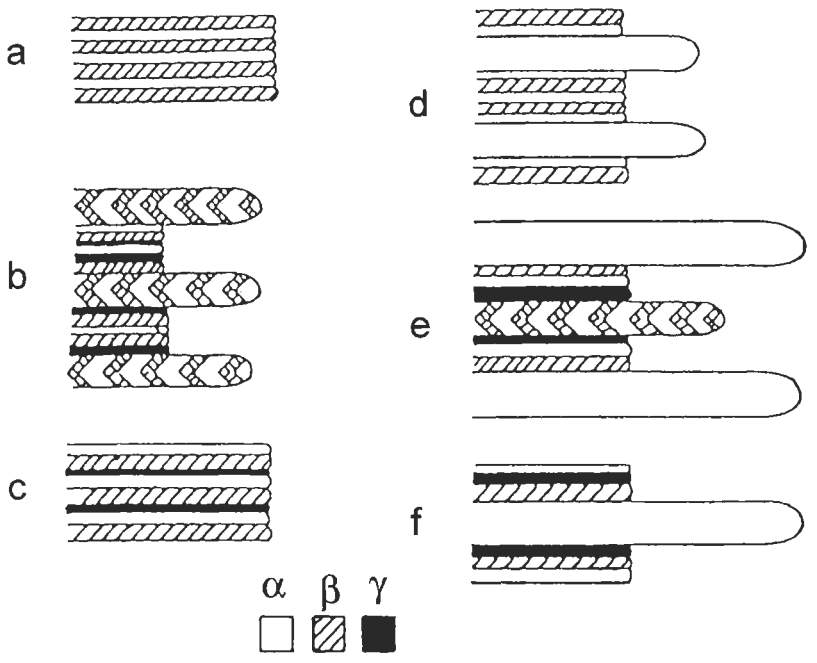

Fig. 43. Possible growth interfaces in a ternary system depending on composition: (a) two phase eutectic (planar growth), (b) two phase cells plus ternary eutectic, (c) three phase eutectic, (d) single phase cells plus binary eutectic, (e) single phase cells, two phase cells and ternary eutectic, (f) single phase cells plus ternary eutectic. McCartney *et al.* [1980a].

utilized, if appropriate, or a dendrite tip model constructed.

The ternary (or higher order) phase diagram is important for either of these approaches. One requires information concerning the relationship between C_{Si}^* and C_{Li}^* for each of the $\underline{i}$ alloying additions. Often values are taken from the binaries, but in general the composition of one species in the solid may depend on the composition of other species as well. This information is given by the tie-lines of the phase diagram that are usually only available through a thermodynamic model of the multicomponent alloy of interest, rather than through experimental studies.

Use of the Scheil approach to determine the solidification path, which is the composition of liquid (and thus solid) as a function of fraction solid, uses a set of equations

$$\frac{dC_{Li}}{df_S} = \frac{(1-k_{0i})C_{Li}}{1-f_S}, \tag{101}$$

that are uncoupled if the k_{0i} $(=C_{Si}/C_{Li})$ do not depend on the composition of the other species. In fact, if the k_{0i} are constants, then for an alloy of initial composition C_{0i},

$$C_{Li} = C_{0i}(1-f_S)^{k_{0i}-1}, \tag{102}$$

for each component during primary solidification. Using the phase diagram, one then determines the fraction solid at which the liquid crosses a monovariant eutectic line. Solidification then follows this line and finally ends with the ternary eutectic. If the solidification path for primary solidification crosses a monovariant peritectic line, solidification switches to single phase growth of the new phase. Calculations of solidification path using full integration of phase diagram tie-lines with the Scheil approach (including solid diffusion) have been conducted by CHEN and CHANG [1992].

For a treatment of the kinetics of the dendrite tip in a multicomponent alloy, Ivantsov solutions are obtained for each solute to determine the composition of each solute at the dendrite tip. The marginal stability criterion for the multicomponent alloy is applied to determine the tip radius as shown by BOBADILLA *et al.* [1988] and RAPPAZ *et al.* [1990].

7.5. New approaches to modeling dendritic growth

Another approach to modeling dendritic growth is the phase-field method (CAGINALP [1986], KOBAYASHI [1991] [1992], WHEELER *et al.* [1992], [1993b]). With this method the interface is treated as being diffuse and the transition from liquid to solid is described by an order parameter called the phase field. For a pure material, equations that govern the phase field and the temperature are solved over a domain of interest without applying boundary conditions along the liquid solid interface. The position of the interface is then determined from the solution as a surface with a constant value of the order parameter intermediate between a homogeneous liquid and solid. This method, which requires time consuming computations on a supercomputer, has succeeded in obtaining realistic dendritic growth forms for pure materials and alloys with no extra conditions required to specify the operating state of the dendrite tip, such as the marginal stability condition, eq. (85). The velocity and tip radius are naturally selected by the solution to the differential equations (WHEELER *et al.* [1993a]). An example of a computed two dimensional alloy dendrite using this method is shown in fig. 44 (WARREN and BOETTINGER [1995]). Presently, computations have been performed using finite difference methods and, due to high computation times, are limited to high supercooling of the order of L/C_p^L.

8. *Polyphase solidification*

The discussion of solidification is now extended to situations where several phases are formed from the melt. Eutectic, peritectic, and monotectic solidification involve the freezing of an alloy at or near a special liquid composition. In a binary system, this special composition is defined thermodynamically as the liquid composition that can be in equilibrium with two other phases at the same temperature. This equilibrium can only occur at a single temperature in a binary system at fixed pressure. For the eutectic and peritectic cases, the liquid is in equilibrium with two solid phases and for the monotectic case, the liquid is in equilibrium with a solid and another liquid phase. The monotectic case involves alloys that exhibit a miscibility gap in the liquid phase.

Fig. 44. Simulation of an alloy dendrite growing into a supercooled liquid using the phase-field method. The shadings show variation of composition (atomic fraction Cu) in the liquid and solid for parameters approximating a Ni–Cu alloy with 0.41 atomic fraction Cu. (WARREN and BOETTINGER [1995].)

8.1. Eutectic solidification

In a binary alloy, eutectic solidification converts a liquid simultaneously into two solid phases. Alloys near eutectic compositions are very important in the casting industry due to several characteristics: (i) low liquidus temperatures compared to the pure component melting points that simplify melting and casting operations: (ii) zero or small freezing ranges that effectively eliminate the dendritic mushy zone thereby reducing segregation and shrinkage porosity while promoting excellent mold filling; (iii) possibil-

ities of forming "in-situ" composites. Among the most common eutectic or near-eutectic alloys of industrial importance are cast irons, Al–Si alloys, wear-resistant alloys and solders. In many other practical alloys that freeze dendritically, secondary phases are formed near the end of freezing by eutectic solidification.

Eutectic solidification involves the following stages: eutectic liquid is supercooled and one of the solid phases nucleates, causing solute enrichment in the surrounding liquid and sympathetic nucleation of the second solid phase. Repeated nucleation and/or overgrowth of one solid phase by the other produces a growth center that defines an individual eutectic grain. For many eutectics, solidification proceeds by simultaneous growth of two interspersed solid-phases at a common liquid–solid interface. The solute rejected into the liquid by each phase is taken up by the adjacent phase particles. As solidification proceeds, spatial and crystallographic rotation of the solid phases together with competitive overgrowth of adjacent eutectic grains lead to a stable solidification front, with the surviving eutectic grains having, as much as possible, maximized the solidification rate, minimized the α–β interfacial energy and oriented the α–β interfaces in the heat flow direction. The ability of one solid phase in the eutectic to stimulate nucleation of the other varies widely for different α–β phases and, in general, knowledge about the nucleation process in eutectic solidification remains rather poor (MONDOLFO [1965]). Thus, this section will treat mainly theory and experiments concerning steady state directional solidification, a method which has furnished, as in the case of dilute alloys, a large number of reliable results. Two excellent summaries of the earlier literature on eutectic solidification can be found in reviews by CHADWICK [1963] and HOGAN *et al.* [1971].

8.1.1. Eutectic classification

When a eutectic liquid solidifies, the resulting material generally consists of a dispersed two-phase microstructure that is approximately ten times finer than cells or dendrites formed under the same conditions. The exact arrangement of the two phases in the eutectic microstructure can vary widely, depending on the solidification conditions and the particular eutectic alloy being solidified. HUNT and JACKSON [1966] provided a simple classification scheme according to the interface kinetics of the component phases. A correlation was found between eutectic morphology and the entropies of fusion of the two solid phases, concepts discussed in § 5.1. The classification refers to: non-facetted–non-facetted eutectics (nf–nf); non-facetted–facetted eutectics (nf–f); and facetted–facetted eutectics (f–f). Very little is known about the solidification of f–f eutectics but extensive research has been performed on nf–nf and nf–f eutectics. KERR and WINEGARD [1967] argued that the facetted or nonfacetted nature of the liquid–solid interface of the phases was better described by the entropies of solution of the individual phases because the (eutectic) liquid composition is generally quite different from the solid phase compositions. CROKER *et al.* [1973] examined a large number of eutectic microstructures and in addition found that the volume fraction of the solid phases in the eutectic structure and the growth velocity must also be considered to obtain a good classification scheme.

8.1.2. Non-facetted – Non-facetted eutectics

Eutectic mixtures of two non-facetted phases tend to form regular microstructures

References: p. 830.

consisting of either alternate lamellae of α and β or rods of α embedded in β that grow in a continuous edgewise manner into the melt. Experimentally, it is found that eutectics in which one phase has a very low volume fraction tend to grow in a rod-like manner. This can be explained on the basis that a rod-like structure has lower total α–β surface energy than a lamellar structure when the volume fraction of one of the phases is less than about 0.3. This assumes that the surface energies are isotropic. A 25% anisotropy of surface energy can stabilize lamellar structures at practically any value of volume fraction. In marginal cases, lamellar-to-rod transitions can occur for a given alloy by changing the growth conditions. Three-dimensional analysis of the eutectic structures shows that both phases are continuous in the growth direction over large distances that are called eutectic grains. A eutectic grain can be described approximately as two interpenetrating single crystals of the two component phases having almost constant crystallographic orientation. HOGAN *et al.* [1971] give a thorough discussion of eutectic grains and a summary of the orientation relationships between phases and the habit plane of the α–β interfaces. The orientation relationship and the orientation of the interfaces usually allow for a high degree of fit between the two crystal structures that minimizes the α–β surface energy.

In lamellar or rod eutectic solidification, the two phases, α and β, solidify side by side with an approximately planar and isothermal S–L interface, supercooled ΔT below the equilibrium eutectic temperature. During solidification of an A–B alloy, the A-rich phase rejects B atoms into the liquid and the B-rich phase rejects A atoms. The interaction of the diffusion fields in the liquid in front of the two phases gives rise to the term *coupled growth*, which is commonly used to describe eutectic solidification. At a given solidification rate V, the spacing of the lamellae or rods, λ_E, and the interface supercooling below the eutectic temperature, ΔT, are controlled by a balance between: (i) the necessity for lateral diffusion of excess A and B in the liquid just ahead of the S–L interface, which favors a small interlamellar or interrod spacing, and (ii) the necessity to create α–β interfacial area, which tends to favor large λ_E (fewer interfaces).

Over the years the theory of lamellar or rod growth for the slow solidification velocities found in castings or in directional solidification when $\lambda_E V/2D_L \ll 1$ has been developed by ZENER [1946], HILLERT [1957], TILLER [1958], JACKSON and HUNT [1966], MAGNIN and TRIVEDI [1991]. The situation for rapid solidification is treated below. The basis of the analysis is illustrated in fig. 45. The interface temperature at each interface point is controlled by the velocity at each point, the composition of the liquid at the interface at each point and the curvature at each point. The supercooling below the eutectic temperature, T_E, for each point on the S–L interface (α–L and β–L) can be described by

$$\Delta T = \Delta T_k + \Delta T_D + \Delta T_c. \tag{103}$$

The first term is the interface attachment kinetic supercooling and is usually neglected compared to the other terms. Thus it is assumed that each point on the α–L and β–L interfaces is at local equilibrium. ΔT_D is the supercooling below the eutectic temperature due to the local variation in composition from the eutectic composition. This local variation is approximated by solving the steady-state diffusion equation in the liquid for

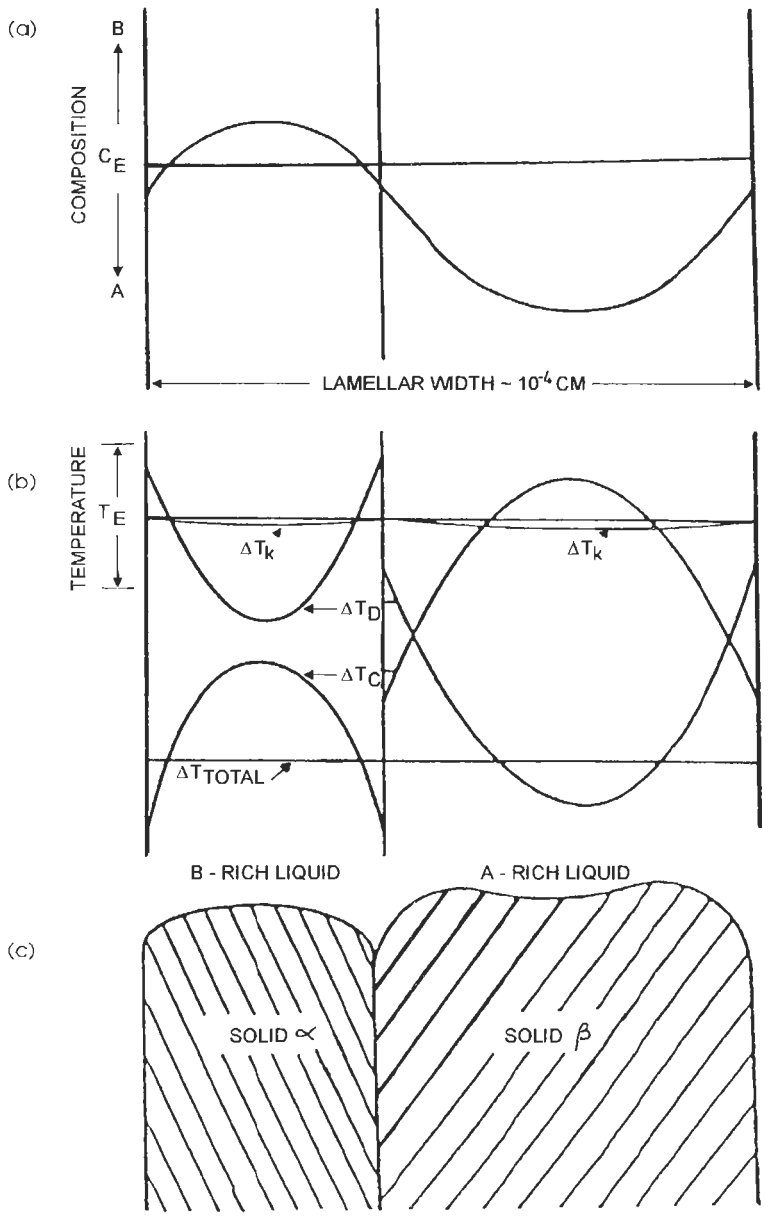

Fig. 45. (a) Liquid composition (% B) across an α–β interface. (b) Contributions to the total supercooling (ΔT) existing at the S–L interface, ΔT_D, ΔT_c, and ΔT_K are the solute, curvature and kinetic supercoolings respectively. (c) Shape of the lamellar S–L liquid interface. HUNT and JACKSON [1966].

a planar α–β interface growing at velocity V and spacing λ_E. ΔT_c is the supercooling due to curvature.

It is then assumed that the total supercooling, ΔT, given by eq. (103) is constant across the interface. Thus across the interface, any variation in ΔT_D must be balanced by a variation in ΔT_c, giving a constant value for $\Delta T = \Delta T_D + \Delta T_c$ at each point of the interface. Due to the solution of the diffusion equation, ΔT_D has a minimum value near the α–β–L groove, and thus ΔT_c has a maximum value there. The radius of curvature is, therefore, smallest near the triple junctions and leads to an interface shape similar to that shown in fig. 45c. JACKSON and HUNT [1966] have shown that the predicted interface shape agrees very well with the interface shape observed in the transparent hexachloroethane–carbon bromide model system.

By averaging the composition deviation from the eutectic composition in the liquid in front of each phase and the interface curvature of each phase (which depends on the width of the phase and the angle the interface makes with the α–β interface), the total supercooling is found to be

$$\Delta T = K_5 \lambda_E V + K_6/\lambda_E, \tag{104}$$

where K_5 and K_6 are constants. For lamellar growth they are given by

$$K_5 = \frac{\overline{m}_L C_0^*}{D_L} \frac{P_E}{f_\alpha f_\beta} \tag{105}$$

and

$$K_6 = 2\overline{m}_L \left(\frac{\Gamma_\alpha \sin\theta_\alpha}{m_{L\alpha} f_\alpha} + \frac{\Gamma_\beta \sin\theta_\beta}{m_{L\beta} f_\beta} \right) \tag{106}$$

with

$$\overline{m}_L = \frac{m_{L\alpha} m_{L\beta}}{m_{L\alpha} + m_{L\beta}} \tag{107}$$

The parameters $m_{L\alpha}$ and $m_{L\beta}$ are the liquidus slopes for the alpha and beta phases, C_0^* is the difference in composition between the solid phases, D_L is the liquid diffusion coefficient, f_α and f_β are the volume fraction of the solid phases in the eutectic, P_E is a series function of the phase fractions and can be approximated (TRIVEDI and KURZ [1988]) by

$$P_E = 0.3383 \left(f_\alpha f_\beta \right)^{1.661}. \tag{108}$$

Γ_α and Γ_β are the Gibbs–Thomson coefficients (surface energy/entropy of fusion per unit volume), and θ_α and θ_β are the angles that the alpha and beta interfaces make with a plane perpendicular to the α–β interface. Because a balance of tensions must exist at the α_E–β_E–L triple point, the solid–solid energy exerts its influence through its effect on these angles. A low value of $\gamma_{\alpha\beta}$ leads to small values for θ_α and θ_β making ΔT_c small.

Very similar expressions are obtained for rod eutectic growth.

Equation (104) is shown schematically for different growth rates in fig. 46. It can be seen that ΔT is biggest for large lamellar spacings because diffusion is difficult, and also for small spacings where curvature effects are dominant. Clearly, the values of λ_E and ΔT are not fixed uniquely by V, yet in experiments it is well established that the value of λ_E generally decreases with increasing V. Hence an additional condition is required to specify the operation point on each λ_E vs. ΔT curve.

The simplest additional condition is obtained by assuming that growth occurs at the minimum ΔT for a given V or, equivalently, a maximum V for a given ΔT. This condition is called the *extremum condition*. Using this condition,

$$\lambda_E^2 V = K_6/K_5, \tag{109}$$

and:

$$\Delta T^2/V = 4K_5K_6. \tag{110}$$

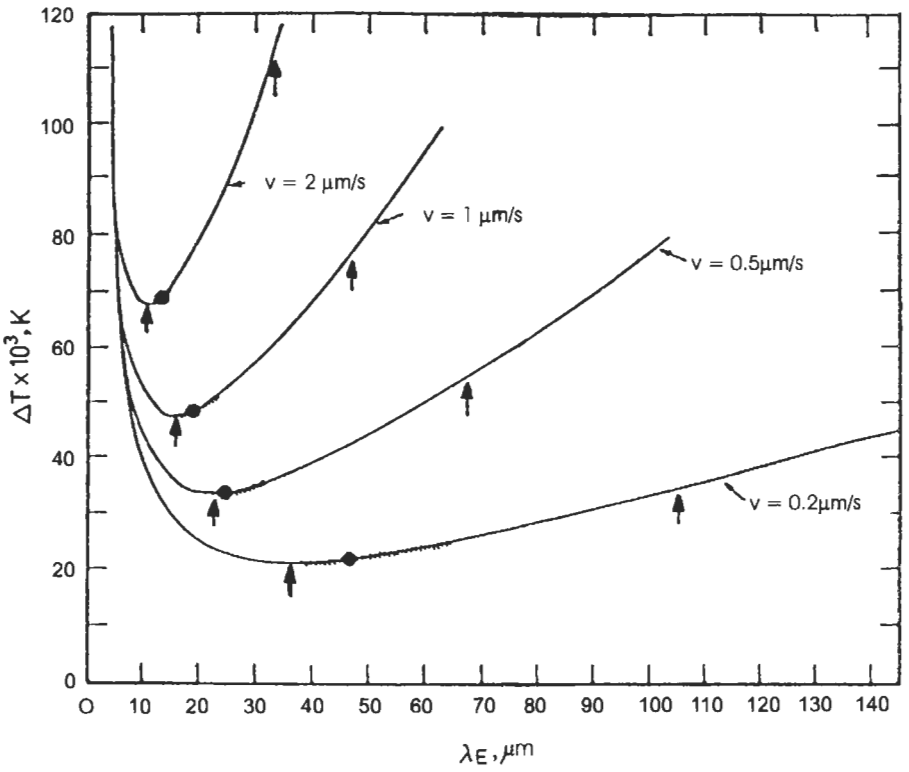

Fig. 46. Interface supercooling, ΔT, as a function of lamellar spacing, λ_E, for different growth rates, V using eq. (104) for CBr_2–C_2Cl_6 organic eutectic. The vertical arrows show the theoretical minimum (extremum) and maximum spacings for stable lamellar growth. The experimentally observed range of spacings (hatch marks) and the mean spacing (filled circles) at the different velocities are shown. (SEETHARAMAN and TRIVEDI [1988]).

References: p. 830.

Many investigators (for example JORDAN and HUNT [1971, 1972], TASSA and HUNT [1976]) have found the average spacing and interface supercooling to be close to the values given by these equations using the extremum condition.

However the use of the extremum condition is rather ad hoc and a more satisfying selection criterion has been sought for years. Indeed the discovery that the dendrite tip radii could not be described by a maximum growth rate hypothesis (see § 7), led to further consideration of this criterion for eutectic growth. Experiments on eutectics (JORDAN and HUNT [1972], SEETHARAMAN and TRIVEDI [1988]) have shown experimentally that a small range of spacings are observed for a given growth rate. They find that the minimum spacing is close to that given by the extremum condition but that the average spacing is somewhat larger than that given by eq. (109). Much research has been focused on defining the allowable range.

The basic concepts were first proposed by JACKSON and HUNT [1966], who indicated that only spacings within a certain range were stable to fluctuations in the shape of the S–L interface as shown in fig. 47. They quoted unpublished work by J.W. CAHN that argued that spacings smaller than that given by the extremum condition are inherently unstable and thus the extremum spacing is expected to be the minimum observed. This instability is due to the pinching off of an individual lamella or rod that locally increases the spacing (fig. 47a). That the extreemum value corresponds to the minimum spacing has been confirmed by extensive theoretical work (LANGER [1980], DAYTE and LANGER [1981] and DAYTE *et al.* [1982].) Less sudden spacing adjustments can occur by the motion of faults (lamellar edges) perpendicular to the growth direction.

A value for the maximum possible spacing at any velocity was first proposed by JACKSON and HUNT [1966]. This maximum spacing also follows a $\lambda_E^2 V$ = constant law. If the spacing exceeds the extremum value by a critical factor, the larger volume fraction phase develops a pocket that drops progressively back from the interface until growth of the other phase ultimately occurs in it (fig. 47b). They took this condition to occur when the slope of the pocket became infinite. For example, this condition yields maximum

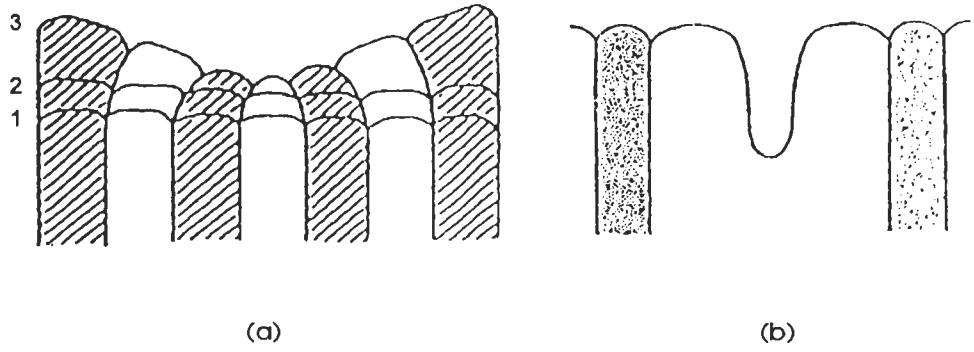

Fig. 47. (a) Schematic illustration of the instability of lamellae with λ_E less than the extremum value. The lamella in the center will be pinched off with time. (b) The shape instability of the interface of one phase that occurs when the spacing becomes too large. A new lamella may be created in the depressed pocket. JACKSON and HUNT [1966]. Figure taken from TRIVEDI and KURZ [1988].

values for the $\lambda_E^2 V$ constant of ten and two times the extremum value for volume fractions of 0.5 and 0.1 respectively. As a consequence of the formation of the new lamella, the local spacing is abruptly reduced by a factor of two. However, the careful experiments of SEETHARAMAN and TRIVEDI [1988] show that the maximum observed spacing is much smaller than this estimate (see fig. 46), giving an average spacing that is only ~20% larger than the extremum value (or minimum stable spacing). Thus the maximum value of spacing occurs before the pocket depression attains infinite slope. While further research is required on this topic, the extremum value is often taken as a good approximation for nf–nf growth. Other stability issues of eutectic growth involving compositions different from the eutectic composition in § 8.1.4 and § 8.1.5.

Convection in the liquid near the interface of a growing eutectic has been found to increase the value of λ_E (JUNZE *et al.* [1984] and BASKARAN and WILCOX [1984]). Flow parallel to the interface distorts the liquid concentration profile in front of the lamellae slightly and alters the diffusion controlled growth. The effect is greatest when the dimensionless parameter, $G_u \lambda_E^2 / D_L$, is large, where G_u is the gradient normal to the interface of the fluid flow velocity parallel to the interface. Vigorous stirring is required to alter the spacing significantly.

8.1.3. Non-facetted–facetted eutectics

The modeling of nf–f eutectics is quite important given the fact that eutectics of technological importance such as Al–Si and Fe–C belong to this class. FISHER and KURZ [1979] and KURZ and FISHER [1979] summarize the main features of (nf–f) eutectic growth. When (nf–f) eutectics are compared with (nf–nf) eutectics, several characteristics can be noted:

i) the degree of structural regularity is much lower and a wide dispersion of local spacing is observed.

ii) for a given growth rate and fraction of phases, the average spacing and the supercooling for growth of a nf–f eutectic are much larger than for a nf–nf eutectic.

iii) for a given growth rate, the supercooling and the spacing decrease as the temperature gradient is increased. No such effect is seen for nf–nf eutectics.

Early investigations introduced interface attachment supercooling for the facetted phase in order to explain the increased supercooling. However STEEN and HELLAWELL [1975] and TOLOUI and HELLAWELL [1976] showed that the kinetic supercooling of Si in Al–Si eutectic is too small to explain the increased eutectic supercooling. Indeed Si in Al–Si and graphite in Fe–C both contain defect planes parallel to the plate growth direction that enable easy growth (twins in Si and rotation boundaries in graphite). TOLOUI and HELLAWELL [1976] suggested that the large supercoolings were due to the difficulties of adjusting the spacing to minimize the diffusion distance. These difficulties are related to the anisotropy of growth of the facetted phase.

Measurement of spacing and supercooling on the model system camphor–naphthalene by FISHER and KURZ [1979] permitted important results to be obtained. The system exhibits two distinct eutectic growth forms: one regular and the other irregular. By assuming that the measured spacing and supercooling for the regular growth were given using the nf–nf theory with the extremum condition, the various materials parameters for

this system were obtained. When ΔT vs. λ_E was plotted for the relevant growth rate, the spacing and supercooling values for irregular growth fell on the same derived theoretical curve for regular eutectic growth but, with spacings much larger than the extremum value. Thus the coarseness of the structure is the cause of the large supercooling of growing nf–f eutectics. Indeed theoretical analysis of the λ_E vs. ΔT curves by MAGNIN and KURZ [1987] that relax the assumption of an isothermal interface made in the nf–nf theory, show a deviation from the nf–nf theory only at very slow growth rates where the constants in eq. (103) become functions of G_L. Thus for growth at more normal speeds, the theory turns to an analysis of why the spacing is so big for nf–f eutectics.

The general argument employed to understand why the average spacing of f–nf eutectics is large focusses on determining the stable range for eutectic spacings at a given velocity. Important contributions have been made by FISHER and KURZ [1980], MAGNIN and KURZ [1987] and MAGNIN *et al.* [1991]. For irregular eutectics the growth directions of different lamellae are not parallel. Thus as growth proceeds, the local spacing decreases between two converging lamellae and increases between diverging lamellae (fig. 48). For converging lamellae, when their separation decreases below the extremum value, one of the lamellae is pinched off, just as for nf–nf growth. For diverging lamellae, when the local spacing increases beyond a critical value, FISHER and KURZ [1980] have suggested that the facetted phases branches into two diverging lamella. The formation of the new lamella decreases the local spacing. The anisotropic growth kinetics

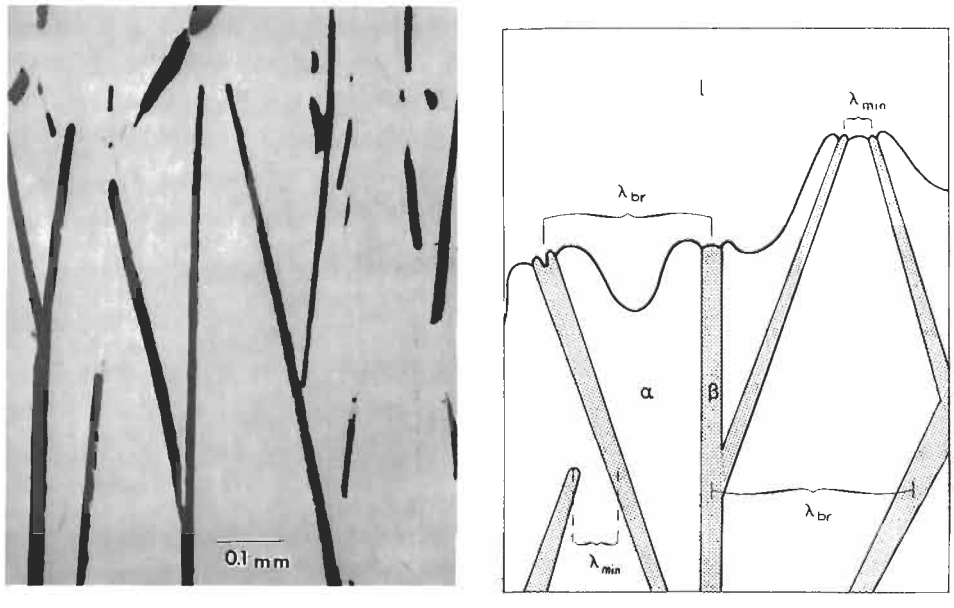

Fig. 48. Proposed growth behavior of irregular eutectics, showing branching at λ_{br} and termination at λ_{ex}. (a) Fe-graphite eutectic growth at $V = 1.7 \times 10^{-2}$ μm/s. (b) schematic representation of solid–liquid interface during growth. MAGNIN and KURZ [1987].

of the facetted phase leads to what is termed *branching-limited growth.* Several criterion have been proposed to determine the maximum value of spacing where the branching takes place (FISHER and KURZ [1980] and MAGNIN and KURZ [1987].) MAGNIN and KURZ [1987] suggest that this branching instability occurs when the facetted phase interface develops a depression of some characteristic depth; e. g., when it drops below a line joining the two triple points for the lamella. The average spacing lies between the minimum spacing and the spacing that cause the branching instability. MAGNIN *et al.* [1991] argue that the mechanism that establishes the minimum and maximum spacings remains undetermined and that the inherently nonsteady solidification of nf–f eutectics plays a fundamental role. Many issues remain to be studied in this area especially those regarding orientation relationships and their relationship to the branching mechanism.

8.1.4. Eutectic cells and dendrites

In addition to consideration of the stability of the eutectic spacing, two other instabilities can influence the microstructure of alloys at or near the eutectic composition. These involve the addition of a ternary impurity or the deviation of the average composition from the thermodynamic eutectic composition in a binary. These will now be discussed in turn.

A ternary impurity added to a binary eutectic can lead to a cellular structure (CHADWICK [1963]). The mechanism is similar to the cellular breakdown in single-phase solidification treated in § 7; for a critical value of G_L/V the average planar S–L interface of the eutectic structure can become unstable and the solidification front becomes corrugated. The cells (often called eutectic colonies) are quite large containing many (10–100) eutectic spacings with the lamellae curving to remain approximately normal to the liquid solid interface. Thus cells are most noticeable for nf–nf eutectics. BERTORELLO and BILONI [1969] propose that the inception of the instability occurs at depressions in the interface due to eutectic grain boundaries or at fault terminations at the S–L interface. It might be noted that near the edge of eutectic colonies there is often a transition to a rod structure.

If an excessive amount of a ternary element is added, the eutectic colony can actually evolve into a two-phase dendrite with secondary arms. In this case, ternary eutectic is usually found between the two-phase dendrite (SHARP and FLEMINGS [1974] (see also fig. 43).

8.1.5. Competitive growth – coupled zone

As a binary alloy with a composition different from the thermodynamic eutectic composition cools from the liquidus to the eutectic temperature, dendritic growth of the primary phase followed by eutectic growth of the remaining interdendritic liquid is expected. However, there is a *range* of alloy composition and growth rate (or interface supercooling) where it is possible to freeze these liquids as eutectic microstructures without dendrites. This range of conditions is known as the *coupled zone.* Pioneering investigations in this field were those of TAMMANN and BOTSCHWAR [1926] and KOFLER [1950] in organic systems, which established that at low or zero temperature gradients, the range of alloy compositions for coupled growth widened with increasing growth

velocity. Later, MOLLARD and FLEMINGS [1967] showed that the widening of the coupled zone was not restricted to high growth rates but, with a positive temperature gradient, could also be obtained at low growth rates with a high G_L/V ratio. Solidification with a high value of G_L/V suppresses the dendritic growth of the primary phase. Other milestones in the development of the knowledge of the coupled zone were the investigations by HUNT and JACKSON [1967], JACKSON [1968], BURDEN and HUNT [1974c], TASSA and HUNT [1976] and KURZ and FISHER [1979].

Taking into account the fact that the description of the microstructural transition from eutectic to eutectic plus dendrites has not yet been successfully modeled using perturbation analysis (JORDAN and HUNT [1971]; HURLE and JAKEMAN [1968]), the coupled zone width can only be obtained using a simpler approach that employs three concepts reviewed by KURZ and FISHER [1979]: For each overall liquid composition, (i) consider all the growth forms possible, i.e., α dendrites, β dendrites, and eutectic. (ii) Analyze the growth kinetics of these forms and determine the interface (or tip) temperatures of the growth forms as a function of V, and possibly of G_L. (iii) Apply the competitive growth criterion, e.g., that the morphology having the highest interface temperature for a given growth rate, or the highest growth rate for a given temperature will dominate. The range of temperatures and compositions, within which eutectic growth is fastest, is called the coupled zone and can be plotted on the phase diagram. The composition range of the coupled zone can also be plotted versus velocity because each value of interface temperature corresponds to a known value of the growth velocity for the dominant growth structure. For growth conditions where the eutectic is not dominant, the microstructure consists of a mixture of dendrites and interdendritic eutectic.

Figure 49 shows an example of a competitive growth analysis for a system involving a f–nf eutectic (the β phase is facetted). The kinetic curves are shown for α dendrites, β dendrites and (planar) eutectic. The curves for the dendrites depend on the value of the

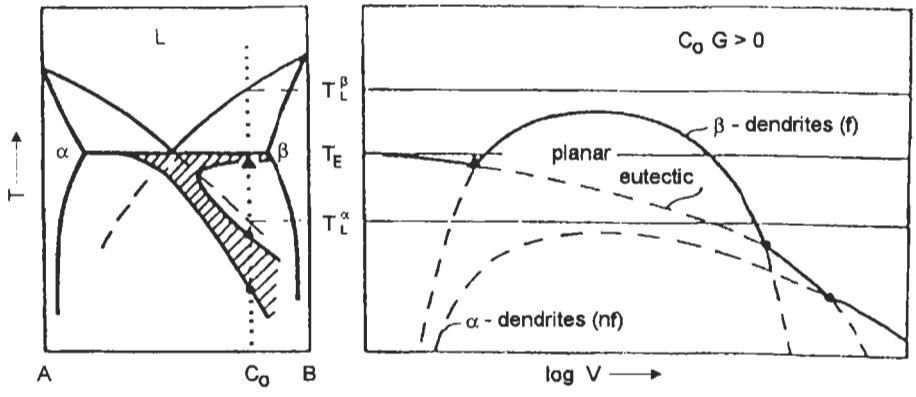

Fig. 49. The origin of the coupled zone (hatched) is understood by considering the variation in eutectic interface temperature and dendrite tip temperatures for an off-eutectic alloy. The dominant microstructure for any composition at a given velocity (or supercooling) is that which grows with the highest temperature (or fastest growth rate given by the solid curves in b). TRIVEDI and KURZ [1988].

temperature gradient and this dependence leads to the decreased interface (tip) temperatures at low velocity and the widening of the coupled zone at high G_L/V ratio. The skewed nature of the coupled zone about the eutectic composition for this f–nf system is due to two factors (KURZ and FISHER [1979]): the nf–f eutectic and the facetted phase dendrite require higher supercooling for a given growth rate than a nf–nf eutectic and a nonfacetted dendrite respectively. The former is due the branching difficulties already discussed and the latter is due to the fact that facetted phase dendrites usually grow as a plate or 2D dendrite rather than a paraboloid or 3-D dendrite. Diffusion of solute away from the tip region of a plate dendrite is more difficult and leads to increased supercooling. Thus for the alloy shown, one expects with increasing growth rate (or supercooling): eutectic, β dendrites (with eutectic), eutectic, and α dendrites (with eutectic). This kind of behavior leads to much confusion if a simplistic, purely thermodynamic view of solidification is employed and leads to difficulty in determining eutectic compositions by purely metallographic methods. For different alloy compositions, the various kinetic curves are raised or lowered leading to a description of the full coupled zone. For a system with a nf–nf eutectic the coupled zone is symmetric about the eutectic composition and the formation of dendrites phase is not observed on the "wrong side" of the eutectic. It is useful to note that near the growth rate where a microstructural transition from dendritic to fully eutectic structure takes place, the interdendritic eutectic will not have an average composition equal to the thermodynamic eutectic composition (SHARP and FLEMINGS [1973]).

The methodology of competitive growth outlined above provides an adequate framework to understand the major features of the transition from eutectic to dendritic growth . However more subtle variations in eutectic microstructure occur under conditions close to the transitions that require a more complete analysis of interface stability. JACKSON and HUNT [1966] observed a tilting of lamellae when the growth rate was suddenly increased. ZIMMERMANN *et al.* [1990] have observed oscillations where the widths of the Al lamellae vary while the Al_2Cu lamellae widths remain fixed in the growth direction in Al-rich Al–Al_2Cu off-eutectic alloys. GILL and KURZ [1993] observed another instability where the widths of both lamellae vary in the growth direction. KARMA [1987] succeeded in simulating these instabilities using Monte Carlo methods. He related the appearance of the instability with increasing velocity to critical values of the concentration gradient in the liquid ahead of the interface.

8.1.6. Divorced eutectics

When the liquid remaining between a primary dendritic phase reaches the eutectic composition, eutectic solidification usually occurs. Typically one observes the same eutectic microstructures already described between the dendrite arms especially if the fraction of liquid remaining between the dendrites when the liquid reaches the eutectic composition is large. If however the fraction of liquid remaining is so small that the width is comparable to the eutectic spacing, the characteristic two-phase structure may not be observed. It is easier for the second phase to form as single particle or layer between the dendrites. This occurs more often for a facetted second phase because coupled nf–f eutectics grow with larger spacings and hence require more space to

develop their characteristic morphology. Thus the final solidified microstructure consists of dendrites or cells with interdendritic single phase. This microstructure is sometimes misinterpreted as resulting from a peritectic reaction in complex alloys where the phase diagram is unknown.

8.1.7. Rapid solidification of eutectic alloys

Rapid solidification produces a very rich variety of microstructures for alloys near eutectic compositions. At extremely high rates of solidification and depending on the thermodynamic structure of the T_0 curves, glass formation or extended crystalline solubility is expected as described in § 3.2, fig. 8. How microstructures and phase distributions evolve from the classical microstructures described above as the solidification velocity is increased has been the subject of intense investigation over the past 15 years.

Eutectic theory – In § 7, the general theory presented for dendritic growth included the modifications necessary to treat high growth rates; viz., modifications of the tip stability condition for high Peclet numbers (of order unity) and the inclusion of non-equilibrium interface conditions (solute trapping). For eutectic growth the Peclet number becomes large at relatively low velocity (~10 cm/s) where the effects of solute trapping are not too important. Thus TRIVEDI *et al.* [1987] recomputed the solute field in the liquid in front of a growing eutectic when the Peclet number is large while maintaining the local equilibrium assumption. The theoretical results are similar to those for nf–nf growth at slow velocity except that the function P_E in eq. (105) depends not only on the volume fractions of the solid phases but also on the Peclet number, the shape of the metastable extensions of the liquidus and solidus curves below the eutectic temperature, and the partition coefficients. Also at high velocity the supercooling can become sufficiently large that the temperature dependence of the liquid diffusion coefficient must be considered (BOETTINGER *et al.* [1984]).

These considerations alter the $\lambda_E^2 V$ "constant" at high speed and the spacing vs. velocity relation (fig. 50) in a way that depends strongly on the equilibrium partition coefficients of the two phases, taken to be equal in the TRIVEDI *et al.* [1987] analysis. Two cases are distinguished depending on whether (a) k_0 is close to unity or (b) k_0 is close to zero. In case (a), the eutectic interface temperature is found to approach the solidus temperature of one of the constituent solid phases as the velocity is increased. During this approach, the eutectic spacing actually *increases* with increasing velocity. Indeed eutectic solidification is replaced by single phase planar growth at high velocities. In case (b) the interface temperature can not reach a metastable solidus curve of either phase. The supercooling becomes so large that the temperature dependence of the diffusion coefficient has a major influence and the spacing decreases with velocity faster than predicted by a constant $\lambda_E^2 V$ value. In both cases there exists a maximum velocity for coupled eutectic growth. In case (a) the eutectic is replaced by single phase growth of one of the phases whereas in case (b) glass formation is possible if the interface temperature reaches the glass transition temperature where the melt viscosity (diffusion coefficient) plummets. In fact, the cases where the k_0's are close to zero are those that would exhibit plunging T_0 curves and lead to glass formation as described in § 3. The symmetry of the coupled zone has an impact on these considerations. Glass formation

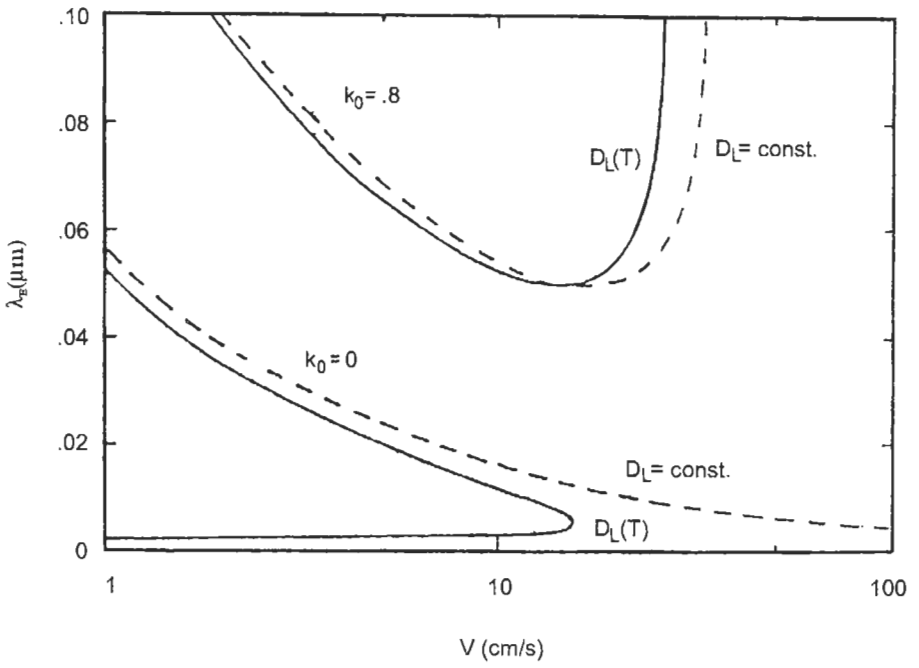

Fig. 50. At high solidification velocities the $\lambda_E^2 V$ "constant" depends on the Peclet number and the relationship between λ_E and V is altered. The changes at high velocity depend strongly on the partition coefficients of the two phases (here taken to be equal). Curves are shown when D_L is assumed constant and when D_L depends on temperature. TRIVEDI *et al.* [1987].

often occurs in systems involving f–nf eutectics. Thus the composition with the smallest maximum growth rate for the eutectic (and hence easiest glass formation) may be shifted towards the direction of the facetted phase. Case (b) may also lead to the formation of a metastable crystalline phase if the eutectic interface temperature drops below the liquidus for such a phase.

Experiments – It is clear from the above that solidification velocity plays a dominant role in controlling microstructure. To control solidification velocity at high rates, surface melting and resolidification employing a moving heat source have been used to create small trails of material that are solidified at speeds close to the scan speed (BOETTINGER *et al.* [1984]). This technique is useful for speeds up to a/d^* where a is the thermal diffusivity and d^* is the diameter of the focussed electron or laser beam. For higher speeds surface melting and resolidification employing a pulsed laser or electron beam must be used. Maps giving the predominant microstructure as a function of speed and alloy composition are then produced. Figure 51 shows such a map for Ag–Cu alloys. Similar maps have been constructed for Al–Al_2Cu (GILL and KURZ [1994]).

In fig. 51 four microstructural domains are obtained: cells/dendrites and eutectic microstructure at slow speed, bands at intermediate speed and microsegregation-free

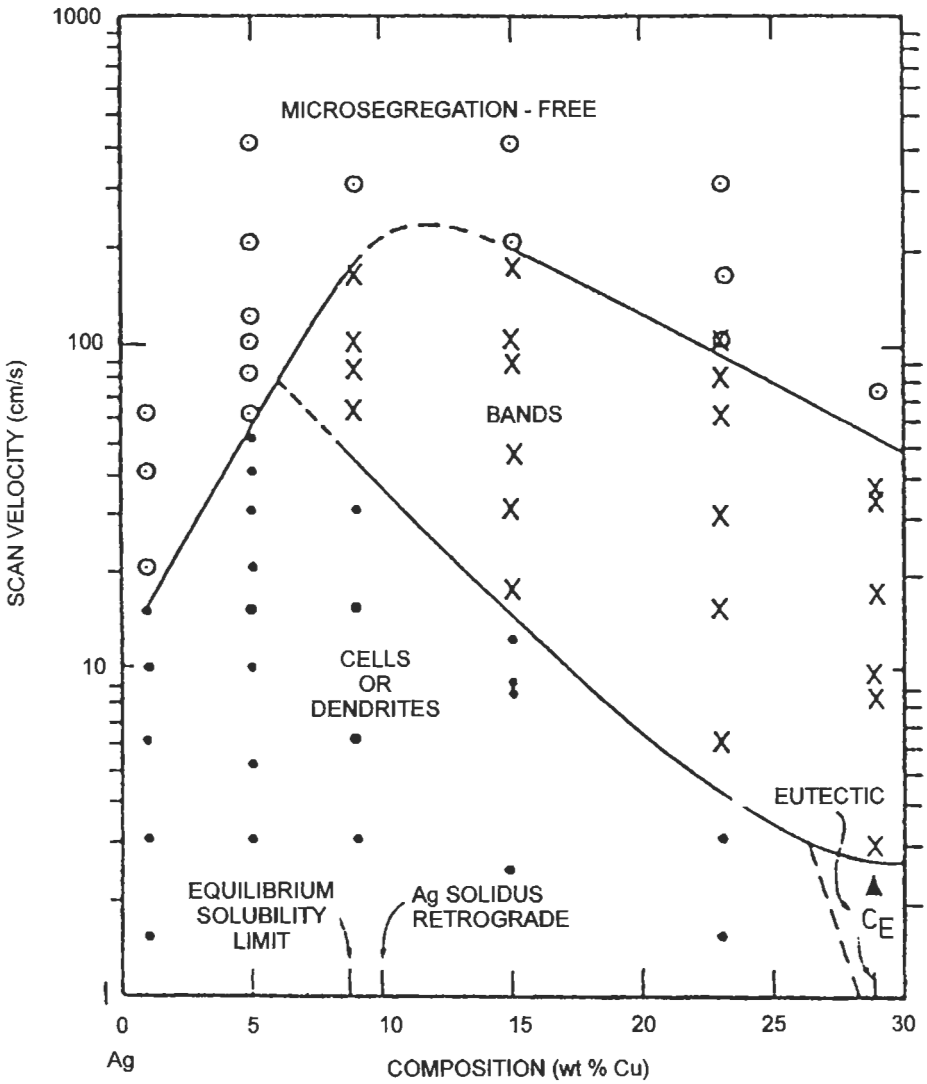

Fig. 51. Experimental results for the variation in microstructure observed for Ag–Cu alloys depending on solidification velocity. BOETTINGER *et al.* [1984].

single phase FCC at high speed. The boundary on the left is due to absolute stability and was described in § 7. Eutectic growth ceases at ~2.5 cm/s generally following the description above except that an intermediate structure of bands is observed before single phase growth dominates at high velocity.

This banded microstructure consist of thin (1 μm) regions *parallel* to the growth front that alternate between cellular solidification and cell-free solidification. The general

character of this structure is due to details of solute trapping (MERCHANT and DAVIS [1990], BRAUN and DAVIS [1991], GREMAUD *et al.* [1991], CARRAD *et al.* [1992]). Ordinarily, interface kinetics requires that the temperature of a planar single phase growth front decrease with increasing velocity. However over the range of velocity where the partition coefficient is approaching unity the interface temperature actually increases with increasing velocity (fig. 20). This reversed behavior is the basic cause of an instability that leads to the banded microstructure. At high speeds in the nondilute Ag–Cu alloys, the microsegregation-free structures are caused by the fact the partition coefficient has gone to unity.

In the Pd–Cu–Si system, maximum growth rates for eutectic and dendritic growth are also observed as shown by BOETTINGER [1981]). However in this case, partitionless growth is not thermodynamically possible and the liquid cools into the glassy state.

Metastable crystalline phase formation – An analysis of growth competition has also been highly successful at explaining observed transitions from microstructures involving stable phases to those involving metastable phases. In the Fe–C system the transition from gray cast iron (Fe-graphite) to white cast iron (Fe–Fe_3C) has been extensively studied (JONES and KURZ [1980]). This transition occurs at relatively slow speeds not normally considered to be rapid. However the same principles can be employed at higher rates for other alloy systems using appropriately modified kinetic laws. The competitive growth analysis must include the dendritic and eutectic growth involving the stable and metastable phases. Figure 52 shows the coupled zones for Al–Al_3Fe (the stable eutectic) and Al–Al_6Fe (the metastable eutectic) summarizing experimental and theoretical work of several groups (ADAM and HOGAN [1972], HUGHES and JONES [1976], GREMAUD *et al.* [1987]). The metastable Al_6Fe phase forms at an increased solidification velocity when the interface temperature drops below about 920K. One of the most striking results of this diagram is the fact that alloys with compositions far on the Fe-rich side of either eutectic can form a microstructure consisting of primary Al at large supercooling and increased velocity; i.e., the Al phase is the first to freeze. Indeed a determination of the powder size dependence of microstructural transitions in Fe-rich Al–Fe alloys from primary Al_3Fe, to eutectic $Al + Al_6Fe$, to primary Al as the powder size decreases is consistent with increasing velocities (supercoolings) calculated for the different size powders (BOETTINGER *et al.* [1986]). Similar microstructural transitions have been observed for other Al based-transition metal alloys. The ability to form a matrix phase of a nf (usually ductile) phase for alloys with a large excess of alloying additions has been a major motivation for alloy development through rapid solidification processing.

8.2. Monotectic solidification

In some metallic systems, the liquid separates into two distinct liquid phases of different composition during cooling. On the phase diagram, the range of temperature and average composition where this separation occurs, as well as the compositions of the two liquid phases are given by a dome-shaped curve that defines the miscibility gap. The maximum temperature of the miscibility gap is called the critical temperature. An example of a miscibility gap is shown in fig. 53 for the Al–In system.

References: p. 830.

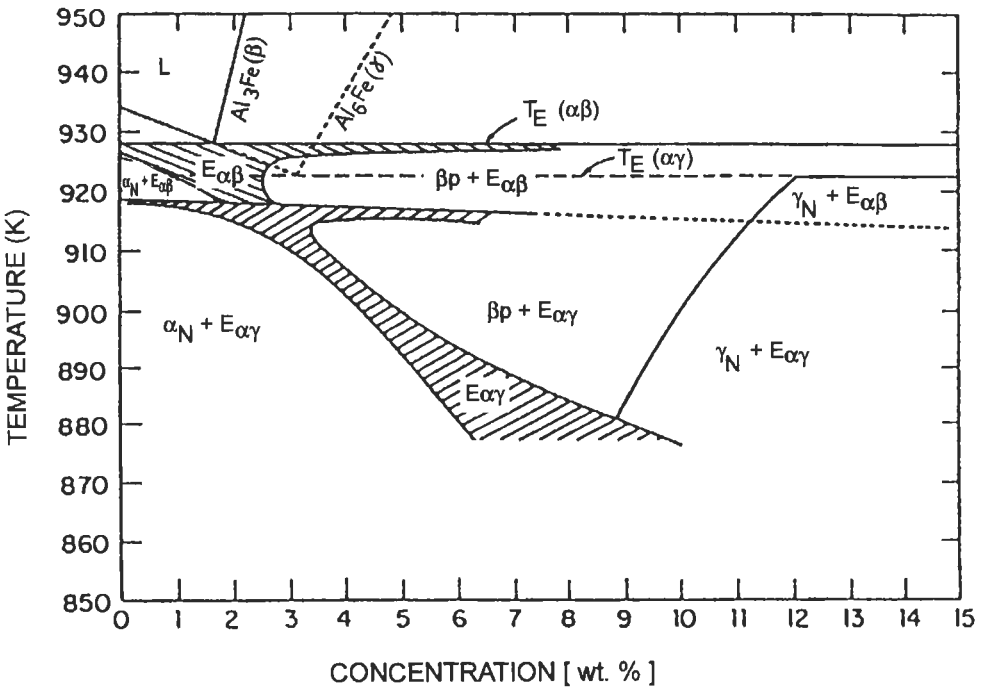

Fig. 52. Theoretical coupled zones for the stable Al–Al_3Fe and metastable Al–Al_6Fe eutectics (hatched). The phases forming outside the coupled zones are also designated. The microstructure present at any value of interface supercooling and average alloy composition has been determine by a competitive growth analysis. TRIVEDI and KURZ [1988]. Subscripts P and N refer to plate (2D) and needle (3-D) dendrites respectively.

Even for alloys outside the miscibility gap, such as for Al-rich alloys in fig. 53, a consideration of the miscibility gap is important in developing an understanding of solidification microstructure. Under ordinary conditions, solidification of these alloys begins with the formation of dendrites of the Al solid phase and enrichment of the liquid remaining between the dendrites with In until the composition reaches the edge of the miscibility gap. This composition (17.3 wt% In, fig. 53) defines the monotectic composition and temperature where the "reaction", liquid $L_1 \rightarrow$ solid $S_1 +$ liquid L_2. Formally this reaction is the same as a eutectic reaction except that on cooling, one of the product phases is a liquid, the liquid defined by the other side of the miscibility gap. At much lower temperatures this liquid usually solidifies in a terminal eutectic reaction $L_2 \rightarrow S_1 + S_2$.

Some sulphide and silicate inclusions in commercial Fe-based alloys are thought to form by monotectic solidification (FLEMINGS [1974]). Free-machining Cu alloys containing Pb also involve this reaction. Considerable research has been focused on directional solidification for fundamental reasons but also because of the potential for producing aligned growth of composites, or (with selective removal of one phase) thin fibers or microfilters (GRUGEL and HELLAWELL [1981]). For this latter purpose it is most

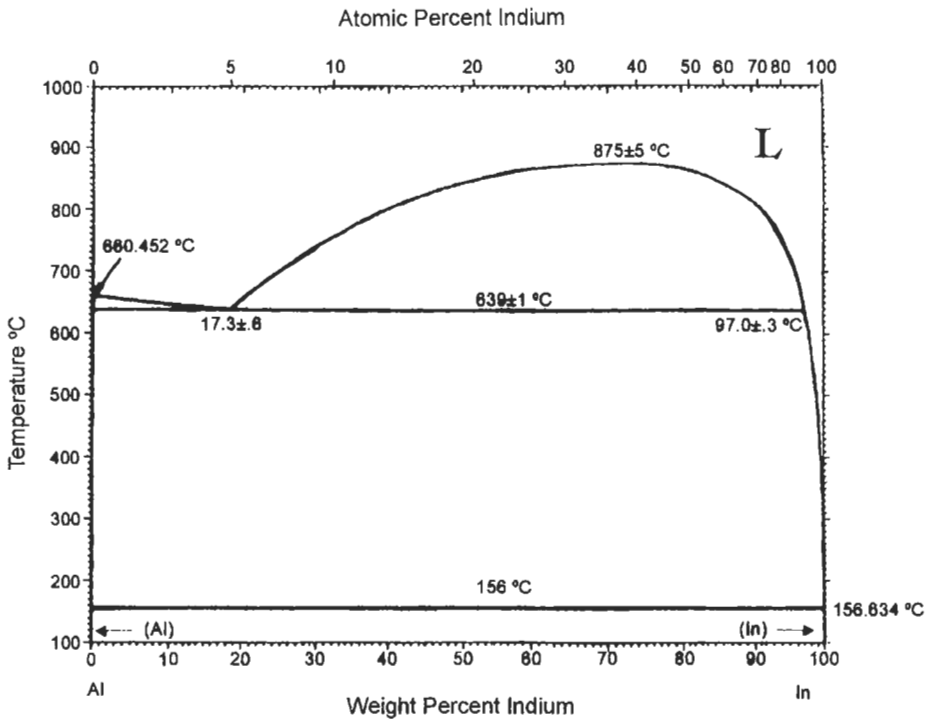

Fig. 53. Al–In monotectic-type diagram. MURRAY [1993b].

important to describe the possibilities of coupled growth of the S_1 and L_2 phases from the L_1 phase of monotectic composition.

8.2.1. Directional solidification of monotectic alloys

As in the case of eutectic solidification, a wide variety of microstructures can be produced by directional solidification of monotectic alloys. Lamellar microstructures are not observed in monotectic systems because the volume fraction of the L_2 phase is usually small. Three types of structures are observed. The first and most interesting and useful, typified by Al–In (GRUGEL and HELLAWELL [1981]), is a regular fibrous or composite structure that consists of closely packed liquid tubes of a uniform diameter embedded in a matrix of the solid phase. These liquid tubes solidify at much lower temperatures to solid rods of In by a divorced eutectic reaction. If the growth rate is increased, the distance between rods decreases, and the structure gives way to a second type of microstructure that consists of discrete droplets of L_2 embedded in a solid matrix. The third type, typified by Cu–Pb (LIVINGSTON and CLINE [1969]), is more irregular consisting of interconnected globules that take on some degree of alignment as the growth rate is increased. Although the L_2 tubes formed at a monotectic reaction are susceptible to

ripening and spheroidization during subsequent cooling, the droplet and irregular structures are not thought to form by coarsening (GRUGEL and HELLAWELL [1981]).

One of the most important considerations for understanding the different microstructures comes from a consideration of whether a stable triple junction can exist between L_1, L_2, and S_1 (CHADWICK [1965]). This condition can only occur if

$$\gamma_{S_1L_1} + \gamma_{L_1L_2} > \gamma_{S_1L_2}. \tag{111}$$

If the inequality is satisfied, regular fibrous structures can be obtained. The eutectic theory for rod growth can then be applied although some modifications are required to treat the increased diffusion in the L_2 phase (GRUGEL and HELLAWELL [1981]). When this inequality is not satisfied, L_2 does not "wet" S_1, and L_1 will tend to coat the interface between L_2 and S_1; i.e., L_1 preferentially wets S_1 to the exclusion of L_2. CAHN [1979] calls this the *perfect wetting case* and during monotectic growth, the L_2 phase will form droplets in the L_1 phase just ahead of the growing S_1 interface. As growth proceeds, the droplets are pushed by the interface and the size of the droplets increase until they reach a critical size where they are engulfed into the growing S_1 solid. The critical size for engulfment is determined by microscopic fluid flow around the droplet. As the solidification velocity is increased, irregular semicontinuous liquid rods can be partially engulfed in the solid as shown schematically in fig. 54. This irregular engulfment is believed to be the origin of the irregular globular microstructure typified by Cu–Pb.

CAHN [1979] showed that in monotectic systems, the perfect wetting case should be expected if the temperature difference between the monotectic temperature and the critical temperature of the miscibility gap is small. Thus irregular composite structures are formed in these systems. When the temperature difference is large, perfect wetting does not occur, a stable triple junction can exist, and regular composite growth is expected. This idea was confirmed by the addition of a ternary element to a binary monotectic alloy. This addition altered the height of the miscibility gap and hence the wetting behavior (GRUGEL and HELLAWELL [1981]). GRUGEL *et al.* [1984] found experimentally that the border between systems with regular and irregular composite

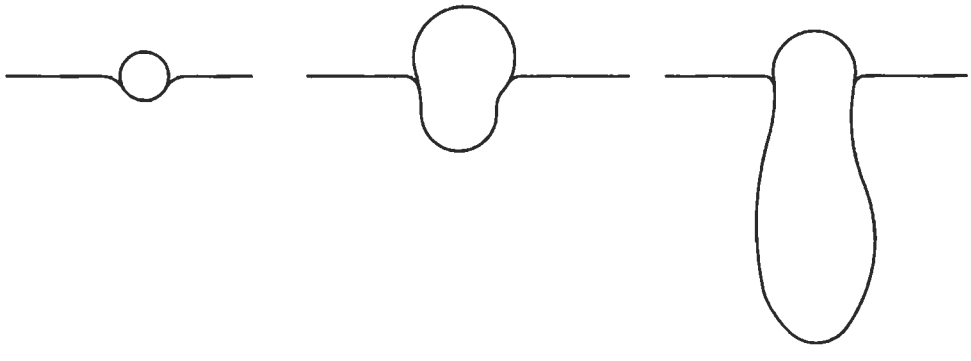

Fig. 54. Schematic sequence to show liquid particle pushing, growth, and engulfment during irregular monotectic growth. GRUGEL *et al.* [1984].

structures occurred when the ratio of the monotectic temperature to the critical temperature is approximately 0.9.

For regular fibrous growth, the spacing varies inversely with the square root of the velocity. GRUGEL *et al.* [1984] showed that the "(spacing)^2 velocity" constant was about an order of magnitude larger for irregular growth than for regular growth. DERBY and FAVIER [1983] have presented a different model for the occurrence of regular and irregular structures similar to those used for irregular eutectics. KAMIO *et al.* [1991] have shown that the value of the temperature gradient has a large effect on the transitions between aligned growth and the formation of droplets.

GRUGEL and HELLAWELL [1981] also examined whether composites could be grown for compositions different than the exact monotectic composition. They found that the dendritic growth of the S_1 phase could be suppressed by sufficiently large values of G_L/V to permit planar composite growth just as for eutectic alloys. Attempts to grow composites with compositions on the other side of the monotectic (within the miscibility gap) failed due to convective instabilities. Reduced gravity experiments have been employed by ANDREWS *et al.* [1992] to avoid these difficulties.

8.2.2. Rapid solidification of monotectic alloys

Some alloys whose phase diagrams do not contain a miscibility gap or a monotectic reaction form microstructures consisting of droplets embedded in a matrix of a primary phase after rapid solidification. If the liquidus curve has a portion where the slope is close to zero, a metastable miscibility gap lies just beneath the liquidus curve. In fact the temperature difference between the liquidus and the metastable critical point is proportional to the liquidus slope (PEREPEZKO and BOETTINGER [1983b]). Thus with the supercooling inherent in many rapid solidification processes, alloy microstructure can be influenced by the presence of the metastable miscibility gap and its associated metastable monotectic reaction. The microstructure of rapidly solidified Al–Be alloys, which consists of fine Be particles in an Al matrix, have been interpreted in this manner (ELMER *et al.* [1994]). In fact even some slowly cooled alloys can exhibit microstructures characteristic of monotectic solidification even though there is no apparent miscibility gap. VERHOEVEN and GIBSON [1978] showed that oxygen impurities raise the metastable miscibility gap in the Cu–Nb system so that it becomes stable and produces droplet microstructures.

8.3. Peritectic solidification

The phase diagram for the Pb–Bi system is shown in fig. 55a. If a liquid with 33% Bi is cooled, and global equilibrium could be maintained (see § 3), the alloy would be composed of $L+\alpha$ at a temperature just above the peritectic temperature of 184°C, denoted T_p, and would be composed of single phase β just below T_p. This gives rise to the notion of a peritectic "reaction" that occurs on cooling that is written as $L+\alpha \rightarrow \beta$. However the diffusion required to accomplish this "reaction" during any realistic solidification process greatly reduces the amount of the β phase formed.

References: p. 830.

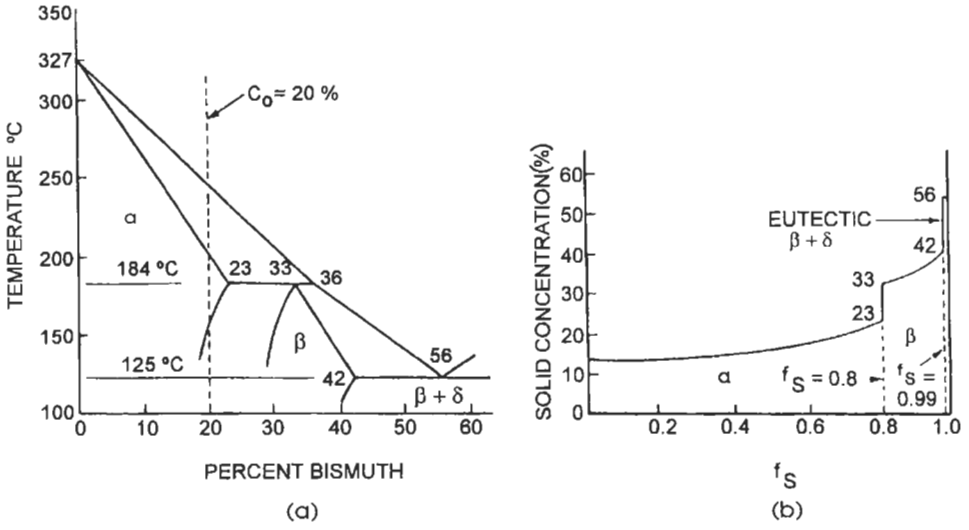

Fig. 55. (a) Pb–Bi peritectic phase diagram. (b) Concentration (% Bi) in the solid according to a Scheil model of solidification. FLEMINGS [1974].

8.3.1. Peritectic solidification during dendritic growth

Under conditions where the α phase grows dendritically, the β phase will usually begin to form along the surface of the α phase. Although the β phase can be formed by three mechanisms, the most important during continuous cooling is the formation of β directly from the melt. The simplest way to treat this situation is to employ the Scheil approach in a small volume of the interdendritic liquid with the usual assumptions: local equilibrium at the solid–liquid interface, uniform liquid composition at each instant (temperature) and no solid diffusion. At small fraction solid, solidification of α phase occurs in the normal way with build up of solute in the liquid between the dendrites following the Scheil equation. When the liquid composition reaches 36%Bi, denoted C_p, solidification switches from the α phase to the β phase. A new value of the partition coefficient given by the β liquidus and solidus must then be employed in the Scheil equation to follow the continued enrichment of the liquid composition in the component Bi. Often one must employ a concentration dependent partition coefficient for the β phase in peritectic systems that requires numerical solution of the differential form of the Scheil equation. The solid composition and the fraction of α and β phases formed by this mechanism using the Scheil model are shown in fig. 55b. For Pb–Bi alloys the final solidification product is eutectic. One notes that using the Scheil approach, *any* alloy composition to the left of 36% will contain α phase in the solidified microstructure. Many systems involve a cascade of peritectic reactions, with solidification switching from phase to phase forming separate layers around the initial α dendrite.

The second and third mechanisms for the formation of β are less important and more difficult to model. The geometry and connectivity of the L, α and β phases determine

their relative importance. Both decrease the fraction of α phase from that predicted above. They have been referred to as the *peritectic reaction* and the *peritectic transformation* by KERR *et al.* [1974]. The peritectic reaction requires that all three phases be in contact with each other. This occurs in the vicinity of the liquid–α–β triple junction and involves partial dissolution of the α phase and solidification of the β by diffusion of solute through the liquid from the L–β boundary to the L–α boundary (fig. 56a). HILLERT [1979] gives an approximate analysis of this process.

The third way that β phase can form, the peritectic transformation, involves solid state diffusion and the motion of the α–β interface during cooling as shown in fig. 56b. This mechanism is very important when the solid diffusion coefficient is large; e.g., for interstitial solutes such as carbon in Fe. Indeed the peritectic reaction in low carbon

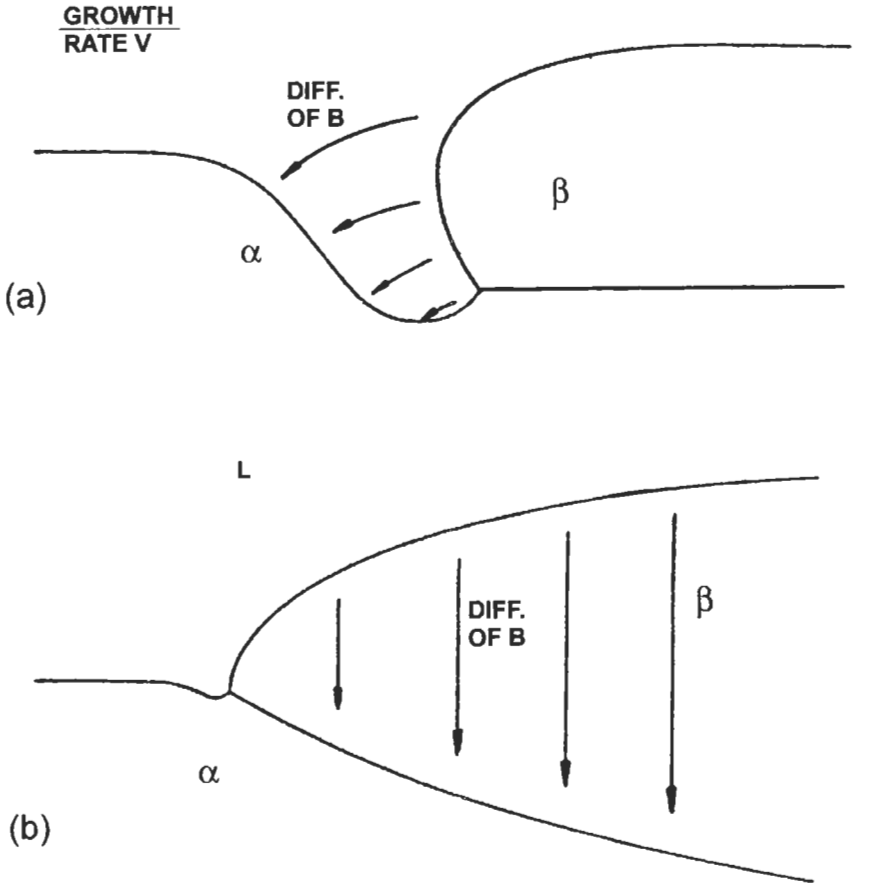

Fig. 56. Peritectic reaction and peritectic transformation on the side of an α dendrite. (a) in the peritectic reaction a second solid phase, β, grows along the surface of the primary phase α by diffusion through the liquid. (b) In the peritectic transformation, diffusion of B atoms through the already formed solid phase β occurs. (After HILLERT [1979]).

References: p. 830.

steels ($L+\delta$–Fe $\rightarrow \gamma$–Fe) seems to go to completion; i.e., no δ–Fe is observed in these alloys. The diffusion problem that governs the motion of the α–β interface involves long range transport of solute from the liquid across the β phase to the α–β interface. At this interface, this flow of solute causes the α phase to dissolve at the expense of the growing β phase. The analysis must use compositions for the interfaces that are given by the $L+\beta$ and $\alpha+\beta$ two phase fields on the phase diagram. HILLERT [1979] has given an approximation for the growth of the β phase by solid state diffusion. Due to the long range diffusion, the thickness of the β phase increases with the square root of time if the interface compositions and diffusion coefficients can be assumed to be independent of temperature.

FREDRIKSSON and NYLEN [1982] have measured the fraction of L, α, and β phases as a function of distance behind the peritectic isotherm by quenching various alloys during directional solidification. The relative contributions of the three mechanisms are analyzed and compared to the measurements. In one alloy (Al–Mn) the β phase did not grow along the L–α interface but grew independently from the melt.

8.3.2. Aligned peritectic growth

Several attempts have been made to grow aligned composites of peritectic alloys by directional solidification. By increasing the temperature gradient or slowing the solidification velocity, it is possible to suppress the dendritic growth of the α phase during directional solidification in peritectic alloys with narrow freezing ranges. When cellular growth of the α phase occurs for alloys whose overall composition falls within the $(\alpha+\beta)$ field, a coarse aligned $(\alpha+\beta)$ two-phase structure can be formed (BOETTINGER [1974]; BRODY and DAVID [1979]).

More interesting were attempts to achieve coupled growth of the α and β phases to produce a fine two-phase structure. It was thought that if the G_L/V ratio were large enough to suppress cellular solidification of the α phase and force a planar solidification front that coupled growth of the two solid phases might be possible. This would also require that the composition of the liquid near the interface be maintained near C_p, a liquid composition from which both α and β could form. However coupled growth has never been observed in peritectic alloys. Instead, coarse alternating bands of α and β form from the melt. (BOETTINGER [1974]; OSTROWSKI and LANGER [1979]; TITCHENER and SPITTLE ([1975]).

BOETTINGER [1974] analyzed the supercooling-velocity-spacing relation for hypothetical coupled growth in a peritectic alloy and showed that it was intrinsically unstable. The formation of bands can be understood through an examination of the stable and metastable liquidus and solidus curves for the α and β phases (HILLERT [1979]). In fig. 57, an alloy of the indicated composition can solidify to single phase α at a planar interface at temperature T_1 if the β phase does not nucleate. Alternately the same alloy composition can solidify to single phase β at a planar interface temperature at T_2 if α does not nucleate. Thus two steady state solidification situations are possible. However each situation is precarious in that nucleation of the other phase can occur in front of the growing phase. The system is extremely sensitive to minor growth rate fluctuations that leads to solidification that alternates between α and β. This situation has been recently analyzed by TRIVEDI [1995].

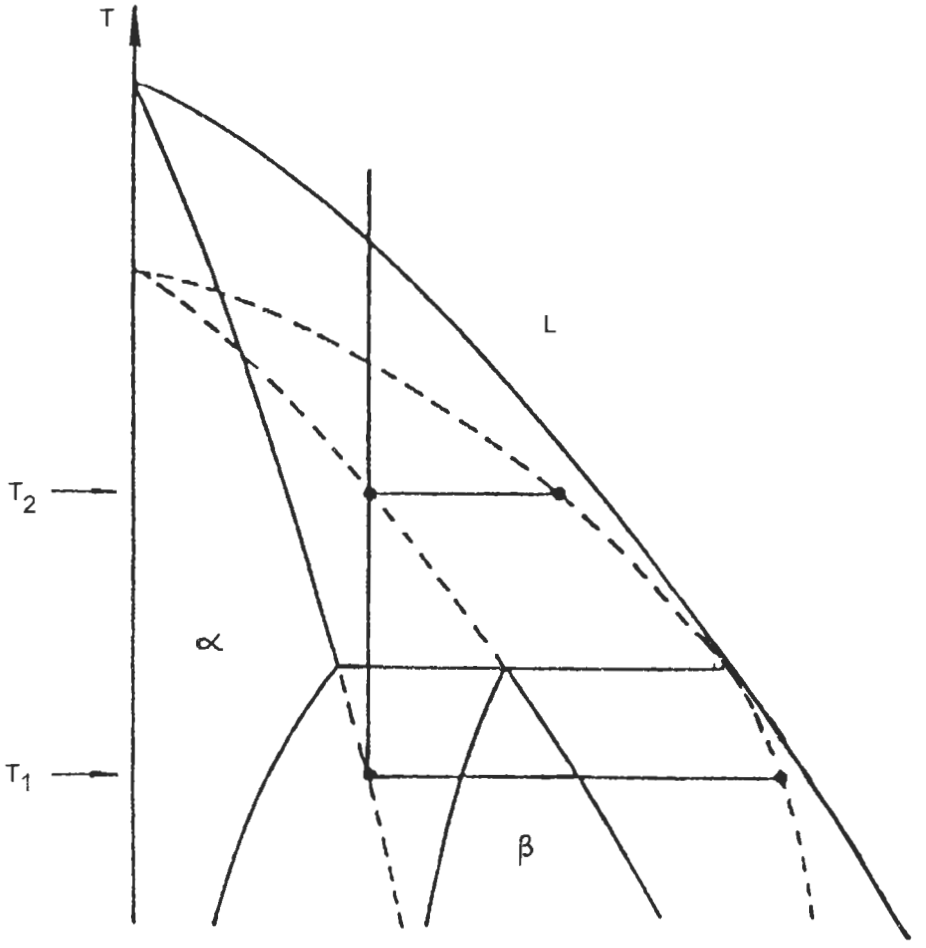

Fig. 57. Peritectic phase diagram with metastable extensions of α and β liquidus and solidus curves below and above the peritectic temperature respectively. For an alloy of the composition of the vertical line, planar steady-state growth of either α or β is possible at the temperatures T_1 and T_2 respectively. After HILLERT [1979].

8.3.3. Rapid solidification of peritectic systems

As shown in fig. 57, the metastable liquidus curve of the α phase below the peritectic temperature must lie below the stable β liquidus. However when compared to a eutectic system, the metastable liquidus is relatively close to the stable β liquidus. Thus there exists considerable opportunity for the formation of the α phase directly from the melt at modest levels of supercooling at compositions where it is not expected. Whether or not this happens depends on the competition of nucleation and growth kinetics for the α and β phases. An example of this kind of behavior is found in the classic experiments of CECH [1956] on solidification of small droplets (3–30 μm) of Fe–30%Ni alloys in a drop tube. This system contains a peritectic reaction, L + bcc → fcc. Experiments showed that

bcc was formed from the melt (and not by solid state transformation) at compositions with high Ni content where only fcc should have formed. In contradiction to the experimental facts, analysis of the dendritic growth kinetics of the competing fcc and bcc structures showed that fcc would be the favored product phase at all supercoolings for Fe–30%Ni (BOETTINGER [1988]). This result is due primarily to the fact that the partition coefficient for bcc is much larger than for fcc. On the other hand, analysis of the nucleation behavior indicates that bcc is favored over fcc if the nucleation is homogeneous or if the contact angle on heterogeneities is greater than about 45° (KELLY and VANDERSANDE [1987]). Thus only nucleation can explain the observed bcc structure.

In alloys containing a cascade of peritectic reactions, the close proximity of stable and metastable liquidus curves can also explain why one or more phases may be skipped over in the layer structure that coats the initial dendritic phase in rapidly solidified alloys.

9. *Fluid flow and casting structure*

The flow of molten metal or alloy is an important consideration during casting. Although the requirements for mold filling especially in narrow cross sections have been considered for centuries, the importance of flow during the freezing process has been recognized much more recently. In this section we consider: i) the general origins of fluid flow in castings; ii) the development of casting macrostructure (grain structure); iii) the macrosegregation observed in ingots and castings due to flow in the mushy zone; and iv) the formation of porosity and inclusions. Finally, the foundry concept of *fluidity* associated with the mould filling capability of alloys will be described.

9.1. Transport processes and fluid flow in casting

There are many sources of material transport that can occur during solidification: i) residual flow due to mold filling, ii) thermal and solute driven bouyancy convection, iii) convection due to expansion or contraction upon solidification, iv) floating or settling of free crystals, v) dendritic breakage and transport, vi) convection driven by thermocapillary forces, vii) pushing of equiaxed crystals by the columnar solidification front, viii) external forces (pressure, rotation, magnetic fields).

COLE [1971] and WEINBERG [1975] extensively studied the flow in the fully liquid part of castings. Weinberg's use of radioactive tracers techniques proved to be very sensitive and overcame the handicap of other experiments performed with transparent model liquids having much lower thermal conductivity than metals. Convection has the largest effect on thermal transport and macrostructure when the S–L interface (position of dendrite tips) is parallel to the gravity vector. Thus horizontal solidification is dramatically affected by convection due to the horizontal temperature gradients. Flows in metals and the heat transfer due to the flow can be reduced by the application of a magnetic field due to the induced eddy current that exerts a body force on the fluid. Rotation of ingots gives a effect similar to the application of a magnetic field; here the body force is a Coriolis force that deflects particles of fluid in a direction normal to the axis of rotation, and normal to the direction of fluid motion. On the other hand, an

increase in heat transfer can be accomplished by vigorous fluid motion near the S–L interface. Rotation or oscillations of the crucible, a rotating magnetic field, or electromagnetic field interactions can be used for this purpose (COLE [1971]).

On a more microscopic scale, fluid flow due to a variety of causes has also been associated with dendrite fragmentation and subsequent crystal multiplication during solidification (JACKSON *et al.* [1966] and O'HARA and TILLER [1967]). In alloys the interaction of natural or forced convection with the dendritic substructure can be rationalized as follows. When secondary branches form, they must grow through the solute-rich layer that exists around the primary stalk. The initial growth through this layer is slow. After the branch passes through the layer, it enters the bulk liquid of lower solute concentration and grows more rapidly. The result is a thin neck of the secondary branch near the primary stalk. Any slight increase in the local temperature or shear force due to local fluid flow can detach portions of the dendrites. These crystals may be able to survive in other portions of the liquid and, if the thermal and constitutional conditions are appropiate, subsequently grow. This leads us into a discussion of ingot macrostructure.

9.2. Ingot structure

The classical representation of ingot macrostructure shows three distinct zones: the chill zone, which is a peripheral region near the mould surface composed of small equiaxed grains, the columnar zone and a central equiaxed zone. Inside each grain a substructure of cells, dendrites, and/or eutectic exists. Fluid flow during solidification affects the origin and development of the three zones. Extensive research has been performed because of the important influence of macro- and microstructure of ingots and castings upon mechanical properties.

9.2.1. Chill zone

The formation of the chill zone structure involves complex interactions of liquid metal flow, metal-mould heat transfer, nucleation catalysis and dendritic growth. CHALMERS [1964] suggested that chill zone grains could form by independent nucleation events or by a *copious nucleation* mechanism. BOWER and FLEMINGS [1967], BILONI and MORANDO [1968] and PRATES and BILONI [1972] experimentally simulated the thermal conditions existing in the chill zone using thin samples filled quickly by a vacuum technique. By controlling the fluid flow, BOWER and FLEMINGS [1967] found a dendritic substructure in the chill grains and established that a *grain multiplication (fragmentation)* mechanism induced by melt turbulence during pouring was quite important. They used moulds coated with lampblack which drastically reduces the value of h_i compared to an uncoated Cu mould. In contrast BILONI and CHALMERS [1965] had earlier found chill grains with a different substructure with uncoated moulds. Predendritic nuclei with solute-rich cores were formed by partitionless solidification. BILONI and MORANDO [1968] used an identical device as BOWER and FLEMINGS [1967], but coated only part of the chill surface with lamp black (fig. 58). The region with lampblack had the same substructure as was previously observed by BOWER and FLEMINGS [1967], but the chill grains in the region without the lampblack were smaller and contained a predendritic

References: p. 830.

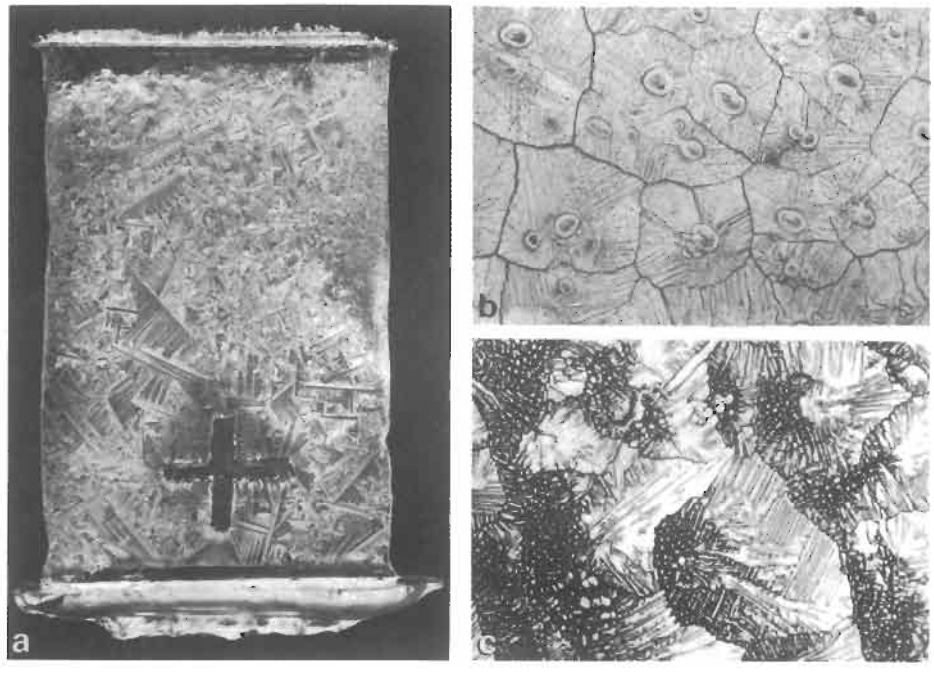

Fig. 58. (a) Chill plate of Al-1% Cu cast in a copper mould coated with lamp black, except in the area of the cross which appears with different reflectivity. (b) Substructure corresponding to the uncoated region of fig. 58a). Each grain has a predendritic region as origin. (c) Substructure corresponding to the coated region; notice the "cells", probably produced by a multipication mechanism, as the origin of the dendrites. BILONI [1980].

substructure. Thus the importance of local values of the heat transfer cannot be neglected even though the grain multiplication mechanism by fragmentation can be active. BILONI [1980] reviewed the origin and development of the chill zone.

The roughness of the mould surface as affected by polishing, machining, or coating can also be important (PRATES and BILONI [1972]). A suitable microprofile design of the surface can promote a specific distribution of predendritic nuclei and fig. 59 (MORALES *et al.* [1979]) shows how the coating microprofile can influence the columnar grains originating from the chill zone.

In summary, a rough surface, a very cold mould, a low pouring temperature and convection currents that stir the melt, all favour a fine grain size in the chill zone through both nucleation and multiplication mechanisms.

9.2.2. Columnar zone

Further from the mould surface, the grain structure evolves into columnar grains growing roughly perpendicular to the mould surface. The origin of the columnar zone was first analyzed by WALTON and CHALMERS [1959]. These authors mention the competitive mechanism through which the favourably oriented grains eliminate those less

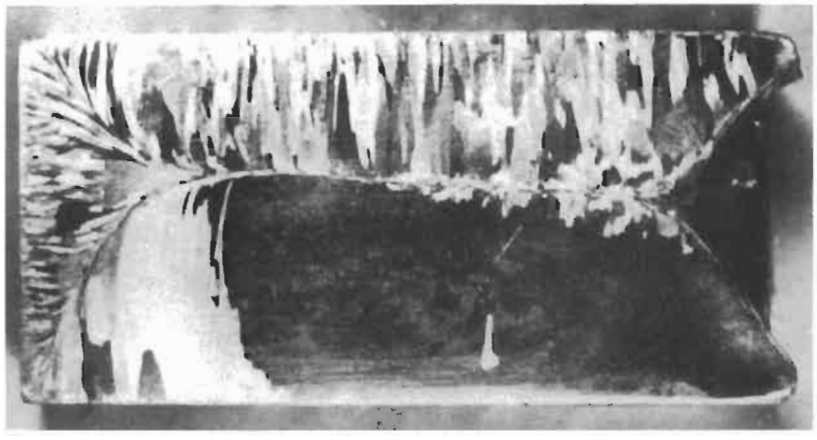

Fig. 59. Longitudinal section of an ingot poured from the bottom (shown to the left), after macroetch. The difference in grain size is due to mould walls with different microgeometries. The small columnar grains start at the asperities of an alumina mould coating presenting a controlled microgeometry; the very large grain started from a wall coated with a very smooth film of lamp black. MORALES *et al.* [1979].

favourably oriented and a texture arises. In fcc and bcc alloys, a preferred <100> orientation is characteristic of the structure.

Figure 60 (RAPPAZ and GANDIN [1993]) schematically shows the competetive columnar growth of three grains. Some equiaxed grains that nucleate and grow in front of the columnar zone are also depicted which will be discussed later. The columnar grains on the left and on the right contain dendrites whose <100> crystallographic orientations are nearly perpendicular to the liquidus isotherm. These dendrites grow with the same velocity V_L, as that of the isotherms. The grain in the middle of the figure, having a deviation of its <100> crystalographic direction from the heat flow direction, grows with a velocity $V_\theta = V_L/\cos\theta$ that is larger than V_L. According to the growth kinetic model of the dendrite tip for constrained growth (§ 7), the faster growing (misoriented) dendrites are characterized by a larger tip supercooling. Thus the tips lie behind those of the better oriented grains. RAPPAZ and GANDIN [1993] give the details of the elimination of the misoriented grains according to the convergence or divergence of the neighbouring grains and the ability or inability to form tertiary arms as shown in fig. 60.

After elimination of misoriented grains, the growth of the columnar front in a casting can be modelled using a macroscopic heat code that solves eq. (7). This requires a fraction solid versus temperature (and other variables) relationship obtained from one of the various dendritic microsegregation models presented in section 7.3. FLOOD and HUNT [1987a] give one approach and the various methods are summarized by RAPPAZ and STEFANESCU [1988] and RAPPAZ [1989].

Several researchers have attempted to provide a more detailed numerical procedure to model the development of the columnar zone including the variation of the transverse

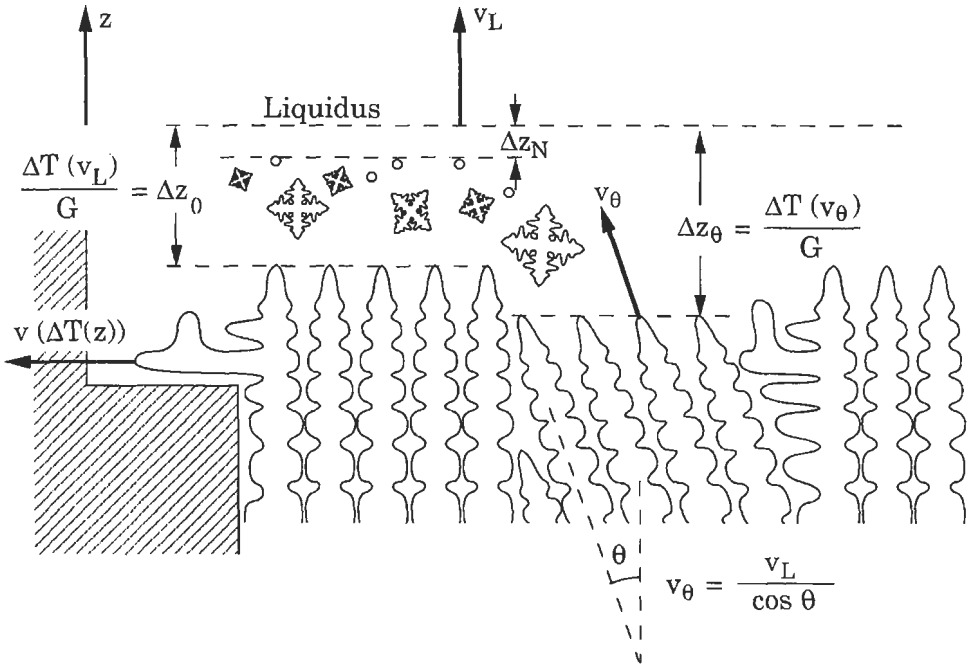

Fig. 60. Competing processes during directional dendritic growth: development of preferred orientation in the columnar region, formation of equiaxed grains ahead of the columnar front. RAPPAZ and GANDIN [1993].

size of columnar grains described by CHALMERS [1964] and to deal with other issues of crystalline anisotropy, and texture formation. BROWN and SPITTLE [1989] and ZHU and SMITH [1992a], [1992b] used Monte-Carlo methods to model the effect of anisotropy. RAPPAZ and GANDIN [1993] developed what they call a *probabilistic model* that includes an orientation variable for each grain and keeps track of the developing grain shape using a cellular automaton technique.

These numerical methods have been able to be compute realistic grain macrostructures as well as crystallographic texture. As predicted by the model, the orientation distribution of the columnar grains narrows as the distance from the mould surface increases and the comparison with the WALTON and CHALMERS [1959] experiments is acceptable. Additionally, the selection of the columnar grains at the chill-columnar transition as well as the columnar extension is also succesfully predicted. This approach is also useful for modeling the grain competition in the grain selector during directional solidification (DS) for the production of modern turbine blades (RAPPAZ and GANDIN [1994]). It must be remembered however, that the success of this approach depends strongly on the input of an accurate nucleation law that generally must be determined from experiments.

Fluid flow can also affect the columnar zone structure. In conventional ingots,

columnar growth may not be perpendicular to the mould wall if convection sweeps past the S–L interface due to horizontal temperature gradients. If convection is diminished through magnetic fields or mould rotation, perpendicular columnar growth can be restored (COLE [1971]).

When columnar growth occurs in concentrated alloys with a low temperature gradient, a substructure other than cellular-dendritic can sometimes appear. Dendrite groups rather than individual dendrites comprise the solidification front. These groups have been called *superdendrites*, where apparently the normal coupling that establishes the primary spacing between dendrites becomes unstable, with certain dendrites grow ahead of their neighbors. (COLE and BOLLING [1968]; FAINSTEIN–PEDRAZA and BOLLING [1975]).

In aluminum-base alloys and under some conditions, another unusual structure can appear. Laminar grains grow from a single origin and form "colonies". These structures have different names in the literature but most commonly are called *feather crystals*. Generally, they appear in continuous or semicontinuous castings and in welding processes. Occasionally they are observed in conventional casting. BILONI [1980], [1983] describes the current knowledge about this structure, which is open to further research.

9.2.3. Equiaxed zone

Equiaxed grains grow ahead of the columnar dendrites and the columnar to equiaxed transition (CET) occurs when these equiaxed grains are sufficient in size and number to impede the advance of the columnar front. Evidence for the collision of the columnar front with equiaxed grains can be found in the work of BILONI and CHALMERS [1965] and BILONI [1968]. When this collision occurs, the heat flow direction in the equiaxed grains changes from radial to unidirectional and a modification of the dendritic substructure can be observed by careful metallography in the solidified samples.

The situation to be modelled therefore corresponds to that shown in fig. 60. The major challenges to predict the columnar to equiaxed transition and the size of the equiaxed zone in castings involve an accurate description of the source of the nuclei and an accurate description of the growth rates of the columnar and equiaxed crystals under the prevailing conditions.

9.2.3.1. Origin of the equiaxed nuclei. Three principal sources of nuclei can be considered. i) *Constitutional Supercooling (CS)* driving heterogeneous nucleation (WINEGARD and CHALMERS [1954]). Because the tips of the dendrites in the columnar grains are at a temperature below the bulk alloy liquidus temperature a region of liquid exists where hetrogenous nuclei may become active. ii) *Big-Bang* mechanism: Equiaxed grains grow from predendritic shaped crystals formed during pouring at or near the mould walls. These crystals are carried into the bulk by fluid flow with some surviving until the superheat has been removed (CHALMERS [1963]). As outlined in § 9.2.1., the origin of the grains could be either by nucleation events or crystal multiplication mechanisms. OHNO *et al.* [1971] has proposed a *separation theory* (OHNO [1970]) for the origin of the equiaxed grains by the big bang mechanism. iii) *Dendritic fragmentation* occurring from the columnar grains (JACKSON *et al.* [1966]), (O'HARA and TILLER [1967]) or from dendritic crystals nucleated at the top of the ingot as a result of the radiation cooling occurring in that region (SOUTHIN [1967]).

References: p. 830.

Many experiments have been performed in metallic alloys and transparent analogues to decide the nucleation mechanism responsible for the equiaxed zone. The available information suggests that in conventional castings there is strong evidence to support the big bang and fragmentation mechanisms, probably a combination of both, in most of the cases where convection is present (MORANDO *et al.* [1970], FLOOD and HUNT [1988]). In these circumstances, the C.S. mechanism would seem not to have a large enough contribution except in the presence of very efficient heterogeneous nuclei. When upward directional solidification experiments are performed and a near-perfect adiabatic lateral mould walls exist, convection is minimized, and the only possible mechanism for equiaxed grain formation is C.S. However, the complete elimination of convection is quite difficult even in this type of growth (CHANG and BROWN [1983], ADORNATO and BROWN [1987]).

9.2.3.2. Columnar to equiaxed transition (CET). If a reliable nucleation model were available, and convection could be ignored, any one of several models could be employed to predict the columnar to equiaxed transition. The model of HUNT [1984] uses selected columnar growth and nucleation models to determine whether the structure will be fully equiaxed or fully columnar. The results depend on whether the temperature gradient is smaller or larger respectively than a critical value given by

$$G_L = 0.617 N_0^{1/2} \left[1 - \left(\frac{\Delta T_n}{\Delta T_c} \right)^3 \right] \Delta T_c, \tag{112}$$

where N_o = density of nucleating sites, ΔT_n = supercooling required for heterogeneous nucleation and ΔT_c = supercooling of the dendrite tips in the columnar grain. This analysis was expanded by FLOOD and HUNT [1987b]. The experimental results by ZIV and WEINBERG [1989] are in close agreement with eq. (112) for Al–3%Cu. Factors which promote a columnar to equiaxed transition by this mechanism are: large solute content (increases the value of ΔT_c for fixed growth conditions), low temperature gradient, which increases the size of the supercooled region in front of the dendritic tips, a small value for ΔT_n (potent nucleation sites), and a large number of nuclei. Hunt's model ignores many complexities of the dendritic growth of equiaxed grains and nucleation was assumed to take place at a single temperature rather than over a range of temperature. It therefore cannot predict the effect of solidification conditions on equiaxed grain size (KERR and VILLAFUERTE [1992]). More detailed models of equiaxed growth employing empirical nucleation laws have been combined with numerical solutions of the heat flow to predict the grain size of fully equiaxed structures (THEVOZ *et al.* [1989], RAPPAZ [1989], STEPHANESCU *et al.* [1990]). These more detailed analyses could be used to predict the columnar to equiaxed transtition. FLOOD and HUNT [1988] have critically reviewed the models and experiments of several researchers.

RAPPAZ and GANDIN [1993] have used the probabalistic model described in § 9.2.2 to simulate the columnar to equiaxed transition. Figure 61a) corresponds to the simulation of the final grain structure of an Al–5%Si casting with no temperature gradients when cooled at 2.3 K/s. Figure 61b) corresponds to an Al–7%Si casting cooled at 2.3 K/s and fig. 61c) to an Al–7%Si casting cooled at 7.0K/s. Comparisons among the

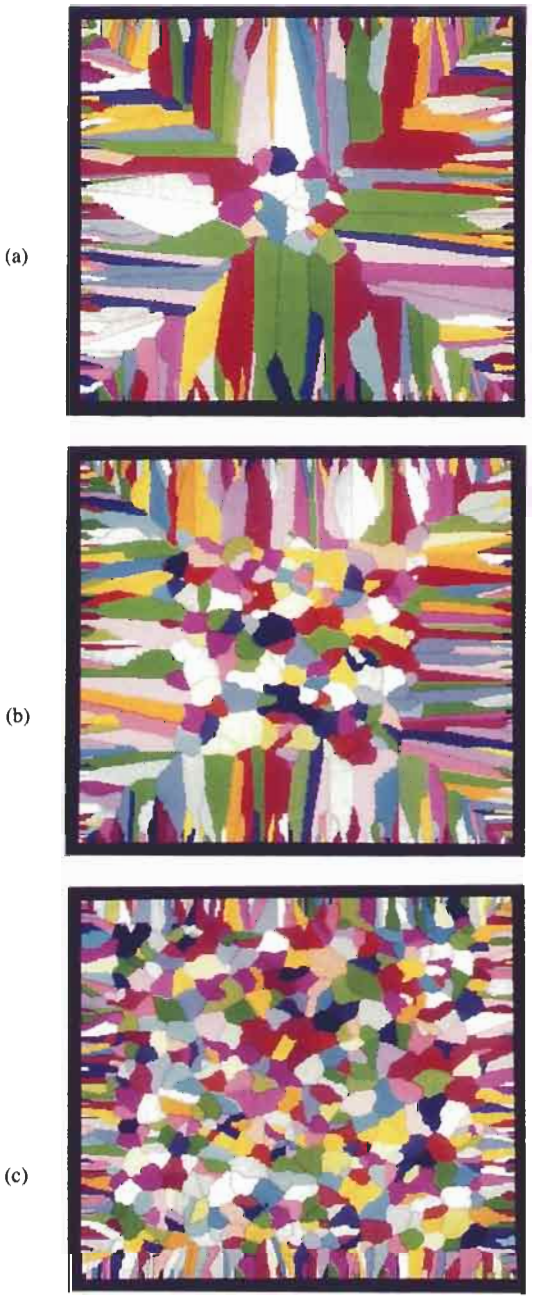

Fig. 61. Simulation of columnar and equiaxed structures by RAPPAZ and GANDIN [1993].

three figures show the effect of the alloy composition and cooling rate upon the grain structure. Very recently RAPPAZ and GANDIN [1994] presented a very comprehensive review of the modeling of grain structure formation in solidification processes.

A set of experiment were performed by BILONI and CHALMERS [1968] which showed that the CET could be stimulated by mechanically disturbing the columnar growth front during upward directional solidification (fig. 62). Experiments were conducted in which the value of $G/V^{1/2}$ decreased with distance down the length of a small ingot. This leads to a columnar to equiaxed transition at some position as previously shown by PLASKETT and WINEGARD [1959] and ELLIOT [1964]. The critical values of $G/V^{1/2}$ obtained by BILONI and CHALMERS [1968] for various Al–Cu alloys are shown in fig. 62 as circles. When the experiment was repeated, but with a periodic disturbance (1 min) of the interface, small equiaxed grains were formed at the position of the disturbance at significantly higher values of $G/V^{1/2}$ as shown by the squares in fig. 62. However this band of equiaxed grains reverted to columnar growth upon further solidification. Presumably the disturbance increased the number of potential growth sites by dendrite fragmentation and acccording to eq. (112) momentarily increased the possibilities for equiaxed growth. However the available growth centers where quickly consumed and the growth reverted to columnar. Finally at a position in the ingot with a low value of $G/V^{1/2}$

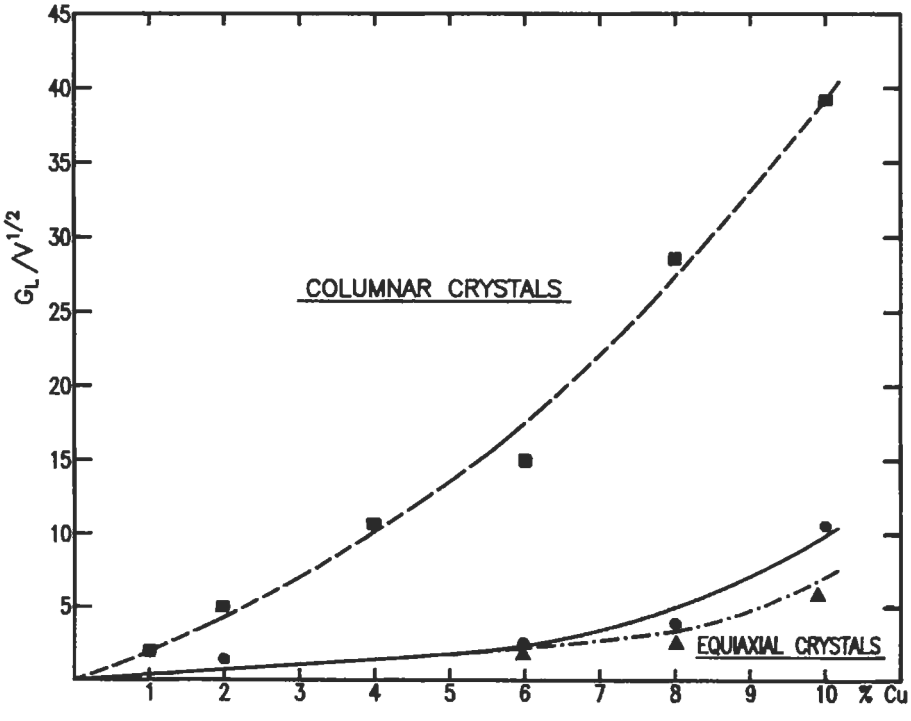

Fig. 62. Critical values of $G/V^{1/2}$ for columnar to equiaxed transition for various Al–Cu alloys. BILONI and CHALMERS [1968].

(triangles, fig. 62) close to that established by the undisturbed experiments, it was found that the equiaxed grains did not revert to columnar grains, but persisted for the remainder of the ingot. These experiments indicate the importance of dendrite fragmentation on the columnar to equiaxed transition.

9.3. Macrosegregation

Macrosegregation is defined as variations in composition that exist over large dimensions, typically from millimeters to the size of an entire ingot or casting. We have already considered one form of macrosegregation in the initial and final transients during planar growth of a rod sample (§ 6.2). However in order to define or measure macrosegregation for dendritically solidified samples, it is necessary to determine an average composition over a volume element that contains several dendrite arms. As we will see, changes in the dendritic microsegregation profile in such a volume element due to settling of free-floating solid or flow of solute-rich liquid in or out of the volume element during solidification will change the average composition of the volume element away from the nominal composition of the alloy. Thus macrosegregation is produced. Figure 63 shows a drawing of a large steel ingot showing some of the major types of macrosegregation commonly found. Positive and negative macrosegregation refer to solute content greater or less than the average.

9.3.1. Gravity segregation

Negative cone segregation has been explained by the settling of equiaxed grains or melted off dendrites into the bottom of a casting if they are of higher density than the liquid. If lighter solids such as nonmetallic inclusions and kish or spheroidal graphite are formed they can float to the upper part of a casting forming positive segregation areas. Centrifugal casting clearly can alter the pattern of macrosegation formed by this mechanism (OHNAKA [1988]). It is important to note that gravity produces negligible macrosegration of a single phase liquid, discrete particles with densities different from the average are necessary.

9.3.2. Interdendritic fluid flow and macrosegregation

The first attempt to create models for macrosegregation due to flow of solute rich material was by KIRKALDY and YOUDELIS [1958]. Later the subject was treated extensively at MIT by FLEMINGS and NEREO [1967]) and MEHRABIAN *et al.* [1970] and has been summarized by FLEMINGS [1974], [1976]. Using a volume element similar to that chosen in fig. 41, a mass balance is performed under the additional possibility that flow of liquid in or out of the volume elements can occur and that the liquid and solid can have different densities. Thus the necessity for flow to feed solidification shrinkage is treated. The result is a modified form of the solute redistribution equation used to describe microsegregation in § 7,

$$\frac{\mathrm{d}f_\mathrm{L}}{\mathrm{d}C_\mathrm{L}} = -\frac{(1-\beta)}{(1-k_0)}\left[1+\frac{\bar{v}\cdot\nabla T}{\varepsilon}\right]\frac{f_\mathrm{L}}{C_\mathrm{L}}, \tag{113}$$

References: p. 830.

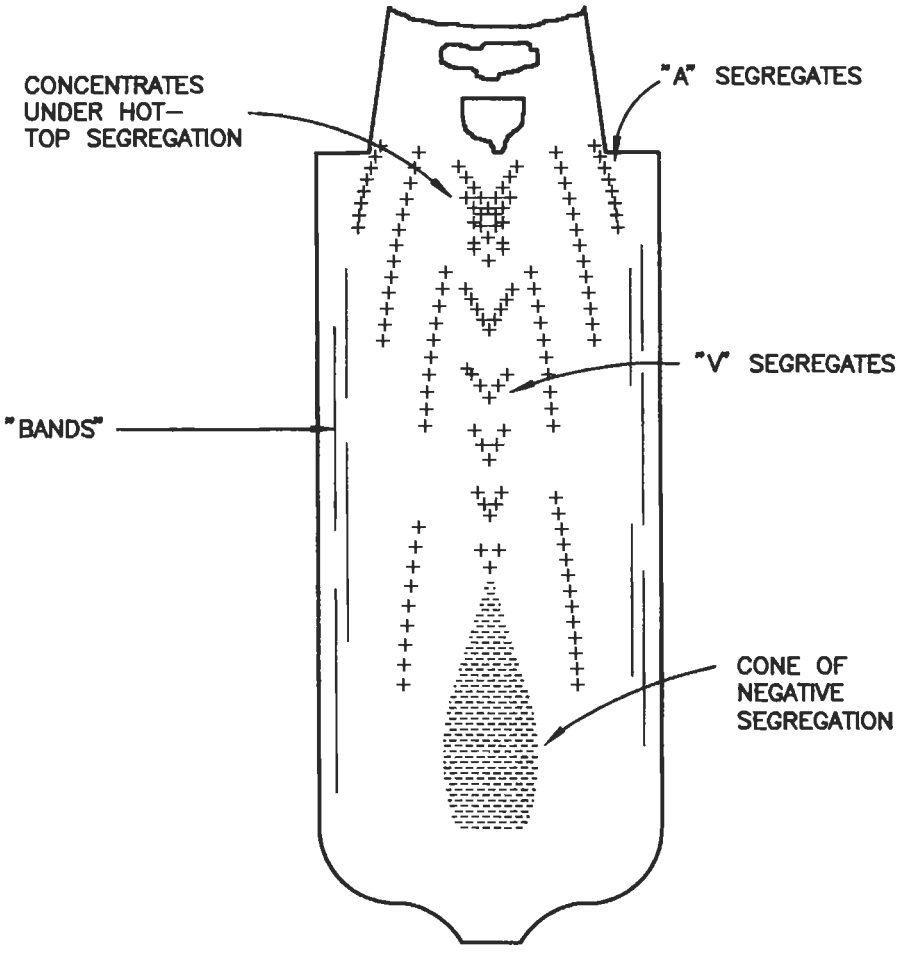

Fig. 63. Different types of macrosegregation in an industrial steel ingot. FLEMINGS [1974].

where: f_L is the fraction of liquid; $\beta = (\rho_S - \rho_L)/\rho_S$ = solidification shrinkage; $\bar{v}$ = velocity vector of interdendritic liquid; ∇T = local temperature gradient vector; ε = local rate of temperature change.

This expression assumes: i) local equilibrium without curvature correction, ii) uniform liquid composition in the small volume of interest, iii) no solid diffusion, iv) constant solid density, v) no solid motion, and vi) absence of voids. In this approach, the appropriate values for $\bar{v}$ and ε at each location must be determined from a separate calculation involving thermal analysis and flow in the mushy zone, which will be outlined below. However given these values for each small volume element, C_L and hence C_S as a function of f_S can be determined along with the fraction of eutectic. The average value of C_S from $f_S = 0$ to 1 gives the average composition at each location in the

casting. The average composition will not in general be equal to the nominal alloy composition.

Several cases can be distinguished. If the interdendritic flow velocity just equals the flow required to feed local shrinkage,

$$\bar{n} \bullet \bar{v} = -\frac{\beta}{1-\beta} \bar{n} \bullet \bar{V}. \tag{114}$$

Then eq. (113) reverts to the Scheil equation and the average composition is equal to the nominal. Here $\bar{n}$ is the unit normal to the local isotherms and $\bar{V}$ is the isotherm velocity. If on the other hand $\bar{n} \bullet \bar{v}$ is greater than or less than this value, negative or positive macrosegregation occurs, respectively. A particularly simple case ocurs at the chill face of a casting. Here $\bar{n} \bullet \bar{v}$ must be zero because there can be no flow into to the chill face. This clearly produces positive macrosegregation (for normal alloys where $\beta > 0$ and $k_0 < 1$). This is commonly observed in ingots and is termed *inverse segregation* (KIRKALDY and YOUDELIS [1958]) because it is reversed from what one would expect based on the initial transient of plane front growth.

In order to compute the fluid velocity of the liquid, the mushy zone is treated as a porous media and *D'Arcy's Law* is used. The pressure gradient and the body force due to gravity control the fluid velocity according to

$$\bar{v} = \frac{K_p}{\eta f_L} \left(\nabla P + \rho_L \bar{g} \right), \tag{115}$$

where:

K_p = specific permeability; η = viscosity of the interdendritic liquid; ∇P = pressure gradient; $\bar{g}$ = acceleration vector due to gravity.

Often, heat and fluid flow in the interdendritic region have been computed by ignoring the fact that the fraction of liquid at each point in the casting depends on the flow itself through eq. (115). This decoupling is thought to cause little error if the macrosegregation is not too severe. FLEMINGS [1974] and RIDDER *et al.* [1981] solved the coupled problem using an iterative numerical scheme for an axisymmetric ingot. In their work the flow in the bulk ingot was also coupled to that in the interdendritic region. Experiments on a model system showed good agreement.

Determining an accurate expression for the permeability of a mushy zone is a difficult problem since the value of K_p depends on interdendritic channel size and geometry. In the case of the mushy zone it has been proposed (PIWONKA and FLEMINGS [1966]) that

$$K_p = \lambda_c f_L^2, \tag{116}$$

where λ_c is a constant depending on dendritic arm spacing. Recently, POIRIER [1987] analysed permeability data available for the flow of interdendritic liquid in Pb–Sn and borneol–paraffin. The data were used in a regression analysis of simple flow models to arrive at relationships between permeability and the morphology of the solid dendrites. When flow is parallel to the primary dendritic arms the permeability depends upon

References: p. 830.

λ_1 (primary arm spacing) but not λ_2 (secondary arm spacing). When flow is normal to the primary arms the permeability depends upon both λ_1 and λ_2. These correlations are only valid over an intermediate range of f_L, roughly between 0.2 and 0.5.

With this model of macrosegregation, FLEMINGS [1974], [1976] was able to explain different types of macrosegregation present in industrial ingots (fig. 63):
a). *Gradual variations in composition from surface to center and from bottom to top* are due to the interdendritic fluid flow with respect to isotherm movement. b) *Inverse segregation* as described above. If a gap is formed between the mould and the solidifying casting surface, a severe surface segregation or *exudation* can arise. c) *Banding* or abrupt variations in composition that result from either unsteady bulk liquid or interdendritic flow, or from sudden changes in heat transfer rate. d) *"A" segregates* or *"freckel"*. These are abrupt and large variations in composition consisting of chains of solute-rich grains. They result from movement of interdendritic liquid that opens channels in the liquid–solid region. Recent work by HELLAWELL [1990] seems to prove that, at least in some cases, the initiation of the channels is at the growth front itself. e) *"V" segregates*. As the fraction solid in the central zone increases in the range of 0.2 to 0.4, the solid network that has formed is not yet sufficiently strong to resist the metallostatic head and fissures sometimes occur. These *internal hot tears* open up and are filled with solute rich-liquid. f) *Positive segregation under the hot top*: Probably occurs during the final stages of solidification when the ingot feeding takes place only by interdendritic flow.

More recently KATO and CAHOON [1985] concluded that void formation can affect inverse segregation. They studied inverse segregation of directionally solidified Al–Cu–Ti alloys with equiaxed grains. MINAKAWA *et al.* [1985] employed a finite difference model of inverse segregation. This model allowed for volume changes due to microsegregation and thermal contractions as well as the phase change.

9.3.3. Further theoretical developments for flow in the mushy zone

Many simplifying assumptions regarding the flow in the mushy zone and its interaction with the bulk flow have been required in the past work. More rigorous approaches have recently been performed. In order to formulate a set of governing equations that determines the flow, temperature and composition fields in the mushy zone as well as in the bulk liquid, two approaches have been employed: *continuum mixture theory* and a *volume averaging technique* as reviewed by VISKANTA [1990] and PRESCOTT *et al.* [1991]. Both approaches have successfully computed macrosegregation patterns in ingots, including freckles. The continuum mixture approach has been used by BENNON and INCROPERA [1987a)], [1987b)], GANESAN and POIRIER [1990], and FELICELLI *et al.* [1991]. The volume averaging technique (BECKERMANN and VISKANTA [1988], NI and BECKERMANN [1991]) may be better suited to flow models involving the formation of equiaxed (free floating) dendritic structures where solid movement must be treated.

9.4. Porosity and inclusions

Porosity and inclusions have a strong effect on the soundness and mechanical properties of castings.

9.4.1. Porosity

For most metals the density of the solid is higher than the liquid. Thus liquid metal must flow toward the solidifying region in order to prevent the formation of voids. Much of foundry practice is involved with the placement of chills and risers that maintain proper temperature gradients to retain an open path of liquid metal from the riser to the solidification front. Indeed the major use of macroscopic heat flow modelling of castings is to identify potential locations in the casting where the solidifying regions are cut off from the risers.

Even if a path of liquid metal remains open to the riser, porosity on the scale of the dendritic structure can still form. When liquid metal flows through the mushy zone to feed solidification shrinkage, the liquid metal pressure in the mushy zone drops below the external atmospheric pressure. The pressure gradient required for flow is given by eq. (115). Microporosity forms when the local pressure in the mushy zone drops below a critical value. Thus detailed prediction of microporosity requires a rather complete description of fluid flow in the mushy zone as does the prediction of macrosegregation. Clearly the larger the freezing range of an alloy and the smaller the temperature gradient, the more tortuous are the liquid channels in the mushy zone. This leads to greatly increased difficulty of feeding the shrinkage and a greater reduction of the liquid metal pressure deep in the mushy zone (far from the dendrite tips).

The critical reduction of the liquid pressure required for the formation of micropores depends on many factors. Indeed the initial formation of a pore is a heterogeneous nucleation problem (CAMPBELL [1991a]) that requires the same consideration as described in § 4, but with pressure substituted for temperature. In principle one needs to know the contact angle of the pore on the solid–liquid interface. It is common to postulate that the critical radius (in the sense of nucleation) of a pore, above which the pore can grow, is related to the scale of the dendrite structure. KUBO and PEHLKE [1985] let the critical radius be equal to the primary dendrite spacing, λ_1, whereas POIRIER *et al.* [1987] relate the critical radius to the space remaining between dendrites. They obtain an expression for the liquid metal pressure where a void can form as

$$P \leq P_G - \frac{4\gamma_{LG}}{f_L}\lambda_1, \tag{117}$$

where P_G is the pressure of gas in the pore if any, and γ_{LG} is the surface energy of the liquid gas interface. If no dissolved gas is present and if the surface energy were zero, porosity would form at locations in the casting where the liquid metal pressure drops to zero. Dissolved gas increases the likelihood of porosity formation whereas the inclusion of the surface energy effect makes it more difficult, possible requiring negative pressure to form a void.

Dissolved gas in a liquid alloy causes porosity because the solubility of gas in liquid metal usually exceeds the solubility in the solid. One can define a partition coefficient for the gas, k_0', as the ratio of the equilibrium solubilities of gas in the solid and the liquid just like any solute. The value of the coefficient as a function of temperature must be known to make predictions. As an alloy solidifies, the dissolved gas is rejected into the

remaining liquid where its level increases. Because the diffusion rate of gas in solid metal is usually quite high, the gas content of the solid phase is usually assumed to be uniform and at the equilibrium concentration. Thus the lever rule can be applied to compute the concentration of gas in the liquid as a function of fraction solid. This increase in the concentration of gas leads to an expression for the equilibrium pressure of the gas in the pores given by

$$P_G = \frac{P'_G}{\left(f_L\left(1 - k'_0\right) + k'_0\right)^2}, \tag{118}$$

where P'_G is the partial pressure of the gas above the melt (given by the initial concentration of gas in the melt (BRODY [1974]). Thus it can be seen how the presence of dissolved gas in the melt (through its effect on P_G) as well as solidification shrinkage both contribute to the formation of dendritic microporosity. This combined effect is particularly important for aluminium castings where the solubility of H in the solid is only tenth of that in the liquid.

Equation (118) for the pressure inside a pore is only valid when the volume fraction of porosity is small. To actually calculate the size and fraction of porosity after solidification is complete, a more complex analysis is required. KUBO and PEHLKE [1985] have calculated the amount and size of the porosity formed in Al-4.5 wt% Cu plate castings containing hydrogen that match experimental measurements. POIRIER *et al.* [1987] perform such calculations for Al–Cu in a directional solidification geometry. ZHU and OHNAKA [1991] have also simulated interdendritic porosity considering both H redistribution in the melt and solidification contraction. With this method, the effect of the initial H content, cooling rate and ambient pressure were simulated.

9.4.2. Inclusions

At present it is very clear that inclusions exert an important influence on fracture behaviour of commercial materials. As a result, this portion of the field of solidification is receiving much greater attention. One type of inclusions, called *primary inclusions*, corresponds to: i) exogeneous inclusions (slag, dross, entrapped mould material, refractories); ii) fluxes and salts suspended in the melt as a result of a prior melt-treatment process; and iii) oxides of the melt which are suspended on top of the melt and are entrapped within by turbulence. These are called primary inclusions because they are solid in the melt above the liquidus temperature of the alloy. In the steel industry a significant reduction of inclusions is obtained by the their floating upward and adhering to or dissolving in the slag at the melt surface. In the aluminum industry filtering has become a common practice and the development of better filters is an important area of research (ROSS and MONDOLFO [1980], APELIAN [1982]).

Secondary inclusions are those which form after solidification of the major metallic phase. Although in industrial practice commercial alloys involve multicomponent systems, a first approach to the understanding of the formation of secondary inclusions has been achieved through the considerations of ternary diagrams involving the most important impurity elements under consideration (FLEMINGS [1974]). Then, the solidifi-

cation reactions occurring during the process, together with the values of the various partition coefficients of the impurity elements in the metallic phase play an important role in the type, size and distribution of inclusions in the final structure. Important ternary systems to be considered are Fe–O–Si, Fe–O–S, and Fe–Mn–S from which the formation of silicates, oxides and sulphides results.

As an example of research in this field FREDRICKSSON and HILLERT [1972], through carefully controlled solidification, were able to determine the formation of four types of MnS inclusions formed by different reactions. CAMPBELL [1991a] and TRAJAN [1988] treat extensively both primary and secondary inclusions and their effect on mechanical properties in ferrous and nonferrous alloys.

An important effect to consider when a moving solidification front intercepts an insoluble particle is whether the inclusion is pushed or engulfed. If the solidification front breaks down into cells, dendrites or equiaxed grains, two or more solidification fronts can converge on the particle. In this case, if the particle is not engulfed by one of the fronts, it will be pushed in between two or more solidification fronts and will be entrapped in the solid at the end of local solidification. STEFANESCU and DHINDAW [1988] reviewed the variables of the process as well the available theoretical and experimental work for both directional and multidirectional solidification. More recently, SHANGGUAN *et al.* [1992] present an analytical model for the interaction between an insoluble particle and an advancing S–L interface. There exists a critical velocity for the pushing-engulfment transition of particles by the interface. The critical velocity is a function of a number of materials parameters and processing variables, including the melt viscosity, the wettability between the particle and the matrix, the density difference as well as the thermal conductivity difference between the particle and the matrix, and the particle size. Qualitatively the theoretical predictions compare favorably with experimental observations.

As an example of the interaction between the formation of inclusions and porosity, MOHANTY *et al.* [1993] present a novel theoretical approach to the nucleation of pores in metallic systems. The proposed mechanism is based on the behavior of foreign particles at the advancing S–L interface. Mathematical analysis has been employed to predict gas segregation and pressure drop in the gap between the particle and the S–L interface. The authors discussed the effect of particle properties and solidification parameters, such as wettability, density, thermal conductivity, solidification rate and S–L interface morphology. They recognize, however, that at present quantitative measurements of materials properties are necessary, in particular for interfacial energies.

9.5. Fluidity

Over the years the foundryman has found it useful to employ a quantity called *fluidity*. The concept arises from practical concerns regarding the degree to which small section sizes can be filled with metal during castings with various alloys. This property is measured through one of several types of fluidity tests. Hot metal is caused to flow into a long channel of small cross section and the *maximum length* that the metal flows before it is stopped by solidification is a measure of fluidity. The solidification process

References: p. 830.

in the channel is under the influence of many variables: metallostatic pressure, heat transfer coefficient, superheat, latent heat of fusion, density of the alloy liquid, viscosity, liquid surface tension, alloy freezing range, and whether the alloy freezes with plane front or with columnar or equiaxed dendrites.

FLEMINGS [1974] reviewed the field and his contributions to the study of fluidity. More recently CAMPBELL [1991a], [1991b] gives a general view of this property and stresses the importance of the factors that influence the fluidity test as they relate to present limitations and future difficulties of numerical modeling of casting. It is worthwhile to follow the approach of CAMPBELL [1991a] who considers three cases: i) *Maximum Fluidity Length*, L_f, determined by an experiment where the cross sectional area of the channel is large enough that the effect of surface tension is negligible; ii) L_f, when surface tension is important, and, iii) *Continuous Fluidity Length*, L_c.

9.5.1. Maximum fluidity

Instead of only determining the total distance travelled, which is the maximum fluidity length, MORALES *et al.* [1977] and AGUILAR RIVAS and BILONI [1980a], [1980b] performed tests on Al–Cu alloys that measured the distance flowed vs. time for different metallostatic pressures, superheats and metal-mould heat transfer coefficients, h_i. In addition, the use of careful metallographic analysis of the fluidity samples gave information about the vein closing mechanism. The measured data have two stages with different slopes. For a given fluidity test, the first stage represents a high percentage of the total distance flowed but depends on variables independent of the true capacity of flow of the metal or alloy, namely, the liquid superheat and the heat transfer coefficient at the metal-channel surface. The second stage, in general, represents a small percentage of the total distance flowed but reflects the intrinsic ability of the metal or alloy to flow. In a complementary study, MORALES *et al.* [1979] determined how the channel microgeometry, as influenced by machining, polishing and coating, affects microstructure and L_f through variations in the local and average heat transfer rates. In summary, the molten metal entering the channel flows until all the superheat is eliminated in the first stage. The liquid can continue to flow primarily because of the delayed cooling due to the latent heat evolution. This second stage is strongly affected by the solidification mechanisms, the $f_S(T)$ relationships, and the nature of the columnar/equiaxed structures.

Until recently all fluidity tests performed in fundamental investigations used binary alloys to establish relationships between L_f and alloy composition (FLEMINGS [1974], CAMPBELL [1991a]). GARBELLINI *et al.* [1990] carried out an extensive study of the fluidity of the Al–Cu rich corner of the Al–Cu–Si ternary system, which serves as a basis for many commercial alloys. This paper developed a correlation between L_f and alloy microstructure in the binary (Al–Cu and Al–Si) and ternary (Al–Cu–Si) systems. CAMPBELL [1991c] discussed this paper expanding on the results. L_f for any composition is a balance among three factors primarily related to the phase diagram: a) the latent heat of the proeutectic phase, i.e., Al, Si or Al_2Cu; b) the amount of interdendritic liquid remaining at the end of the proeutectic solidification; and c) The value of the fluidity for the specific eutectics (binary and/or ternary) that complete solidification. These considerations led to the conclusion that minor changes of compositions can be quite

important, for example for metal matrix composites (MMC) obtained by infiltration. Also due to the latent heat effect, the high fluidity of alloys with proeutectic Si phase in hyper eutectic alloys was confirmed. The important industrial Al–Si alloys do not display a peak fluidity at the eutectic composition. Typically alloys with the smallest freezing ranges show the best fluidity (FLEMINGS [1974], CAMPBELL [1991a]). Small amounts of Si in hypereutectic alloys dramatically increased L_f because of the extraordinarily high latent heat of Si that maintains the fluid state of the alloys for longer times. The relationships that exist between fluidity length and solidification microstructure are open to further research. As examples, there is a large difference in fluidity between binary Al–Al_2Cu, a regular eutectic and Al–Si, an irregular eutectic (GARBELLINI *et al.* [1990]). In eutectic cast irons the fluidity is determined by the morphological changes of the graphite phase as documented by fluidity tests on laminar, vermicular and nodular cast irons (STEFANESCU *et al.* [1988]).

9.5.2. Combined effects of surface tension and fluidity

When the channel section becomes thinner than a critical value, considered to be ~0.30 cm for most metals and alloys by FLEMINGS [1974], the resistance to liquid flow increase because of surface tension. This is particularly critical in technologies such as aerofoils, propellers, and turbine blades (CAMPBELL [1991a]). CAMPBELL and OLLIF [1971] distinguish two aspects of filling thin sections: *flowability*, essentially, following the rules discussed above and *fillability* limited by surface tension.

9.5.3. Continuous fluidity length

Figure 64a is a schematic representation of the solidification into a channel when a nondendritic S–L interface is considered (MORALES *et al.* [1977]). In region I, no solidification occurs; in region II the solidification occurs in the presence of a decreasing amount of superheat. Region III corresponds to the liquid and solid at the melting temperature, i.e. with no superheat. The length, L_c, defines a critical value known as the continuous fluidity length. The physical meaning of L_c has been defined by FELIU *et al.* [1962], who introduce the concept of the flow capacity of a channel. In the case of a very long channel the flow capacity is just the volume of the cast fluidity length L_f. In the case of a channel of intermediate length, the flow capacity is the total of the amount which has flowed through, plus the amount which has solidified in the channel. For a channel shorter than L_c the flow capacity becomes infinity (fig. 64b). CAMPBELL [1991a] gives technological applications of these concepts for different types of alloys and moulds.

10. Solidification processes

This section will treat two conventional solidification processes that have an important impact in current technology: continuous casting and welding.

10.1. Continuous casting

Continuous casting has emerged as one of the great technological developments of

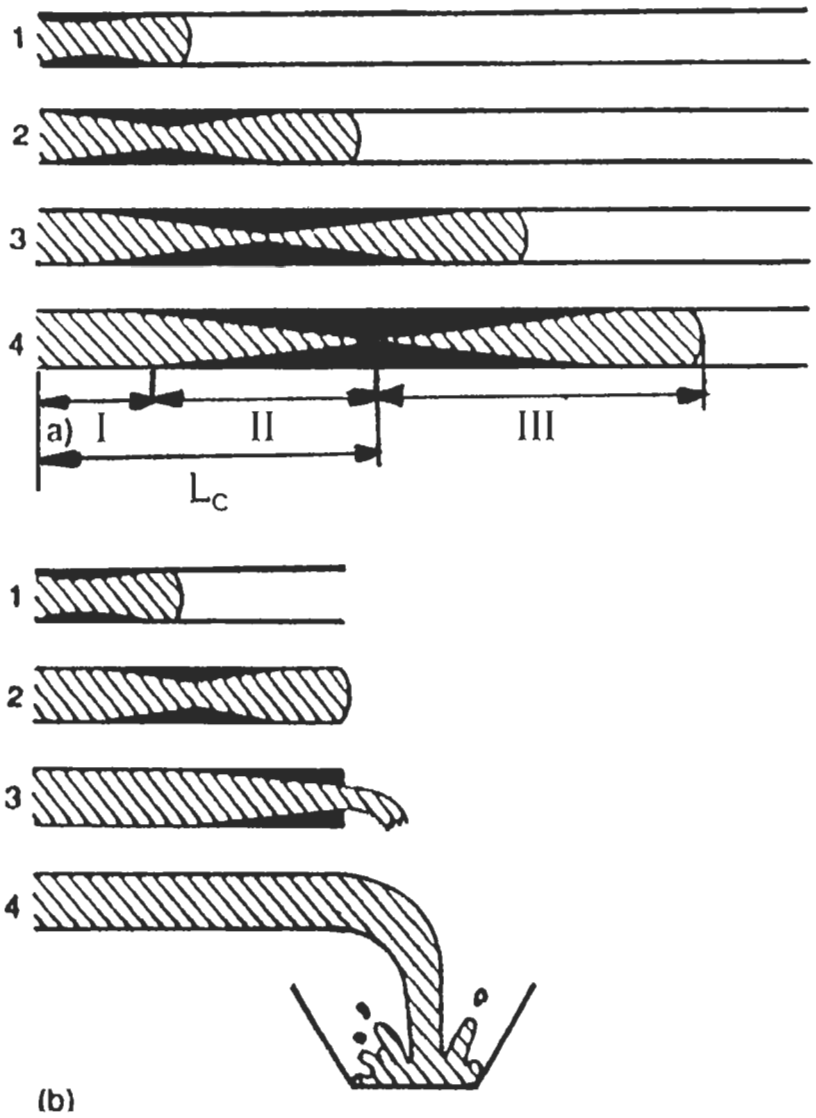

Fig. 64. The concepts of: (a) maximum fluidity length showing the stages of freezing leading to the arrest of flow in a long mould; and (b) the continuous flow which can occur if the length of the mould does not exceed a critical length, defined as the continuous-fluidity length. CAMPBELL [1991a]. In (a) has been included the schematic representation of the solidification considered by MORALES *et al.* [1977].

this century, replacing ingot casting and slabbing/blooming operations for the production of semi-finished shapes: slabs, blooms and billets. More recently even continuous production of single crystals for research and sophisticated technology has been

developed. Excellent reviews of the research and technology involved in this field have been presented by TAYLOR [1975], WEINBERG [1979a] [1979b] and BRIMACOMBE and SAMARASEKERA [1990] for steels and EMLEY [1976] and BAKER and SUBRAMIAN [1980] for aluminum and its alloys. Additionally PEHLKE [1988] and MINKOFF [1986] present comprehensive details of the process both in ferrous and nonferrous alloys together with technical details of the industrial installations currently used.

10.1.1. Continuous casting of steels

Figure 65 shows the main components of a continuous casting machine. Molten steel is delivered from a ladle to a reservoir above the continuous casting machine called a *tundish*. The flow of steel from the tundish into the water cooled mould is controlled by a stopper rod nozzle or a slide gate valve arrangement. To initiate a cast, a starter, or *dummy bar* is inserted into the mould and sealed so that the initial flow of steel is contained in the mould and a solid skin is formed. After the mould has been filled, the dummy bar is gradually withdrawn at the same rate that molten steel is added to the mould. Solidification of a shell begins immediately at the surface of the water cooled copper-mould. The length of the mould and the casting speed are such that the shell thickness is capable of withstanding the pressures of the molten metal after it leaves the mould. Usually a reciprocating motion is superimposed on the downward travel to prevent sticking.

Figure 66 shows schematically the role of fundamental knowledge in analyzing the process for the achievement of quality products (BRIMACOMBE and SAMARASEKERA [1990]). Determination of the *heat flow* is important because it allows the prediction of the shell profile, the pool depth and temperature distribution as a function of casting variables. In the mould heat transfer, the gas gap separating the mould and the strand casting and its relationship to mould heat flux is very important. MAHAPATRA *et al.* [1991a] [1991b] employed measured mould temperatures and mathematical modeling in order to predict formation of oscillations marks, longitudinal or corner depressions and subsurface cracks. Additionally, laboratory experiments and in-plant studies have been undertaken to determine the relationship between spray heat transfer coefficient and spray water flux. As, a result, mathematical models of spray systems have been developed.

The main aspects of solidification that must be understood in continuous casting are: i) the cast structure; ii) growth of the solid shell encasing the liquid pool and, iii) segregation. For the first concern, as with static casting, the structure consists of both columnar and equiaxed grains. The lower the pour temperature, the higher the fraction of equiaxed grains. The equiaxed structure is favoured in the medium carbon range, from about 0.17% to 0.38%C. Also induced fluid flow, for example by electromagnetic stirrers, enhance the growth of equiaxed grains. Shell growth is affected by all the variables that influence the mould heat flux distribution. When microsegregation is considered the models discussed in § 7 can be applied but the macrosegregation associated with the fluid flow during the solidification process is still not completely understood in continuous casting. However it is recognized that the same factors favoring an equiaxed structure diminish the macrosegregation.

Very recently BRIMACOMBE [1993] stressed the challenges of transferring knowledge

References: p. 830.

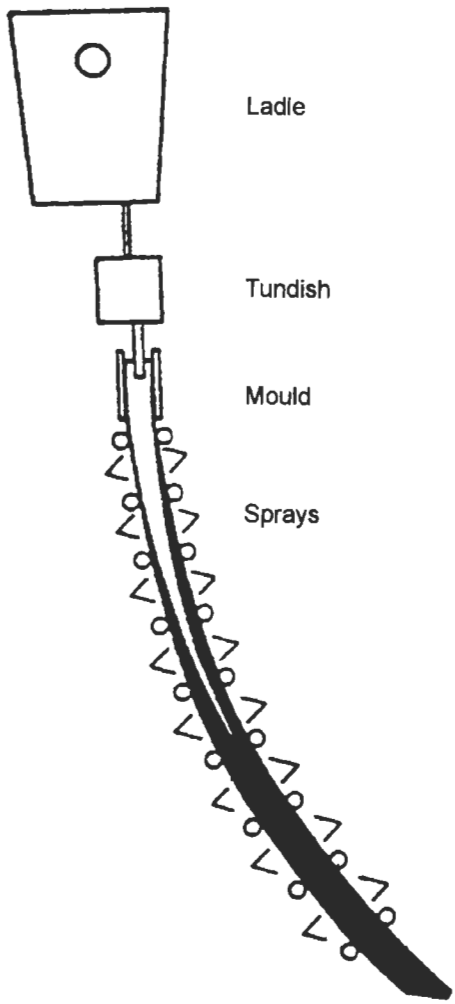

Fig. 65. Schematic diagram of continuous-casting machine. BRIMACOMBE and SAMARASEKERA [1990].

from R & D to the steel continuous casting industry. He suggests the development of *expert systems* in the form of an *intelligent billet casting mould*. This system effectively transfers knowledge on line to the shop floor through the combination of thermocouple and load cell information, signal data recognition based on years of research, mathematical models of heat flow in the solidifying shell and mould, understanding of the mechanism of quality problems, and the formulation of a response to a given set of casting conditions.

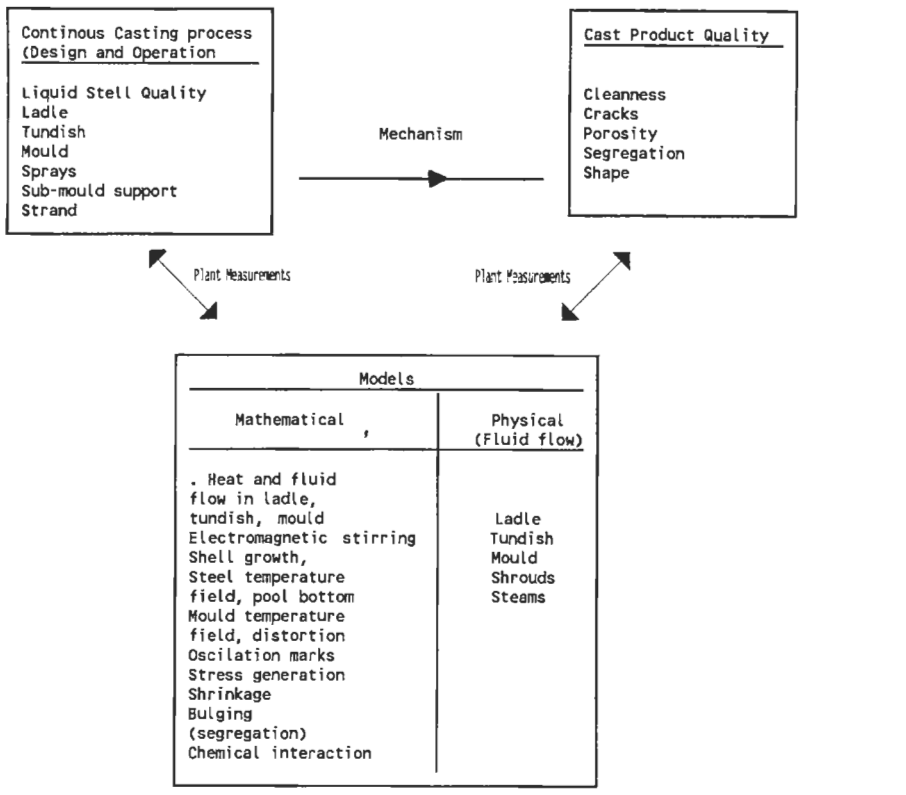

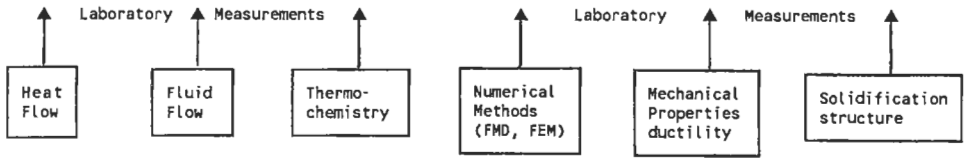

Fig. 66. Knowledge-based approach to analysis of continuous casting. After BRIMACOMBE and SAMARASEKERA [1990].

10.1.2. Continuous casting of light alloys

The principal casting process for light metals, such as Al, is the *direct chill process*. Figure 67 shows a schematic representation of the D.C. casting components for conventional open mould casting, the most common method used for blocks and billets

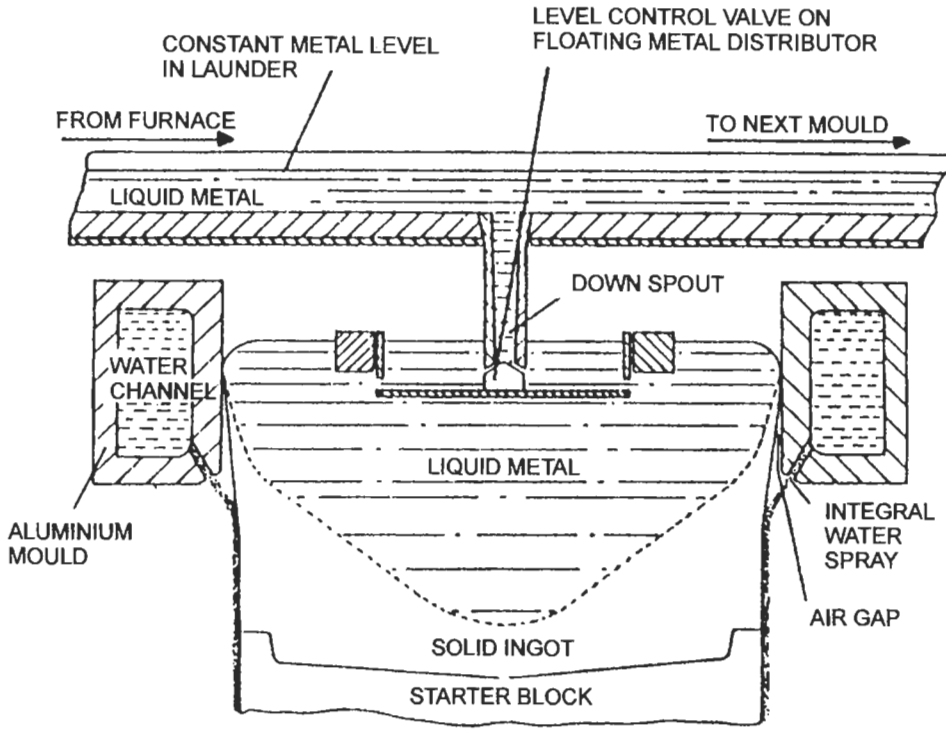

Fig. 67. Schematic diagram of vertical DC casting as commonly practiced. EMLEY [1976].

(BAKER and SUBRAMANIAN [1980]). There are three factors that influence the separation of the ingot shell from the mould: (i) shrinkage at the ingot shell itself; (ii) thermal strain within the ingot shell; (iii) shrinkage in the block section below the mould and the associated mechanical strains in the shell. All are influenced by the primary and secondary water cooling system and can affect the ingot structure, principally at the surface of the ingot. The air gap developed when the shell separates from the mould can give rise to defects of various types. When gap formation occurs there is increased resistance to heat transfer and, consequently, reheating of the skin. Reheating results in macrosegregation, exudation, runouts, retardation of the solidification in the subsurface zone, and variations in the cell/dendrite size of the outer surface of ingots. Zones of coarse dendritic substructure may extend 2–3 cm below the surface. Associated with the coarse cells are large particles of intermetallic constituents, formed by eutectic reactions, which may be exposed by surface machining that is usually performed before fabrication (BOWER *et al.* [1971]). Several methods have been proposed to reduce surface defects. The most succesful are those that reduce the heat extraction at the mould through the control of the microgeometry of the mould surface, for example by machining fine

grooves in the face of the mould. The molten aluminum does not fill the grooves due to surface tension.

More recently, *mouldless electromagnetic casting* has been developed to improve the metal surface quality. Electromagnetic casting was invented by GETSELEV [1971] and the principle behind this process is simple. Molten metal is supported slightly away from a mould by radial electromagnetic body forces concentrated within the upper part of the ingot. These forces are generated by a one-loop induction coil supplied with 5000 A at 2000 Hz (VIVES and RICOU [1985]).

SATO *et al.* [1989], [1991], [1992] studied extensively the production of Al, Al–Cu, and Al–Si rods with different cross-sectional geometries by a mouldless vertical continuous casting process. The main advantages consist of: (i) near net shape material having small and complex cross sectional configuration; (ii) full automation preventing break-out of molten metal and permitting easy start-up and easy shut down; (iii) cast material having unidirectional solidification structures; iv) geometries having changeable cross sectional configuration along their axes.

Elimination of the nucleation source for new crystals during solidification permits long single crystals to be continuously cast. Figure 68 shows the principle of the ingenious Ohno Continuous Casting process (OCC) (OHNO [1986]). The mould is heated to a temperature above the melting point of the metal to prevent the formation of new crystals on the surface of the mould. Cooling is arranged so is that the ingot maintains a small region of molten metal when leaving the mould, which solidifies immediately after leaving the outlet of the mould. If many crystals are nucleated at the end of the dummy, where the ingot begins to solidify, the combination of dendritic growth competition and macroscopic interface curvature eliminates all grains except one having a direction of preferential growth in close proximity to the casting direction. As a consequence a single crystal is formed. The process can also be used with a seed crystal of desired crystal orientation at the end of the dummy. Excellent results have been reported with Al, Pb, Sn, Cu and their alloys (OHNO [1986]). More recently KIM and KOU [1988] and WANG *et al.* [1988] studied the experimental variables of the OCC process and performed numerical modeling of heat and fluid flow. TADA and OHNO [1992] extended the OCC principles to the production of aluminum strips using an open horizontal, heated mould. The method was patented under the name, Ohno Strip Casting process (OSC).

As in most solidification processes, mathematical modelling of continuous casting of nonferrous alloys has also been undertaken. In the particular case of aluminum alloys, SHERCLIFF *et al.* [1994] present a comprehensive review.

10.2. Fusion welding structures

In most metallurgical processes the scientific approach to process improvement is to obtain relations between operational variables, metallurgical structures and properties. However, for many years in fusion welding technology, only relations between operational variables and mechanical properties were considered. In the last thirty years, the scientific approach has begun to be applied in cases where quality assurance is man-

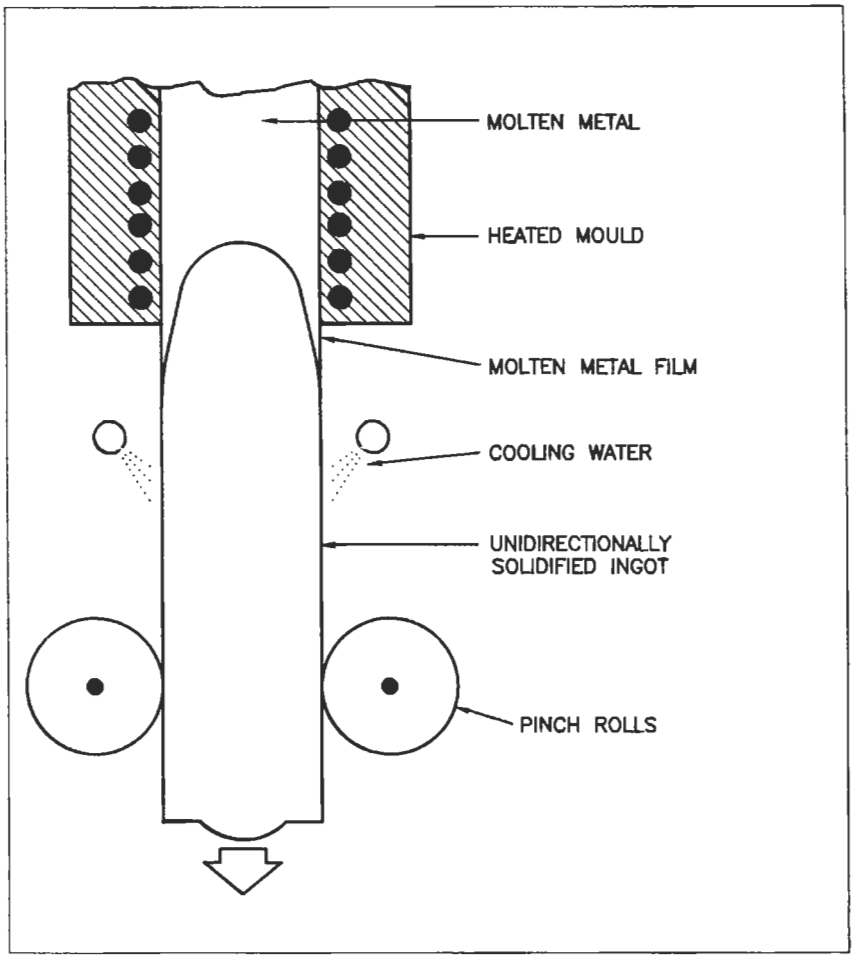

Fig. 68. The principle of the OCC process. After OHNO [1986].

datory for sophisticated technologies.

The fusion welding structure is a result of complex transformations and interactions starting with metal–gas and metal–flux reactions in the liquid state followed by the formation of the *primary structure* by solidification. Pioneering work by SAVAGE and co-workers at R.P.I. initiated the correlation between operational variables and primary structures (SAVAGE *et al.* [1965]). More recently, DAVIES and GARLAND [1975], EASTERLING [1984] and DAVID and VITEK [1989] have presented comprehensive reviews of the correlation between solidification parameters and weld microstructures.

Metallurgically, a fusion weld can be considered to consist of three major zones, namely the *fusion zone* (FZ), the *unmelted heat affected zone* (HAZ) and the *unaffected*

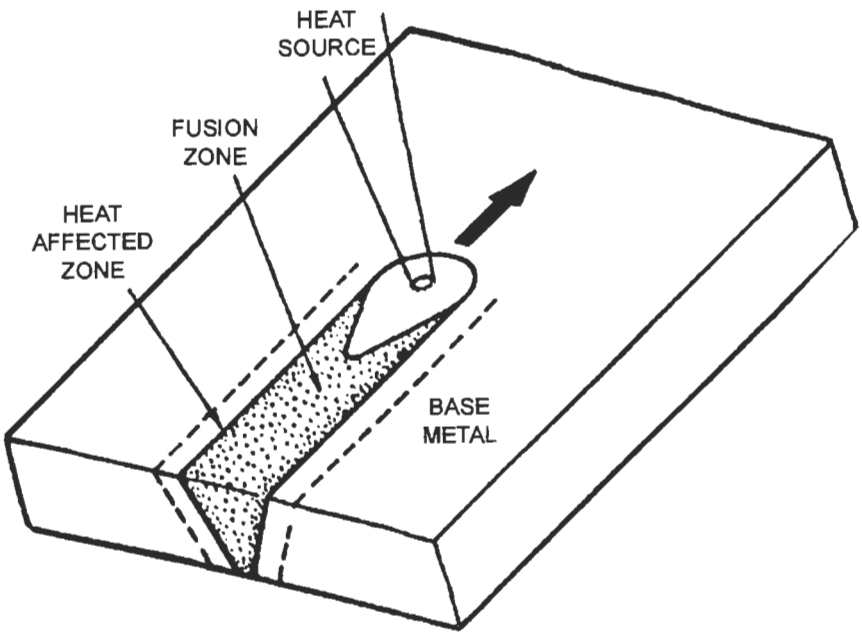

Fig. 69. Schematic diagram showing the three zones within a weldment. After DAVID and VITEK [1989].

base metal (BM), fig. 69. However careful metallographic analysis reveals the zones schematically shown in fig. 70 (SAVAGE and SZEKERES [1967]). The (FZ) can be divided into subzones: the *composite zone* (CZ) and the *unmixed zone* (UZ). In addition between

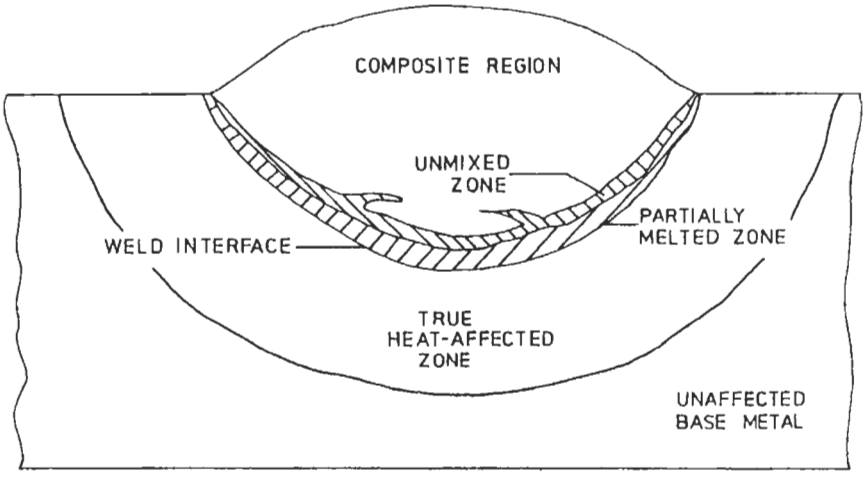

Fig. 70. Schematic representation of the different zones of a weld. After SAVAGE and SZEKERES [1967].

References: p. 830.

the (FZ) and the (HAZ), a *partially melted zone* (PMZ) exists.

The (UZ) appears in welds made with filler metal additions. It is a thin zone composed of base metal that is melted and resolidified without mixing with the filler metal during the passage of the weld puddle. This zone can be the location of initiation sites of microcracking as well as corrosion susceptibility in stainless steel. The PMZ is a region where the peak temperatures experienced by the weldment falls between the liquid and the solidus. As a consequence, only inclusions of low melting point as well as segregated zones can be melted. These areas resolidify and the contraction during the subsequent cooling can be a source of microcracks (BILONI [1983]).

In solidification processes, cooling rates range from 10^{-2}–10^{2} Ks^{-1} in casting technology to 10^{4}–10^{7} Ks^{-1} for rapid solidification technology. Cooling rates in welds may vary from 10–10^{3} Ks^{-1} for conventional processes, but when modern high energy beam processes such as electron beam (EB) and laser welding (LW) are considered cooling rates may vary from 10^{3} to 10^{6} Ks^{-1}. Furthermore the local conditions and cooling rates vary significantly within the weld pool. Therefore weld pool solidification incorporates aspects of both extremes of solidification, i.e. traditional casting as well as rapid solidification. Thus, most of the solidification concepts discussed previously may be applied to the understanding of the different weld microstructures. The most important subjects to be considered are: weld pool geometry and macro- and microstructures of the welds.

10.2.1. Weld pool geometry

Figure 69 schematically describes an autogeneous welding process in which a moving heat source interacts with the metal parts to be joined. The weld pool geometry is a function of the weld speed and the balance between the heat input and the cooling conditions. For arc welding processes the puddle shape changes from elliptical to tear drop shaped as the welding speed increases. For high energy processes such as EB or LW, the thermal gradients are steeper and as a result the puddles are circular at lower speeds becoming more elongated and elliptical in shape as the welding speeds increases. Eventually at high speeds they become tear drop shaped.

The heat transfer equation for a moving heat source was developed by ROSENTHAL [1941]. MINKOFF [1986] and KOU *et al.* [1981] reviewed this type of analytical model of heat transfer for welding. They consider only heat transfer by conduction neglecting the important convective heat transfer existing in the weld pool. In recent years much effort has been focussed on the dynamics of the heat and fluid flow in the weld puddle through experimental work and mathematical modeling. The goal is to reproduce actual weld pool shapes and eventually to develop the capability of predicting weld geometries (DAVID and VITEK [1989], [1992]), (DAVID *et al.* [1994]).

Convection is produced by: a) buoyancy effects; b) electromagnetic forces and, c) surface tension forces. The interactions among these three driving forces have been modeled by WANG and KOU [1987] showing the effects on the shape and weld penetration in G.T.A. (Gas Tungsten Arc) aluminum welds and by ZACHARIA *et al.* [1992] in G.T.A. welding of type 304 stainless steel. It is important to keep in mind that impurities in weld metal are often surface active and alter the surface tension of the liquid metal and its temperature dependence. For pure metals and high purity alloys the surface

tension decreases with increasing temperatures and the resultant flow is outward, away from the center of the weld pool. The result is a wide and shallow weld pool. When surface active elements exist, a positive temperature coefficient of the surface tension can occur in some cases and the resultant inward flow promotes a deeper and narrower weld pool. An example is the presence of small amounts of O and S (less than 150ppm) in stainless steel (HEIPLE *et al.* [1984]).

As already mentioned, computational models have been developed in order to predict the weld pool shape. Figure 71 shows calculated profiles superimposed on a macrograph of a cross section of an aluminum G.T.A. weld (ZACHARIA *et al.* [1988]). Although the correlation is reasonable, improvement of the model is necessary considering that the calculations underestimate the depth of penetration.

10.2.2. Macro- and microstructures of welds

A weld pool solidifies epitaxially from the parent grains in the (PMZ) surrounding it. As a consequence of competitive growth controlled by the orientation of the temperature gradients and the easy growth direction, favourably oriented grains survive. As in castings, a columnar region develops, favoured by the presence of a continuous heat source, which keeps thermal gradients high at the S–L interface. Figure 72 corresponds to an elliptical weld pool. The *local thermal gradient*, G_L and the *local solidification rate*, R_w changes from the fusion line to the weld center line. If crystal growth is considered isotropic (fig. 72a)

$$R_w = V_w \cos\theta_1. \tag{119}$$

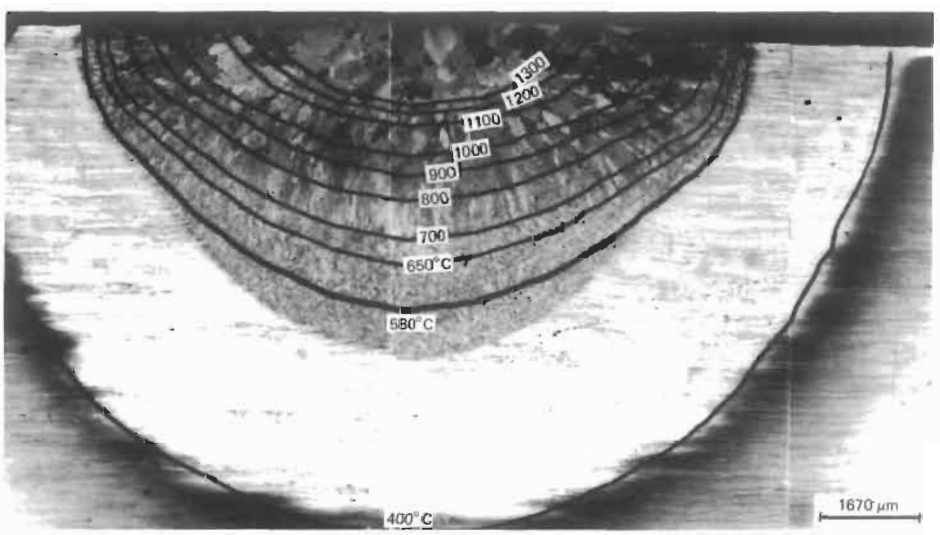

Fig. 71. Calculated temperature profiles superimposed on a macrograph of a cross-section of an aluminium alloy. DAVID and VITEK [1989].

References: p. 830.

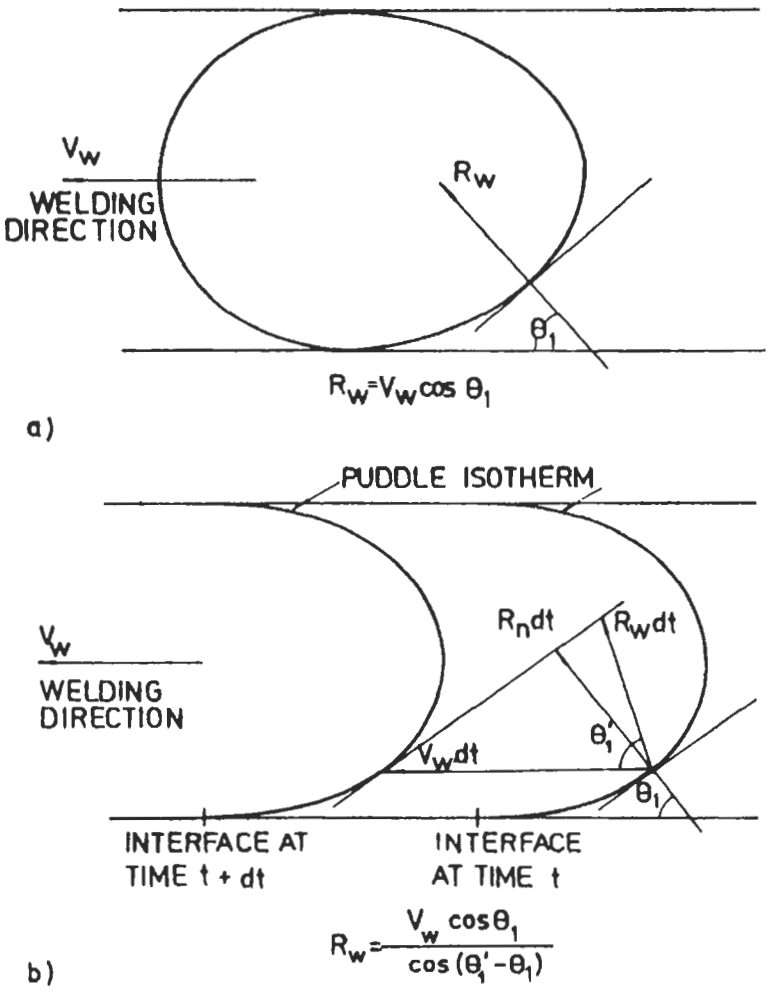

Fig. 72. (a) Solidification rates at different positions of the weld pool if isotropic growth is assumed. (b) Relationship between welding speed and actual growth rate if anisotropic growth is assumed. NAKAWAKA *et al.* [1970].

where V_w is the velocity in the welding direction. If crystal growth is anisotropic, R_w must be corrected according to the expression developed by NAKAGAWA *et al.* [1970],

$$R_w = \frac{R_n}{\cos(\theta_1' - \theta_1)} = \frac{V_w \cos\theta_1}{\cos(\theta_1' - \theta_1)}, \tag{120}$$

where R_n is the growth rate in a direction normal to the isotherm and θ_1' is the angle between the welding direction and the direction of favoured growth (fig. 72b). Thus in welding the solidification rate is greatest on the weld center line where $\theta_1 = 0°$. At this

point the temperature gradients are shallow because of the large distance from the welding heat source.

The liquid pool shape determines the columnar growth direction as well as the solidification rate and thermal gradient into the liquid. Columnar-grain substructures are determined by the S–L interface morphology. Thus, most of the concepts discussed in § 6 and § 7 for unidirectional solidification of alloys and in § 9 for columnar growth in conventional castings can be applied to columnar growth in welding: micro- and macrosegregation, banding, inclusions, porosity, etc. In addition, when situations involving rapid solidification arise, significant departures from local equilibrium at the S–L interface may occur (see § 5) and as a result metastable structures may be obtained. VITEK and DAVID [1992] reported recent research showing that in LW or EB welding, metastable microstructures can be produced in stainless steel welds. Laser surface melting and alloying will be treated in § 11. Regarding the classification of welding macrostructures, PEREZ *et al.* [1981], BILONI [1983] shown schematically nine types of macrostructures obtained with different fusion welding processes. All of them show a columnar zone which may occupy the entire weld, or be accompanied by grains growing along the welding direction, by feathery crystals (see § 9), by equiaxed grains or by mixed coarse and fine grains, the last being characteristic of electroslag welding (PATON [1959]). Recently RAPPAZ *et al.* [1989] and DAVID *et al.* [1990] examined the effect of growth crystallography and dendrite selection on the development of the FZ microstructures. Using single crystals and geometrical analysis that provides a three dimensional relationship between travel speed, solidification velocity and dendrite growth velocity, they were able to reconstruct a three dimensional diagram of a weld pool. The presence of equiaxed grains near the center of welds is believed to be beneficial in preventing solidification cracking and in maintaining good ductility in alloys subjected to brittle fracture. KERR and VILLAFUERTE [1992] reviewed the mechanisms and conditions which give equiaxed grains in castings (see § 9) and compared them to the situation in welds.

11. Structure manipulation and new processes

The concepts discussed in previous sections are the basis used by metallurgists to manipulate microstructure and thus obtain better physical and mechanical properties. However, the manipulation of structure is closely related to the continued development of processing methods. In this section we describe a few examples: single crystal growth from the melt, grain refinement, eutectic modification, rapid solidification, microgravity processing, metal matrix composite fabrication, and semi-solid metal forming.

11.1. Single crystal growth from the melt

Single crystal growth is useful to study the laws governing solidification of metals and alloys, to prepare samples for scientific studies, especially mechanical properties, and for technological devices such as those used in the electronics industries or the production of gas turbine blades. Thus, we consider single crystal production an important example of structure manipulation.

References: p. 830.

CHALMERS [1964] and THORTON [1968] present reviews of the different methods available for single crystal preparation. In general, the same methods can be used for the growth of *bicrystals* if grain boundaries are to be studied. Four main methods and their variations are employed. (i) In the *Bridgman method* the mould containing the melt is lowered through the furnace and the solidification begins either at the lowest point of the mould or on a seed located in the bottom of the mould. (ii) The *Chalmers method* is a variation of the above using a horizontal boat. An advantage of these methods is the fact that the remaining liquid can be decanted by electromagnetic devices. However with horizontal growth, problems arise due to excessive convection during growth (see § 6). (iii) The *Czochralski or pulling method* consists of a melt contained in a crucible and a seed crystal that is lowered into it from above and then slowly rotated and withdrawn. The purpose of the rotation is to maintain axial symmetry of the crystal and decrease the solute enriched layer at the S–L interface. HURLE [1987] discussed the evolution of the method, mathematical modeling, and the advantages and future potential of this technique. (iv) The *floating zone method* employs zone melting principles (PFANN [1966]) and, uses no mould. Essentially, the molten zone is held in place by surface tension forces, sometimes aided by magnetic fields.

In § 6 the importance of maintaining a flat interface has been discussed in detail as well as the relationship between different types of convection and stable interfaces. PIMPUTKAR and OSTRACH [1981] present a comprehensive review of convective effects in crystals grown from the melt, especially when Czochralski and Bridgman methods are considered.

The directional freezing technique has been applied extensively to turbine blade manufacture. The techniques are employed in preparing aligned eutectic structures, directional columnar structures, and single crystal turbine blades. Unlike single crystals grown for electronic applications, single crystal turbine blades solidify with a dendritic structure. Therefore even though the crystallographic orientation of all the dendrites is the same, the turbine blades contain microsegregation and occasionally second phase particles formed by eutectic reactions. PIWONKA [1988] reviewed the different methods used. In the case of single crystal turbine blades, the alloys have no grain boundaries and thus need no grain boundary strengtheners. Elimination of these elements permits solution heat treatment at higher temperatures. Consequently, new high temperature Ni base alloys have been developed having better high temperature properties because they contain a higher percentage of the γ' strengthening phase. In addition, because no grain boundaries exist, monocrystal turbine blades have better corrosion resistance.

11.2. Grain refinement

Various techniques may be used to produce fine grained structures during solidification: thermal methods, innoculation and energy induced methods (BOLLING [1971]). Each of these operates principally through one mechanism: nucleation or multiplication.

11.2.1. Thermal methods

From a thermal point of view we are concerned principally with two possibilities, rapid chilling and bulk supercooling.

(i) ***Chill effect***: when molten metals contact the cold walls of a mould, the melt superheat is removed from the liquid and it becomes locally supercooled. The number of nucleation centres increase and nucleation takes place catastrophically in the liquid. Techniques such as splat cooling (see below) and die casting, as well as applications using chills employ this approach with varying efficiencies according to the sample size. The reader is referred to § 9 regarding the influence of wall microgeometry on the grain size in the chill zone of ingots and castings as well as the columnar zone grain size.

(ii) ***Supercooling methods***: WALKER [1959] published the first observations of grain refinement phenomena due to bulk supercooling. Samples of about 500 g were cooled under a glass slag and/or inert gas atmosphere and were contained in a fused silica crucible to reduce the probability of heterogeneous nucleation on the crucible walls, and, thus, aid the achievement of large supercooling of the melt. With this method Ni samples doped with Ag (to preserve the grain structure) were supercooled in the range from 30 to 285K. From 30 to about 145K of supercooling the grain size decreased monotonically but at this *critical supercooling* (ΔT^*), a sharp decrease in grain diameter from about 20mm to 2mm arose. WALKER [1964] found a similar grain size transition in Co but at $\Delta T^* = 180K$. WALKER measured the pressure pulse associated with the solidification of Ni and found that it showed a maximum in the vicinity of ΔT^*. He suggested that the grain refinement was brought about by homogeneous nucleation in the liquid ahead of the S–L interface due to a transient local elevation in melting temperature caused by the pressure pulse. Subsequently, many researchers tried to understand the grain refinement mechanism associated with high supercooling. Other containerless processes, such as electromagnetic levitation and drop tubes have been used (HERLACH *et al.* [1993]). These authors have analyzed most of the previous results and the proposed mechanisms as well as the effect of minor amount of impurities on the grain refined structure, which can be columnar and/or equiaxed. The large number of proposed mechanisms fall into three broad categories having much overlap: (i) multiple nucleation in the melt arising from a mechanical disturbance of some kind, generally associated with a pressure pulse generated by the solidification itself. (WALKER [1959]; COLLIGAN *et al.* [1961]; GLICKSMAN [1965]; HORVAY [1965], POWELL [1965]). (ii) Dendrite fragmentation arising in a number of possible ways including remelting and mechanical fracture (KATTAMIS and FLEMINGS [1966]; JONES and WESTON [1970a]; MCLEOD [1971]; TARSHIS *et al.* [1971]; SOUTHIN and WESTON [1973], [1974]; KATTAMIS [1976], MCLEOD and HOGAN [1978]; KOBAYASHI and HOGAN[1978]; KOBAYASHI and SHINGU [1988]; DEVAU and TURNBULL [1987]). (iii) Recrystallization of the solidified structure (POWELL and HOGAN [1968], [1969]; JONES and WESTON [1970a], [1970b]).

The study of the segregation substructure of the grains obtained at different supercooling seems to support the fragmentation mechanism. KATTAMIS and FLEMINGS [1966], [1967] and KATTAMIS [1976] observed a gradual change in dendrite morphology from a normal branched form to a more cylindrical form with decreasing side branching as the supercooling increased. At ΔT^*, the transition from coarse columnar grains to fine equiaxed grains was accompanied by a change in the solute segregation pattern from dendritic to spherical. Each of these spherical patterns corresponded to a refined grain. The evolution of the spherical morphology is assumed to occur in two steps: detachment

References: p. 830.

of the secondary dendrite arms and subsequent coarsening into spherical elements during recalescence. Regarding the short time available for the remelting/coarsening mechanism during recalescence, COCHRANE *et al.* [1991] have shown that in drop tube processed Cu–30%Ni and Fe–35%Ni alloys, local solidification times as short as 200 μs cannot retain the dendrite structure formed during the rapid growth phase. In addition, WILLNECKER *et al.* [1989], [1990] measured dendrite growth velocities and grain refinement in Cu–30%Ni and Cu–30%Ni–1%B as a function of supercooling. The addition of 1at % B shifted ΔT^* from 193 to 255 K. The grain refinement transition occurred in both cases at the same supercooling that a sharp change in V–ΔT behavior occurred (fig. 73). These results open the possibility of a link between grain refinement with the onset of complete solute trapping during the rapid growth phase (see § 5). As HERLACH *et al.* [1993] pointed out, there are many issues to be resolved in determining the mechanism responsible for grain refinement in highly supercooled melts and containerless processing. SCHWARZ *et al.* [1994] have presented a simple model of dendrite fragmentation by a Rayleigh instability that appears to predict the correct value for ΔT^* for Cu–Ni alloys.

A variant of the supercooling method uses so-called *denucleation*, a concept introduced by MARCANTONIO and MONDOLFO [1974], working with aluminum alloys. If the nucleants that act at low supercooling can be removed (by centrifuging during freezing, among other methods) a denucleated melt can be supercooled well below its freezing point where it can be made to freeze rapidly on a chosen nucleant. These authors were able to reduce considerably the grain size of commercial purity Aluminum and Al–Mn alloys by this method. Also in Al–Mn alloys the method permits the retention of a higher percentage of Mn in solid solution.

11.2.2. Innoculation methods

One of the most important examples of structure modification in industry is the grain refinement of Al and its alloys using innoculants that increase heterogeneous nucleation (See § 4). A fine grain size in shaped castings ensures the following: (i) mechanical properties that are uniform throughout the material, (ii) distribution of second phases and microporosity on a fine scale, (iii) improved machinability because of (ii), (iv) improved ability to achieve a uniformly anodizable surface, (v) better strength, toughness, and fatigue life, and (vi) better corrosion resistance.

The grain refining inoculants used in the aluminum industry employ so-called "master alloys" containing Al with Ti, B and C. Several mechanisms have been proposed for grain refinement and critical reviews exist in the literature (GLASSON and EMLEY [1968], ROSS and MONDOLFO [1980], PEREPEZKO and LEBEAU [1982], PEREPEZKO [1988], MCCARTNEY [1989]). It is agreed that when master alloys are added to aluminum alloy melts, the aluminum mattrix dissolves and releases intermetallics into the melt, probably Al_3Ti and various borides and carbides. Some compounds appear to act as effective nucleants with disregistry values below 10% and nucleation supercooling of less than about 5°C. In the past, the identities of the active nucleants have typically been studied from thermal and structural results obtained from standard bulk refinement tests. However more recently HOFFMEYER and PEREPEZKO [1989a], [1989b], [1991] utilized the Droplet Emulsion Technique (DET) (see § 4) to produce a fine dispersion of master alloys powders containing innoculant particles. In this way the response of Al to specific

effective and ineffective nucleants can be separated and identified through highly sensitive DTA and metallographic analysis. On the other hand, very recently JOHNSSON

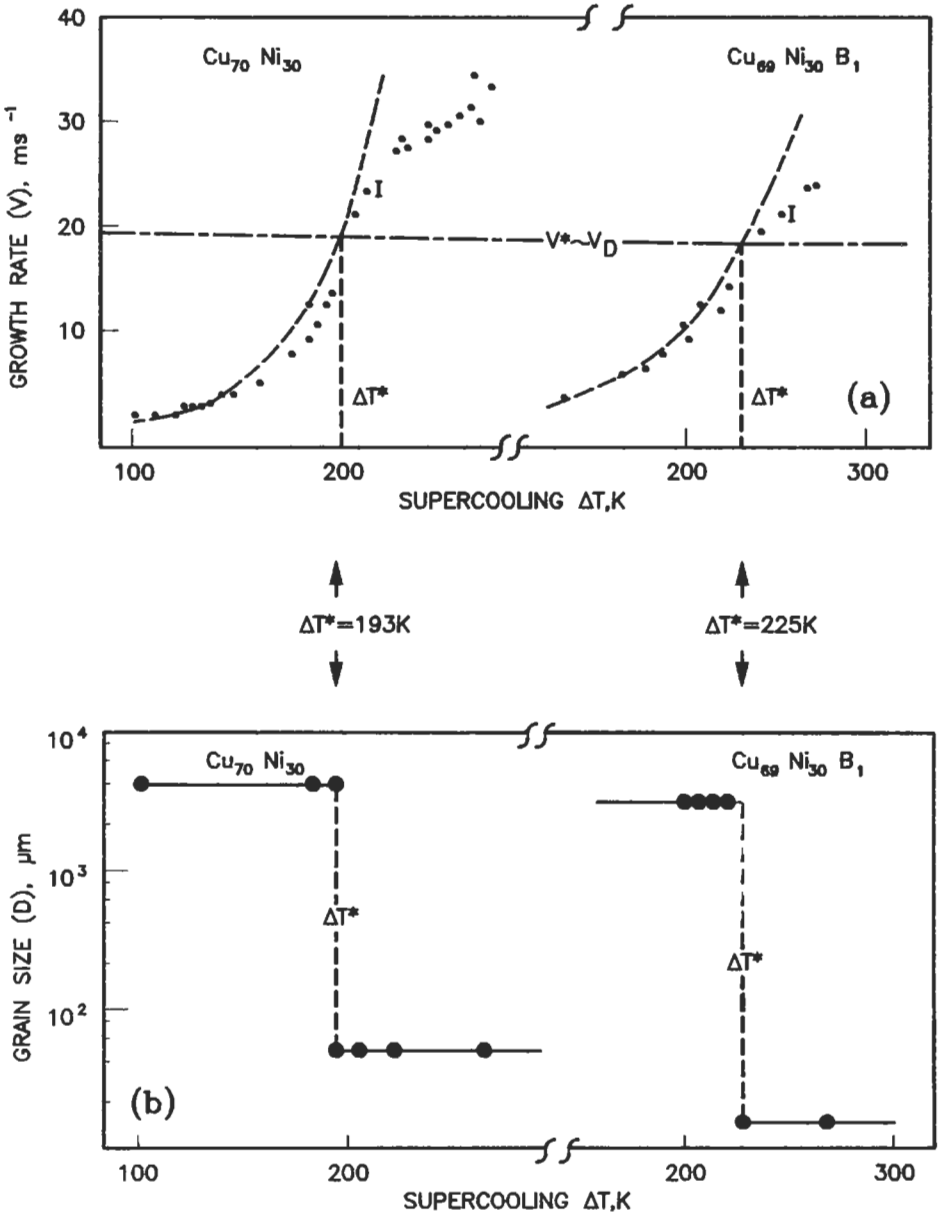

Fig. 73. Dendrite growth velocity and grain diameter as function of supercooling for $Cu_{70}Ni_{30}$ and $Cu_{69}Ni_{30}B_1$. WILLNECKER *et al.* [1990]. See HERLACH *et al.* [1993].

et al. [1993] used highly sensitive thermal analysis in bulk experiments to study the mechanisms of grain refinement in high purity Al by master alloys. The use of high purity material and a computer automated thermal analysis technique, permitted them to isolate the effect of the Ti and B containing particles. Both types of work are complementary and promise to elucidate the quite complicated refinement mechanisms.

Despite the uncertainty about the details of nucleation mechanisms, improvements have been made in theory in order to predict the final grain size as a function of the dispersion and density of nucleant particles. MAXWELL and HELLAWELL [1975] and HELLAWELL [1979] treat the ability of a substrate to act as a surface for heterogeneous nucleation simply using the *wetting angle*, θ, without entering into the details of the nucleation mechanism. A comparison is made between the final grain density and the initial nucleant density for various freezing conditions. As the melt cools below the liquidus, two processes take place concurrently. Solid nucleates on the available substrate surfaces at a rate which rises exponentially with the supercooling and, when the temperature has fallen below a certain limit, nucleated particles start to grow and evolve latent heat. The local cooling rate decreases as nucleation and growth accelerate until the temperature reaches a minimum and recalescence begins. The nucleation rate rises rapidly to a maximum at a temperature just before the minimum in the cooling curve. Afterwards the number of nucleation events decreases quickly as the available particles are exhausted and particularly because recalescence begins. Consequently, nucleation is almost complete just beyond the minimum temperature in the cooling curve. Subsequently, there is only growth. The number of grains varies according to the nucleation rate and is determined by the time recalescence begins.

The minimum temperature reached and the recalescence rate are strongly influenced by the growth rate from each nucleation center. MAXWELL and HELLAWELL [1975], and HELLAWELL [1979] employ a purely solute diffusion model for growth of spheres. More recently the *deterministic* model of RAPPAZ [1989] employs a more realistic dendritic growth model to predict final grain size for different inputs of nucleation and cooling conditions. An important effect is how grain size is decreased, for fixed nucleation and cooling conditions, by increasing the level of solute in the alloy. This occurs because of the reduction of the dendritic growth rate with increasing composition as described in § 7. The important effects of convection are not included in these models.

11.2.3. Energy-induced methods

A large number of methods have been employed to refine the grain structure through energy-induced methods that increase nucleation through cavitation or that promote crystal multiplication, principally through mechanical vibration, bubbling agitation, rotating magnetic fields, magnetic–electric interactions and mould oscillation. COLE and BOLLING [1969] and CAMPBELL [1981] present comprehensive reviews in the field. Although cavitation may be responsible for grain refinement under some experimental conditions, today it is generally accepted that the best, and cheapest method of grain refinement using energy-induced methods is to *promote crystal multiplication during the solidification process.* The multiplication occurs primarily by fragmentation of the

incipient dendritic structure by forced convection. FLEMINGS [1991] gives a summary of the possible dendrite fragmentation mechanism existing in the literature.

11.3. Eutectic modification

Among the most important foundry alloys are those based on the Fe–C and Al–Si systems. The mechanical properties of these metal–nonmetal (nonfacetted–facetted) eutectics are dominated by the morphologies in which the non-metals solidify. As nonfacetted–facetted eutectics, the asymmetry of the couple zone must always be considered in the interpretation of microstructure regarding the presence or absence of primary phases as described in § 8.1.5. In both systems the structure can be *modified* either by rapid cooling or by controlled addition of specific elements. The use of elemental additions has an advantage because their effect is essentially independent of the casting section thickness. Thus we shall only discuss modification by additives. The modification of the structure of these alloys and the resultant effect on the mechanical properties is a clear example of the manipulation of the structure based on the application of fundamental principles.

11.3.1. Aluminum–silicon alloys

Many studies have been focussed on the mechanism of modification in Al–Si alloy and several reviews are available (CHADWICK [1963]; SMITH [1968]; HELLAWELL [1970]; GRANGER and ELLIOTT ([1988]). Most important is the change of the morphology of the silicon phase in the eutectic mixture. In unmodified alloys, the Si phase in the eutectic appears as coarse flakes that grow more or less independently of the Al phase. With small additions of alkaline or alkaline earth metals (especially Na and Sr), the Si phase takes on a somewhat finer branched fibrous form that grows at a common liquid–solid interface with the Al phase to form a composite-like structure with improved properties. The easy branching of the modified Si leads to a more regular and finer structure as described in § 8.1.3. Modifiers also change the morphology of primary Si in hypereutectic alloys. Although nucleation studies have been performed (CROSSLEY and MONDOLFO [1966]; ROSS and MONDOLFO [1980]), the modifying effects of Na and Sr are now thought to be growth related (HANNA *et al.* [1984]). Nucleation remains important however, through the addition of Al–Ti–B master alloys to control the Al grain size in hypoeutectic alloys (§ 11.2.2) and through the addition of P (usually Cu–P) to promote heterogeneous nucleation (on AlP) and refinement of primary Si in hypereutectic alloys.

During the growth of unmodified Al–Si eutectic, the Si flakes contains widely spaced {111} twins that provide for easy growth in the [111] direction and difficult growth normal to [111]. This is called twin plane re-entrant edge (TPRE) growth. In modified alloys the Si fibres contain a much higher density of twins that exhibit an internal zig-zag pattern (LU and HELLAWELL [1987], [1988]). Since both Na and Sr are concentrated in the Si phase, these authors proposed a mechanism whereby the modifying elements are adsorbed on the growth ledges spewing out from the re-entrant corner. These adsorbed atoms cause the formation of new twins due to stacking errors on the growing interface due to size mismatch of the Si and the modifier. A hard sphere model for atomic packing

was used to define a critical ratio (1.65) of modifier to Si atomic size that promotes twinning. The growth of the Si is then thought to occur by repeated twin formation in a more isotropic manner than by TPRE governed growth. This more isotropic growth permits the Si fibers to branch and adjust eutectic spacing. The formation of the internal zig-zag twin structure is also consistent with the observation of microfaceting on the Al–Si interface (LU and HELLAWELL [1987]).

MAJOR and RUTTER [1989] proposed that a certain concentration of Sr is required at the interface to achieve modification (CLAPHAM and SMITH [1988]). Below a critical concentration, growth of the Si is by the twin plane re-entrant edge (TPRE) mechanism typical of unmodified eutectic. If growth occurs for a sufficient distance to accumulate Sr concentration at the solid–liquid interface above a critical level, the re-entrant edges are poisoned. Then, new twins form as described above. A continuous cycle of twin formation, TPRE growth, poisoning, new twin formation and so on can occur. More recently QIYANG *et al.* [1991] confirmed the adsorption of Na on $\{111\}_{Si}$ in agreement with the poisoning of the twin re-entrant edges. The phenomenon of overmodification can be explained as complete suppression of the TPRE mechanism resulting from elevated quantities of the modifying addition. In this way, formation of Al bands in overmodified structures (FREDRIKSSON *et al.* [1973]) may be explained.

11.3.2. Cast iron

It is known that cast iron, belonging to the family of high carbon Fe alloys, can solidify according to either the stable iron-graphite system (grey iron) or to the metastable Fe–Fe_3C system (white iron). As a consequence, the eutectic may be austenite–graphite or austenite–cementite (ledeburite). Furthermore, the complex chemical composition of the material has important and powerful effects on the structure of cast iron. Commercial alloys usually contain Si, minor addition of S, Mn and P and usually trace elements such as Al, Sn, Sb and Bi as well as the gaseous elements H, N and O. Both forms of cast irons (white and grey) have technological importance. Several comprehensive reviews and books have been published in the last decades both from fundamental and technological points of view (MORROG [1968a], [1968b]; MINKOFF [1983]; ELLIOT [1988]; STEFANESCU [1988]; CRAIG *et al.* [1988]; HUGHES [1988]; STEFANESCU *et al.* [1988]). Grey iron is the most interesting because of the different morphologies that the graphite can achieve and the resulting differences in mechanical and physical properties. Although semantic problems have confused scientists and foundrymen in the past, a general understanding of the mechanisms of nucleation, growth and modification of the graphite phase has occurred in the last 15 years. In this section, the present status of knowledge in the area will be discussed briefly.

It is known that the growth of the stable Fe–G eutectic is favoured over the metastable Fe_3C eutectic by slow freezing (See § 8.1.7.) or by addition of elements such as Si and Al. These elements increase the temperature difference between the stable Fe–G and metastable Fe–Fe_3C eutectic temperatures. In addition a wide variety of compounds have been claimed to serve as nuclei for graphite, including oxides, silicates, sulphides, nitrides, carbides and intermetallic compounds. Most of the nucleation mechanisms are connected with impurities existing in the melt or with inoculants that promote heterogen-

eous nucleation of the graphite. Although other inoculants are used, Fe–Si alloys are the most powerful and popular (ELLIOT [1988], STEFANESCU [1988]), SKALAND *et al.* [1993]).

11.3.3. Cast iron eutectic morphology

The morphology and characteristic of the eutectic, whether stable or metastable, with or without modification, are very important in determining the physical and thermal properties. Thus, it is worthwhile to consider the most important eutectic structures observed. The microstructure of these major forms are shown for example by STEFANESCU [1988].

White Irons: The metastable unalloyed Fe–Fe_3C ledeburite eutectic is classified as quasi-regular. HILLERT and SUBBARAO [1968] described the mode of growth of the eutectic as well as the orientations arising between Fe_3C and austenite(γ). POWELL [1980] has shown that the eutectic structure can be modified by quenching. By adding Cr or Mg, a plate-like Fe_3C structure associated with equiaxed grains can be achieved (STEFANESCU [1988]).

Grey Irons: For high purity Fe–C–Si alloys, the structure of the Fe–G eutectic is *spheroidal* (SADOCHA and GRUZLESKY [1975]). However in practice the presence of impurities in the melt cause the graphite to take a flake morphology and grey flake iron is considered to be the *characteristic* form from a practical point of view. Modification of this structure gives different graphite morphologies: *nodular*, *compact* or *vermicular*, and *coral*. We shall be concerned only with the growth of eutectic structures without a primary phase and we will refer mainly to the three structures widely used in industry: flake, compact or vermicular, and nodular or spheroidal cast iron.

At present there exists a theory for the mechanisms of the evolution from flake to compact and nodular graphite (MINKOFF [1990]): (i) fig. 74 corresponds to cooling curves for the three types of structure (BACKERUD *et al.* [1975]). The major characteristics of these cooling curves is the increase of supercooling on going through flake, compact and spheroidal graphite forms. The rate of recalescence after nucleation is determined by the nucleation rate and the growth rate. (ii) *Grey flake irons*: the growth of the flake structure is well understood. Once graphite has nucleated, the eutectic cell or colony grows in an approximately radial manner and each flake is in contact with austenite up to the growing edge. The crystals of graphite grow in the close packed strong bonding "a" direction using steps created by rotation boundaries. These rotation boundaries are defects in the crystals in the form of rotations of the lattice around the <0001> axis. According to MINKOFF [1990], the screw dislocations on $\{10\bar{1}0\}$ planes, which have been proposed as an alternative growth mechanism, are inactive (fig. 75a).

ELLIOTT [1988], STEFANESCU [1988] and SKALAND *et al.* [1993] discuss the effect of S and O as promoters of the flake graphite morphology on the basis of their adsorption on the high-energy $(10\bar{1}0)$ plane. Thus, growth becomes predominant in the "a" direction. The result is a *plate like* or *flake* graphite. (iii) *Nodular or Spheroidal Irons*. This is considered a divorced eutectic. Until recently has been widely accepted that the growth of this eutectic begins with nucleation and growth of graphite in the liquid, followed by early encapsulation of these graphite speroids in austenite shells. The result is eutectic grains (often named "eutectic cells") presenting a single nodule (WETTERFALL *et al.*

References: p. 830.

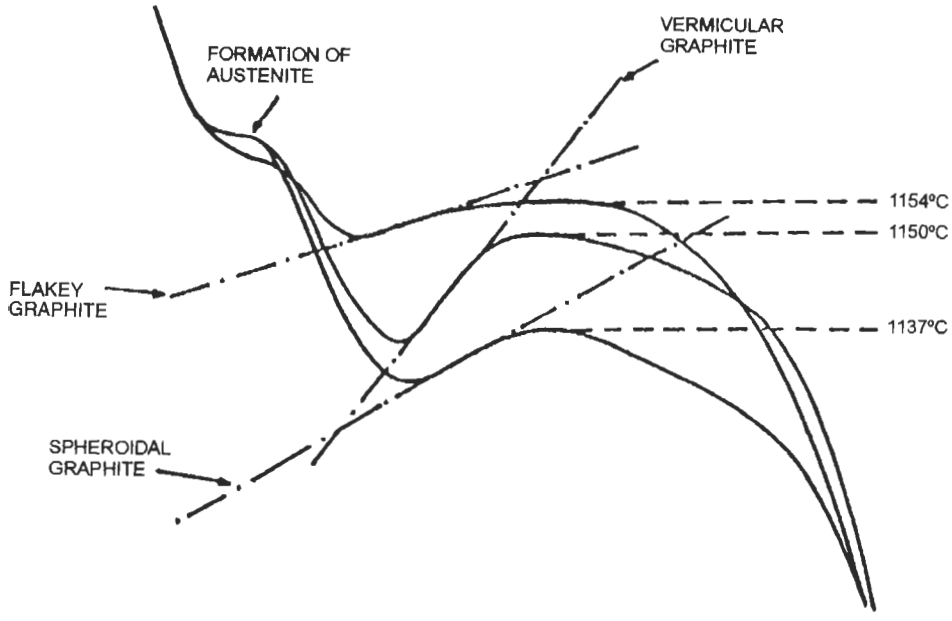

Fig. 74. Cooling curves for laminar, vermicular and nodular cast irons. BACKERUD *et al.* [1975].

[1972]). Thus, it is common practice in the foundry industry to associate the number of nodules to the number of eutectic grains. However recent research by SIKORA *et al.* [1990]) and BANERJEE and STEFANESCU [1991] indicated the existence of simultaneous nucleation of both the dendritic austenite and the spheroidal graphite. The interaction between both phases during solidification gives rise to the formation of eutectic grains presenting several nodules. This is a fact to be taken into account when micromodelling of the structure is attempted. Regarding the spheroidal growth of the graphite, several theories exist in the literature and they have been reviewed by MINKOFF [1983], ELLIOT [1988] and STEFANESCU [1988]. MINKOFF [1990] considers that the relationship among supercooling, melt chemistry and crystalline defects determine the spheroidal growth of the graphite. In this case the screw dislocation mechanism is considered dominant in causing repeated instability of the pyramidal surfaces, so that a radial array of pyramids is formed (fig. 75b). (iv) *Compact or Vermicular Graphite Irons*: This intermediate graphite morphology has been studied extensively due to its technological importance (RIPOSAN *et al.* [1985]). The graphite is interconnected within the eutectic cell but its growth differs from flake graphite. As in the case of spherulitic growth, several theories exist (STEFANESCU [1988], ELLIOT [1988]). The influence of the melt chemistry is very important. The occurence of compact graphite form requires a balance between flake-promoting elements, such as S and O, spheroidizing elements such as Mg, Ce and La, and antispheroidizing elements such as Ti and Al (SUBRAMANIAN *et al.* [1985]).

MINKOFF [1990], in his general approach to the interdependence of supercooling,

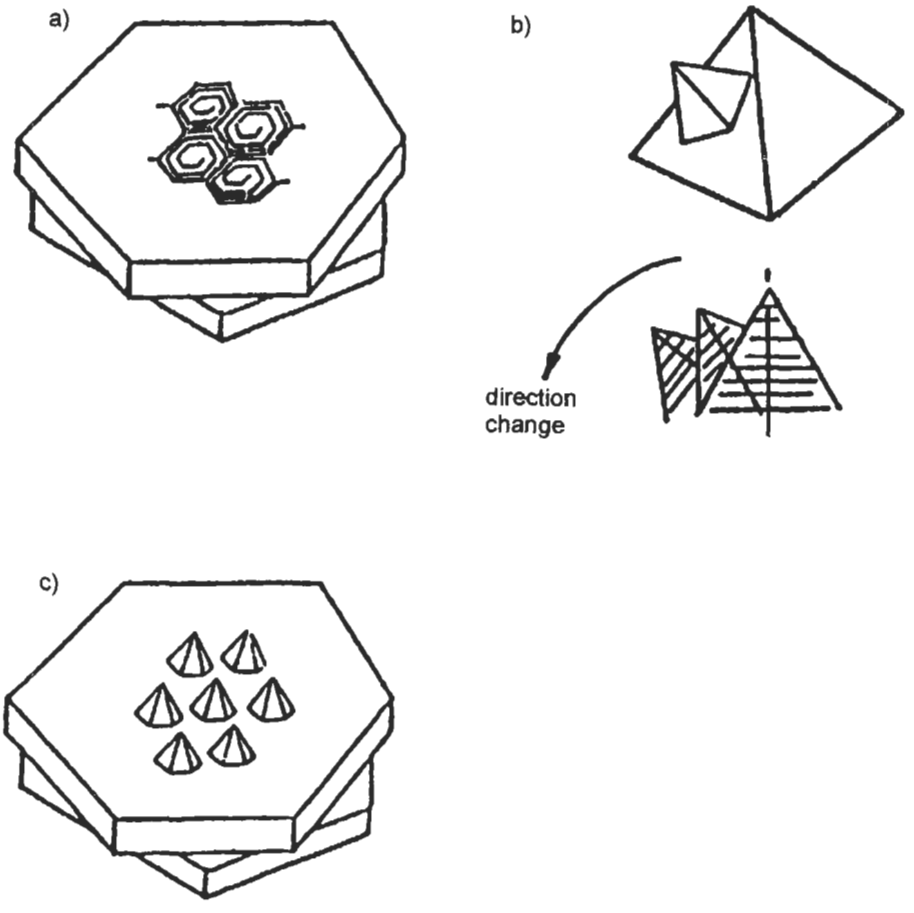

Fig. 75. (a) Mechanism of growth of flake graphite from a rotation boundary which provides steps for the nucleation of (1010) faces. (b) Mechanim of growth of spheroidal graphite by repeated instability of pyramidal surfaces forming a radial array. (c) Mechanism of growth of compacted graphite by development of pyramidal forms on the crystal surface at steps due to screw dislocations. MINKOFF [1990].

chemical composition and crystalline defects, considered that compact or vermicular graphite forms are intermediate between flake and spherulitic formation, and that the rounded morphology of the structure is a result of the thickening of graphite crystals at small values of supercooling by growth from the steps of screw dislocations, which have Burgers vector in the <0001> direction (fig. 75c). We consider that the mechanisms of graphite growth as well as modification by proper chemical agents is an open research field. Recent unidirectional solidification of flake and compact graphite irons with and without "in situ" modification in front of the S–L interface open questions about the forms of crystalline growth of the graphite phase, as well as the influence of the impurities and chemical agents on the surface tension of the Fe–G eutectic phases (ROVIGLIONE and HERMIDA [1994], ROVIGLIONE and BILONI [1994]).

References: p. 830.

11.4. Influence of rapid solidification processes (RSP)

Most of the fundamentals of RSP have been included in § 2–8 and grain refinement due to high supercooling was described in § 11.1.2. The present section considers how RSP can be used to manipulate microstructure.

11.4.1. Experimental and production methods

The evolution of RSP methods goes back to the last century and its potential for the modification of microstructure were initiated by DUWEZ and his collaborators at the beginning of the 60's. They designed the *Duwez Gun*, a device in which a gaseous shock wave smashes a drop of about 10mg of molten alloy into contact with a copper substrate or *chill block* to produce small foils or *splats*. This method usually is called *splat cooling*. These authors were successful in making a continous series of Cu–Ag alloys without any two-phase structure. In the same year the first *metallic glasses* were also discovered (DUWEZ *et al.* [1960]) (see chapter 19, §§ 2 and 3). Much earlier work in the field focused on equipment invention and evaluation, for example, the invention of *melt spinning* by POND [1958]. Subsequently many other methods have been developed and they have been reviewed by JONES [1982], CAHN [1983], LAVERNIA *et al.* [1992], and SURYANARAYANA *et al.* [1991]. In all the methods a *cast* sample is produced where at least one physical dimension is small assuring a rapid removal of the latent heat of fusion by an appropriate heat sink. The methods developed to achieve rapid solidification have been categorized into three main categories, (i) *atomization*, (ii) *chill methods*, and (iii) *self substrate quenching*. (See also detailed discussion in ch. 19, § 3).

In *atomization* a fine dispersion of droplets is formed when molten metal is impacted by a high energy fluid; as a result of the transfer of kinetic energy from the atomising fluid (gas or liquid) to molten metal, atomization occurs. For example LAVERNIA *et al.* [1992] summarize the phenomena associated with the method considering that the size distribution of atomized droplets will depend on: (a) the properties of the material, such as liquidus temperature, density, thermal conductivity, surface tension, heat capacity and heat of fusion; (b) the properties of the gas, such as density, heat capacity, viscosity and thermal conductivity and (c) the processing parameters such as atomization gas pressure, superheat temperature and metal/gas flow ratio. One of the most important applications of the atomization method is powder fabrication. Powder is convenient for subsequent consolidation into near final shapes. Variants of the method include, among others, gas atomization, centrifugal atomization and spark erosion (KOCH [1988]). A recent review by GRANT [1992] indicates that in recent years, atomization processes have been improved, new alloy compositions have been developed, hot isotatic pressing (HIP) has become an important processing tool, and new commercial product areas have emerged.

One extension of the atomization method is *spray atomization and deposition*. Pionneering work in this area was performed by SINGER [1970], [1972]. The general principle of the method is to atomize a stream of molten metal and to direct the resulting spray onto a shaped collector, or mandril. On impact with the collector, the particles, often partially liquid, flatten and weld together to form a high density preform which can be readily forged to form a product. LAVERNIA *et al.* [1992] and GRANT [1992] reviewed

the different variables involved in the method. Additionally, GRANT [1992] reviewed further application of the method to the formation of continuous sheet. It seems clear that high potential exists for continuous forming of steel and other metals as strips, sheet, plate and other forms. Recently ANNAVARAPU and DOHERTY [1993] have developed an understanding of the microstructural development in spray forming.

Chill Methods: *Melt spinning* is the technique most widely used in rapid solidification because it is easy to execute and the quenching rates compare favorably with other available processes. Melt spinning makes possible the production of long narrow ribbons up to a maximum width of 3 mm. This limitation has led to the development of a patented method, *planar flow casting* (fig. 76a), and to renewed interest in the melt *overflow process* originally patented in 1911 by STRANGE (fig. 76b) and now not protected by patents. Both methods can yield large quantities of wide ribbons cooled at rates approaching 10^6 Ks^{-1}.

Self-Substrate Quenching Methods: In this method the main objective is the modification of surface layers by rapid solidification. The heat source is typically a scanned or pulsed laser or electron beam focussed onto the specimen surface to cause rapid melting and resolidification. Spark discharge has also been used as a localized heat source. This field, especially when laser beams are used, have been reviewed among others by DRAPER and POATE [1985] and SURYANARAYANA *et al.* [1991]. Because of the intimate thermal contact within the different regions of the sample, the flow of heat during solidification can be modeled simply by conduction into the underlying cold material. In addition resolidification does not require nucleation: the unmelted portion of a crystalline sample provides a growth source. Then the supercooling that exists in the process is only associated with the S–L interface and is due to kinetics of the growth.

11.4.2. Relationships between RSP and solidification structures

The principal changes which can be brought about in crystalline alloys by RSP include, (i) Extension of solid-state solubility; (ii) refinement of grain size, with possible modification of grain shapes and textures; (iii) reduction or elimination of microsegregation; (iv) formation of metastable phases; (v) achievement of high density of point defects; (vi) surface alloying. Many aspects of RSP have been discussed earlier from thermodynamic and /or kinetic points of view. Several papers and reviews exist for particular metals and alloys as a consequence of the increasing importance of RSP. Among these contributions the reader is referred to LAVERNIA *et al.* [1992] for aluminum alloys; KOCH [1988] for intermetallic compounds; SURYAMARAYANA *et al.* [1991] for titanium alloys; GRANT [1992] for powder production by RSP methods; PAWLOSKI and FUCHAIS [1992] for thermally sprayed materials; DRAPER and POATE [1985] for laser surface alloying; CHEN *et al.* [1988a] [1988b] for laser surface modification of ductile iron. KURZ and TRIVEDI [1989] have modeled the selection of the microstructure under given laser processing conditions.

11.5. Low gravity effects during solidification

The common features of research in this area are the drastic reduction of sedimentation and buoyancy driven convection. Space flight provides solidification research with

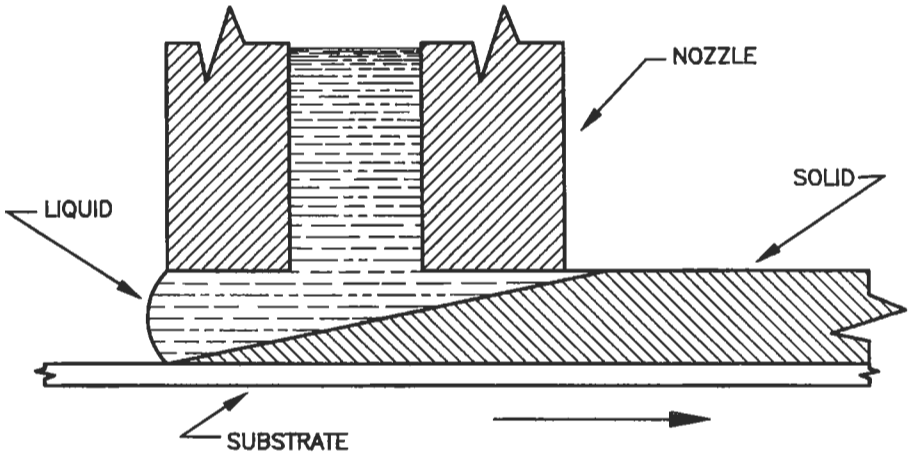

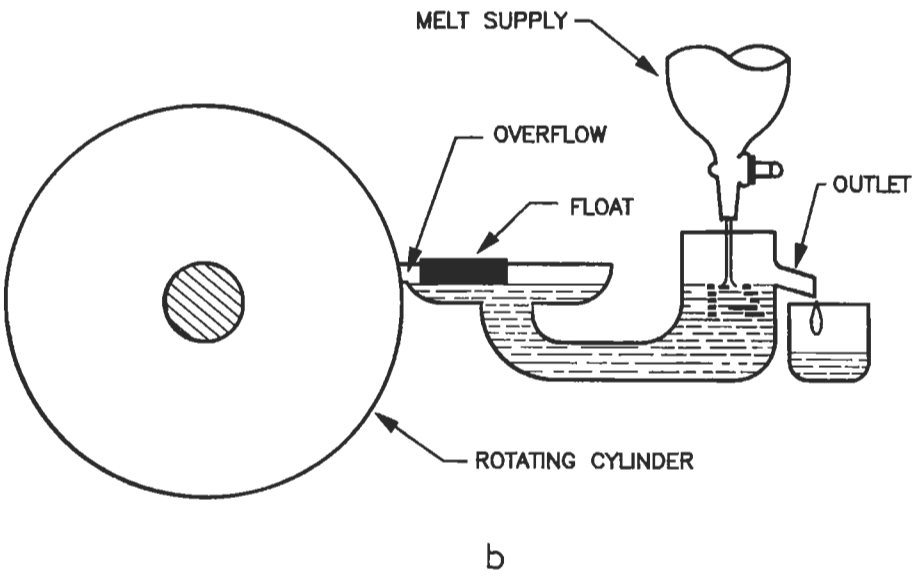

Fig. 76. (a) Planar flow casting in which the nozzle is positioned near the moving substrate to control the thickness of the cast tape. NARASHIMAM [1980]. See LAVERNIA *et al.* [1992]. (b) Melt overflow process as described by Strange in 1911 patent. STRANGE [1911]. See LAVERNIA *et al.* [1992].

long duration access to *microgravity*. However there also exist several short duration free fall facilities. Figure 77 shows the available low-g experimental systems (CURRERI and STEFANESCU [1988]). Both drop tubes and drop towers are used extensively. A *drop tube* is an enclosure in which a molten droplet can solidified while falling freely either in vacuum or in a protective atmosphere. Microgravity conditions are obtained up to a maximum of about 2 s. By contrast in a *drop tower* an entire experimental package, which may include furnace and instrumentation as well as the specimen is dropped within an enclosure. At present the best facilities are at NASA-LRC and at ZARM (Bremen) with drop towers of 145 m and 110 m height where 10^{-6} and 10^{-5} g during free fall times of 5.2 and 4.7 s respectively are obtained. However, the 500 m drop tower planned at Sunagawa (Japan) and the Eurotube-Saar project of 1200 m high drop tower would give microgravity periods of 10 s and 12 s respectively (HERLACH *et al.* [1993]). On the other hand parabolic flight and suborbital sounding rockets (fig. 77) provide microgravity levels between 30 s and 5 min.

The wide variety of experiments and disciplines involved in microgravity research opens a new field where solidification and mechanisms as modified by the near null value of gravity may be studied. On the basis of different reviews (JANSEN and SAHM

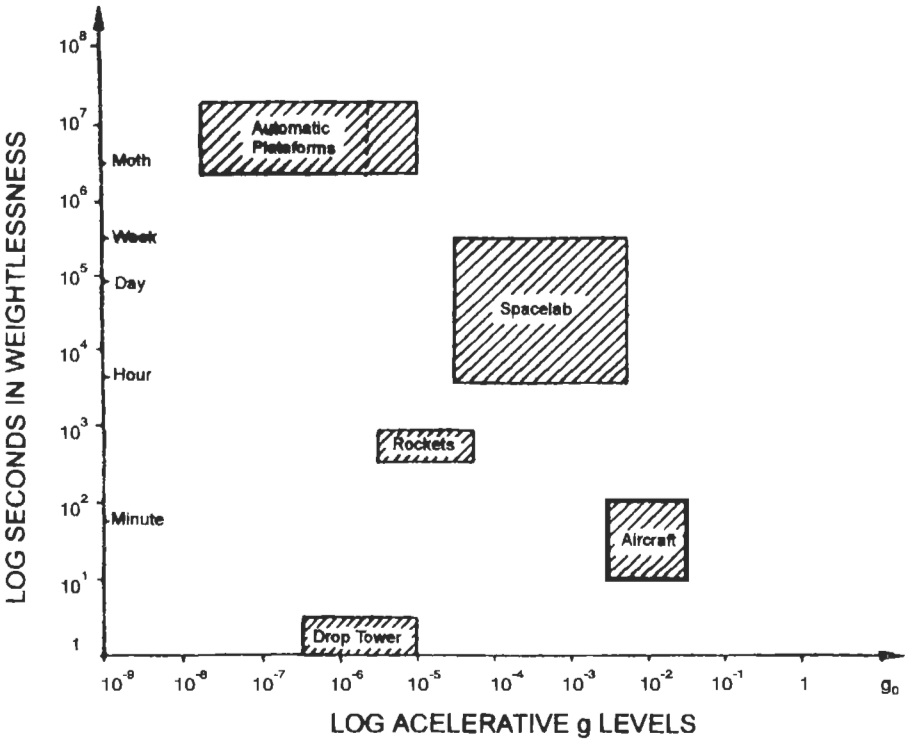

Fig. 77. Regimes of microgravity experimentation in terms of time in weightlessness and accelerative g-levels. CURRERI and STEFANESCU [1988].

References: p. 830.

[1984], MINKOFF [1986], CURRERI and STEFANESCU [1988], HERLACH *et al.* [1993]) among others, and the numerous proceedings of microgravity symposia quoted by the preceding authors, the mechanisms under study can be summarized: (i) distribution of the constituents in the initial fluid phase; (ii) phenomena of mass and heat transfer in the absence of bouyancy-driven convection. The drastic reduction of this source of convection leads to the increased influence of other mechanisms, which in general are masked on earth, namely: a) *Marangoni* convection; b) fluid movement as a result of expansion associated with phase changes or in the presence of electric, magnetic or thermoelectric fields; c) mechanisms of solute redistribution through diffusion; d) damping of temperature fluctuations in the fluid phase; e) effect of the absence of gravity on phase interfaces or meniscuses. iii) Techniques for forming or preparing materials without crucibles, direct formation of whiskers, thin films without substrates, production of hollow spheres with extremely thin walls, and float zone melting with large diameter; iv) in the more specific case of alloys in connection with casting structures: a) convection and solute distribution, b) solidification of off-monotectic and eutectic alloys, c) morphological stability of the S–L interface, d) micro- and macrosegregation, e) grain multiplication and casting structures.

11.6. Solidification processing of metal matrix composites

Thirty years ago KELLY and DAVIES [1965] and CRATCHLEY [1965] summarized their own and other pioneering efforts on metal matrix composites. Recently there has been a surge of interest in using reinforced metal matrix composites as structural materials. ASHBY [1993] indicates that any two materials can, in principle, be combined to make a composite in many geometries. A review of the processes for fabrication of MMCs is presented by GOSH [1990] covering a wide range of materials such as light alloy matrices, high temperature matrices and other special cases such as high thermal conductivity matrices and a variety of particulates, whiskers and fibers as reinforcements. Process methods may be divided as follows (i) liquid metal processes, (ii) solid state processes, (iii) deposition processes and (iv) deformation processes. Of these, solidification processing of MMC is gaining more and more importance because liquid metal is relatively inexpensive, and can flow easily to surround the reinforcing phases and create composites having a wide variety of shapes. ROHATGI [1988] has presented the state of the art related to the technical aspects of solidification processing for metal matrix composite fabrication. MORTENSEN [1991b] and MORTENSEN and JIN [1992] have reviewed the fundamentals. MORTENSEN [1991b] has classified the methods for production of MMCs into four classes on the basis of the mechanism by which the reinforcement and metal are combined (fig. 78 a–d).

1. ***Infiltration***. (fig. 78A) The reinforcement phase is stationary and essentially constitutes a very fine and intricate mould into which the liquid metal flows to fill all open porosity.
2. ***Dispersion processes*** (fig. 78B) The reinforcement phase is discrete and is added to the metal. Entrainment of the reinforcing phase into the melt is affected by agitation, which acts on the reinforcement via viscous shear stresses.
3. ***Spray processes*** (fig. 78C) The metal is divided into molten droplets and sprayed with,

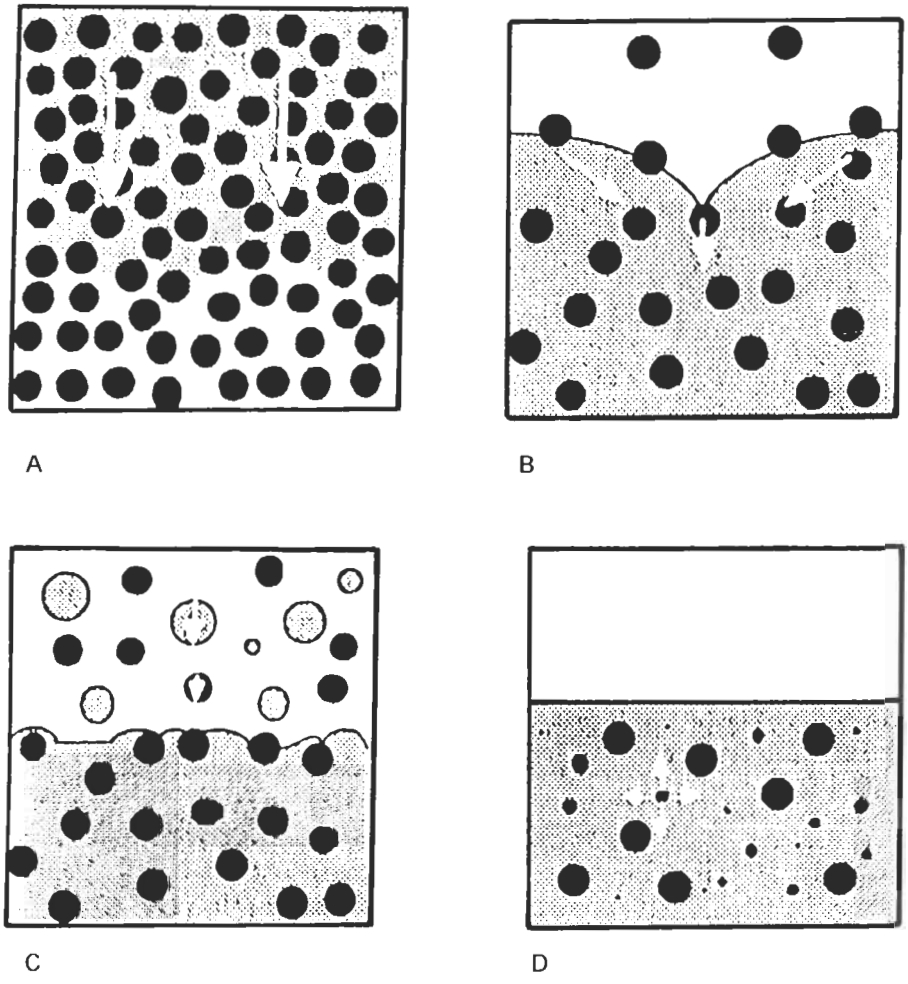

Fig. 78. Schematic representation of the principal classes of metal matrix composite solidification processes: A: infiltration, B: dispersion, C: spray-casting and D: in-situ processes. The reinforcing phase is black, the metal gray. MORTENSEN [1991b].

or onto, the reinforcement. Incorporation of the reinforcement into the matrix is affected by the added surface energy of the metal and the kinetic energy of moving droplets and particles.

4. ***In situ-processes*** (fig. 78D) Essentially consists of obtaining composites via directional solidification. In contrast with the above methods, "in-situ" processes use conventional alloying and not an artificial combination of two phases. Thus the material can have exceptional high temperature capabilities.

MORTENSEN and JIN [1992] present a comprehensive review of the physical phenom-

ena that govern infiltration and dispersion processes, which describes the governing phenomena of the process as being connected with the three main steps of metal matrix composite solidification.

The *first step* involves the interaction between the liquid matrix and the reinforcement material. This step is governing by the *wetting* between the metal and the reinforcing phase that are being combined. In most cases wetting is generally unfavorable and positive pressure and hence external work must be provided to create the composite (MORTENSEN [1991b]). From an elementary thermodynamic analysis a minimum amount of energy W per unit volume of composite is equal to

$$W = A_i(\gamma_{LR} - \gamma_{AR}), \tag{121}$$

where A_i is the surface area of the reinforcement/matrix interface per unit volume of composite; γ_{LR} = reinforcement/molten metal interfacial energy; γ_{AR} = reinforcement/atmosphere interfacial energy. MORTENSEN and JIN [1992] discussed the methods to measure wettability and to improve it namely by: (a) reinforcement pretreatment, (b) alloying modification of the matrix and (c) reinforcement coating. From a chemical point of view, knowledge about the surface of the metal matrix, the reinforcement surface and the interface chemistry as well as the influence of alloy additions and reactive wetting are described.

The *second step* corresponds to fluid flow, heat transfer and solidification phenomena that takes place in the composite material during infiltration and before it is fully solidified. The mechanics of infiltration and thermal and solidification effects, as well as processing of metal matrix composite slurries, (rheology and particle migration) must be considered.

The *third step* corresponds to completion of the solidification process. The solidification of the metal matrix is strongly influenced by the presence of the reinforcing phase that can affect the nucleation, coarsening, microsegregation and grain size. In the case of particulate composites, particle pushing theories and experiments discussed in § 9 are very important.

In conclusion it appears that the solidification processing of MMCs is an open and fascinating research area. It now stands at a point where the most essential phenomena are beginning to be clarified. On the other hand, the engineering potential of metal matrix composites is continuously increasing. Reinforced metals have been introduced in a growing number of applications, ranging from the sports industry, electronics and aerospace to the automotive sector. Current estimates indicate that the number of applications and their commercial significance will grow significantly over the next decade (WHITE and OLSON [1990]).

11.7. Semisolid metal forming processes

When metals or alloys solidify in castings and ingots, a dendritic structure forms that develops cohesion when the alloy is as little as 20% solid. Thereafter strength develops rapidly. When the casting is deformed during solidification, deformation takes place preferentially along grain boundaries; grains slide and roll over one another with small welds forming and breaking. Occasional bending of dendrite arms in the neighbourhood

of the region of deformation also occurs. As deformation proceeds, open fisures may form (*hot tears*) and be fed by liquid. In this case segregated regions, sometimes called *filled hot tears* result, yielding *V* segregates as mentioned in § 9 (FLEMINGS and MEHRABIAN [1971]). In the course of this type of macrosegregation research, METZ and FLEMINGS [1969a], [1969b] performed experiments where small blocks of Al alloys were isothermally sheared. They found negligible strength below about 0.2 fraction solid. SPENCER *et al.* [1972] carried out similar tests of Sn–15pct Pb alloy. Their test apparatus consisted of two grooved, counter-rotating cylinders. Figure 79a) shows the result obtained. Cleverly SPENCER [1971] decided to use the same apparatus to conduct a quite different type of test. Instead of partially solidifying the alloy before beginning the shear, they began the shear above the liquidus and then slowly cooled the alloy into the solidification range (fig. 79b). Two major differences are noted: (i) there is a change from

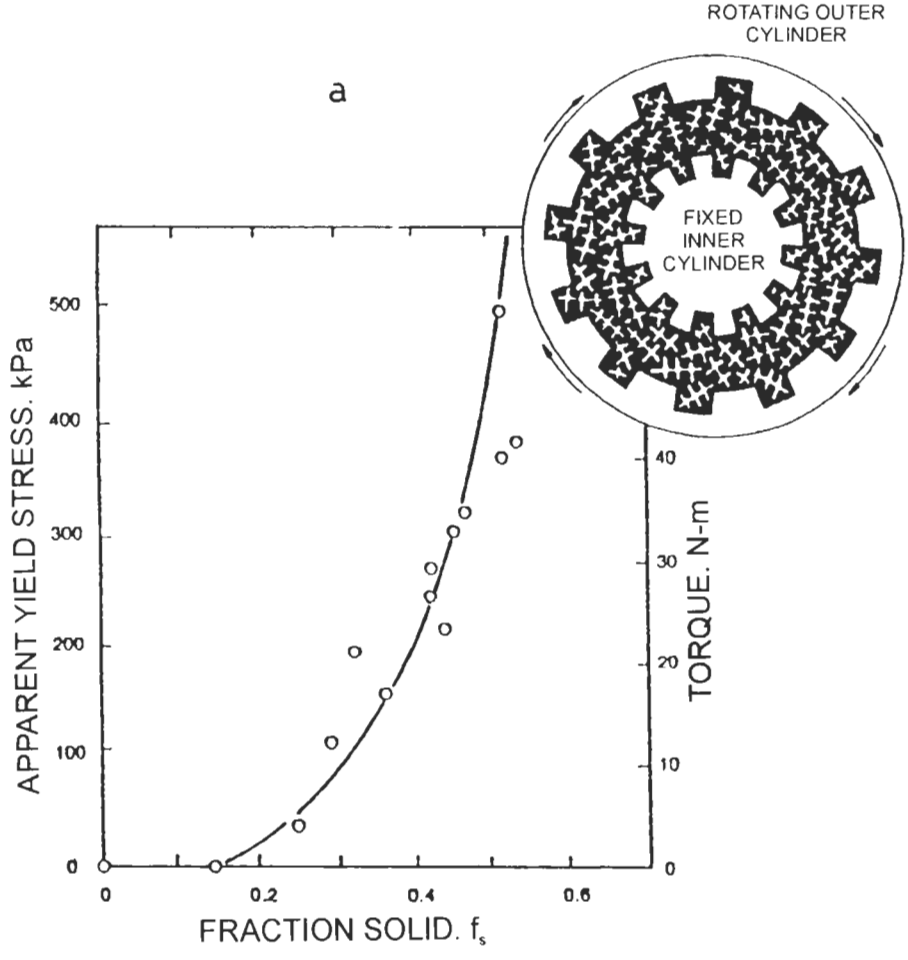

Fig. 79a

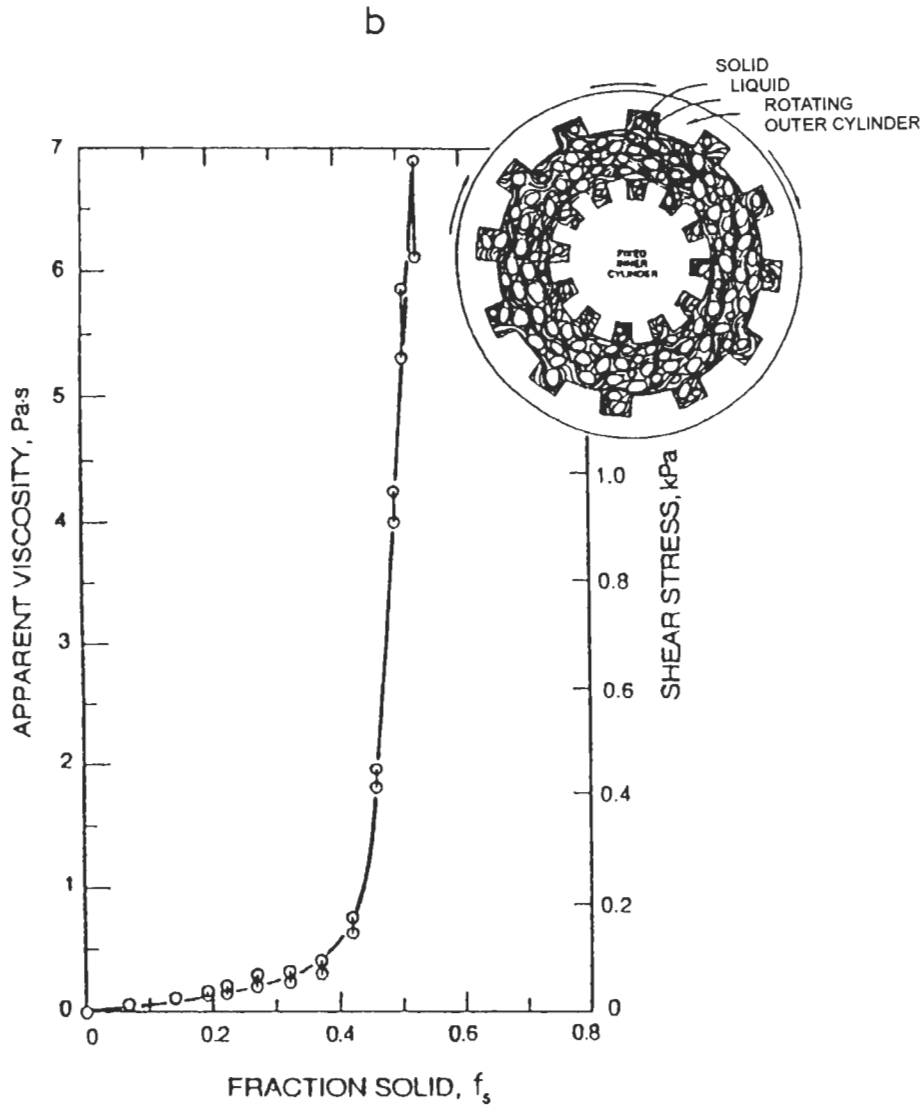

Fig. 79. (a) Maximum shear strength of semisolid dendritic Sn-15wt pct Pb alloy vs. fraction solid obtained in isothermal experiments. (at a shear rate of 0.16 s^{-1}). Schematic upper right shows test arrangement. (b) Viscosity and shear stress vs. fraction solid for Sn-15 wt pct Pb alloy cooled at 0.006 Ks^{-1} and sheared continuously at 200 s^{-1}. Schematic at upper right is an illustration of the test specimen. FLEMINGS [1991].

dendritic to non-dendritic structure; (ii) the shear stress is diminished for the dendritic structure compared to the nondendritic structure. For example, at $f_s = 0.4$ the shear stresses are 200 KPa and 0.2 KPa respectively. The material behaves as a liquid-like

slurry to which an apparent viscosity can be assigned, as has been done in fig. 79b). The fundamentals of the semi-solid metal (SSM) forming processes lie in these results. Recently FLEMINGS [1991] presented an extensive review of the development of this processes during the last 20 years as well as the current industrial applications. Also KENNEY *et al.* [1988] reviewed this area, especially from an applied and technological point of view.

Different names to characterize SSM forming processes exist in the literature. In *rheocasting* (from the Greek "rheo" to flow) strong shear forces break off dendrite fragments. If the alloy is poured when the viscosity is still low, it can be made to fill the mould. Each dendrite fragment becomes a separate crystal and a very fine grain size can be achieved without the disadvantages inherent in the use of grain-refining additions. The process also affects other casting features because the alloy is already partialy frozen when cast. Thus, shrinkage is reduced and economy in risers and gating may be substantial. Pouring temperature can also be much lower and as a consequence the amount of heat to be removed is lower and thermal stresses are reduced. Through this method all kinds of castings can be made including *continuous rheocasting* with or without electromagnetic stirring. The method can be used to prepare material to be utilised in subsequent casting processes. The prepared slugs are heatly rapidly to the partially molten state, dropped in the die-casting machine and forged under pressure into the mould. This method is named *thixocasting*. One important advantage is the dramatic improvement in die life due primarily to reduced metal temperature.

Compocasting corresponds to the development and production of metal-matrix composites containing nonmetallic particles, taking advantage of the rheological behaviour and structure of the partially solidified and agitated matrix. The particulate or fibrous nonmetals are added to the partially solid alloy slurry. The problems of wettability and their solutions are similar to those discussed in § 11.6. and the reader is referred to the MORTENSEN and JIN [1992] review of MMC processes. The high viscosity of the slurry and the presence of a high volume fraction of primary solid in the alloy slurry prevents the nonmetallic particles from floating, setting or aglomerating. With increasing mixing times, after addition, interaction between particles and the alloy matrix promotes bonding. The composites are subsequently reheated to the partially molten state in a second induction furnace and forged into shape with hydraulic presses. Very promising wear-resistant alloys have been obtained based on work by SATO and MEHRABIAN [1976] in Al alloys containing particulate additions of Al_2O_3 and SiC. MATSUMIYA and FLEMINGS [1981] extended the application of SMM to strip-casting and the basic technology of SMM provides a potential means of metal purification (MEHRABIAN *et al.* [1974]).

Acknowledgements

The authors wish to acknowledge the contributions of their various co-workers over the years and the financial support of many agencies. Special thanks are in order for S.R. Coriell and F. W. Gayle for criticisms of this manuscript, and to Miss Graciela Martínez for her effort and patience in the elaboration of the manuscript.

References: p. 830.

*References**

ADAM, C. M. and L. M. HOGAN, 1972, J. Australian Inst. of Metals, **17**, 81.

ADORNATO, M. and R. A. BROWN, 1987, J. Cryst. Growth **80**, 155.

AGUILAR RIVAS, R. A. and H. BILONI, 1980 a), Z. Metallk. **71**, 264.

AGUILAR RIVAS, R. A. and H. BILONI, 1980 b), Z. Metallk. **71**, 309.

ANDREWS, J. B., A. L. SCHMALE, and A. C. SANDLIN, 1992, J. Cryst. Growth **119**, 152.

ANNAVARAPU, S. and R. D. DOHERTY, 1993, Int. J. of Powder Metall. **29**, 331.

APELIAN, D., 1982, in: Aluminum Transformation Technology and Applications 1981, eds. C. A. Pampillo, H. Biloni, L. Mondolfo and F. Sacchi (ASM, Metals Park, OH) p. 423.

APTEKAR, J. L. and D. S. KAMENETSKAYA, 1962, Fiz Metal, Metalloved, **14**, 123.

ASHBY, M. F., 1993, Acta Metall Mater. **41**, 1313.

AUDERO, M. A. and H. BILONI, 1972, J. Cryst. Growth **12**, 297.

AUDERO, M. A. and H. BILONI, 1973, J. Cryst. Growth **18**, 257.

AZIZ, M. J., 1982, J. Appl Phys. **53**, 1158.

AZIZ, M. J. and T. KAPLAN, 1988, Acta Metall. **36**, 2335.

AZIZ, M. J. and W. J. BOETTINGER, 1994, Acta Metall. Mater. **42**, 527.

BACKERUD, L., K. NILSSON and H. STEEN, 1975, in: Metallurgy of Cast Iron (Georgy Pub. Co., St. Saphorin, Switzerland), p. 625.

*BAKER, J. C., 1970, Interfacial Partitioning During Solidification, Ph. D. Thesis, Massachusetts Institute of Technology, Chapter V, (see also CAHN *et al.* [1980]).

BAKER, J. C. and J. W. CAHN, 1971, in: Solidification (ASM, Metals Park, OH), p. 23.

BAKER, C. and V. SUBRAMANIAN, 1980, in: Aluminum Transformation Technology and Applications 1979, eds. C. A. Pampillo, H. Biloni and D. E. Embury (ASM, Metals Park, OH.) p. 335.

BANERJEE, D. K. and D. M. STEFANESCU, 1991, Trans. AFS, **99**, 747.

BASKARAN, V., W. R. WILCOX, 1984, J. Cryst. Growth **67**, 343.

BATTLE, T. P., 1992, Int. Mat. Rev. **37**, 249.

BATTLE, T. P., and R. D. PEHLKE, 1990, Metall. Trans. **21B**, 357.

BECKERMANN, C. and R. VISKANTA, 1988, Physicochem. Hydrodyn. **10**, 195.

BENNON, W. D. and F. P. INCROPERA, 1987 a), Int. J. Heat Mass Transfer **30**, 2161.

BENNON, W. D. and F. P. INCROPERA, 1987 b), Int. J. Heat Mass Transfer **30**, 2171.

BERRY, J. T. and R. D. PEHLKE, 1988, in: Metals Handbook, ninth ed., **15**: Casting (ASM, Metals Park, OH), 858.

BERTORELLO, H. R., and H. BILONI, 1969, Trans. Met. Soc. AIME **245**, 1375.

BILLIA, B. and R. TRIVEDI, 1993, in: Handbook of Crystal Growth 1B: Fundamentals, Transport and Stability, D. T. J. Hurle, ed., (North-Holland, Amsterdam) p. 899.

*BILONI, H., 1968, in: The Solidification and Casting of Metals (Iron and Steel Inst., London) Pub. 110, p. 74.

BILONI, H., 1970, Metallurgia ABM (Aso. Brasileira de Metais) **26**, 803.

BILONI, H., 1977, Ciencia Interamericana **18** (3–4), 3.

BILONI, H., 1980, in: Aluminum Transformation Technology and Applications 1979, eds. C. A. Pampillo, H. Biloni and D. E. Embury (ASM, Metals Park, OH) p. 1.

BILONI, H., 1983, Solidification, in: Physical Metallurgy, 3rd. ed, Ed. R. W. Cahn and P. Haasen (North Holland, Amsterdam), p. 478.

BILONI, H. and B. CHALMERS, 1965, Trans. Met. Soc. AIME, **233**, 373.

BILONI, H., G. F. BOLLING and H. A. DOMIAN, 1965 a), Trans. Met. Soc. AIME **233**, 1926.

BILONI, H., G. F. BOLLING and G. S. COLE, 1965 b), Trans. Met. Soc. AIME **233**, 251.

BILONI, H., G. F. BOLLING, and G. S. COLE, 1966, Trans. Met. Soc. AIME **236**, 930.

BILONI, H., R. DI BELLA and G. F. BOLLING, 1967, Trans. Met. Soc. AIME **239**, 2012.

BILONI, H. and B. CHALMERS, 1968, J. Mat. Sci. **3**, 139.

* References marked with an asterisk are suitable for Further Reading.

BILONI, H. and R. MORANDO, 1968, Trans. Met. Soc. AIME **242**, 1121.
BLODGETT, J. A., R. J. SCHAEFER, and M. E. GLICKSMAN, 1974, M. E., Metallography **7**, 453.
BOBADILLA, M., J. LACAZE, G. J. LESOULT, 1988, J. Cryst. Growth **89**, 531.
BOETTINGER, W. J., 1974, Metall. Trans. **5**, 2023.
BOETTINGER, W. J., 1981, in: Proc. Fourth Intl. Conf. on Rapidly Quenched Metals, edited by T. Masumoto and K. Suzuki, (The Japan Institute of Metals, Sendai, Japan), p. 99.
BOETTINGER, W. J., 1982, in: Rapidly Solidified Crystalline and Amorphous Alloys, B. H. Kear and B. C. Giessen, eds., (Elsevier North Holland, NY), p. 15.
BOETTINGER, 1988, unpublished research, NIST, Gaithersburg, MD, U.S.A.
BOETTINGER, W. J., D. SHECHTMAN, R. J. SCHAEFER, and F. S. BIANCANIELLO, 1984, Metall. Trans. **15A**, 55.
*BOETTINGER, W. J. and J. H. PEREPEZKO, 1985, in: Rapidly Solidified Crystalline Alloys, S. K. Das, B. H. Kear, C. M. Adam, eds., (TMS-AIME), p. 21.
BOETTINGER, W. J., L. A. BENDERSKY and J. G. EARLY, 1986, Metall. Trans. **17A**, 781.
BOETTINGER, W. J., and S. R. CORIELL, 1986, in: Science and Technology of the Supercooled Melt, P. R. Sahm, H. Jones and C. M. Adam, eds., (NATO ASI Series E-No. 114, Martinus Nijhoff, Dordrecht), p. 81.
BOETTINGER, W. J., L. A. BENDERSKY, S. R. CORIELL, R. J. SCHAEFER, and F. S. BIANCANIELLO, 1987, J. Cryst. Growth **80**, 17.
BOETTINGER, W. J., L. A. BENDERSKY, F. S. BIANCANIELLO and J. W. CAHN, 1988a), Mater. Sci. Eng. **98**, 273.
BOETTINGER, W. J., S. R. CORIELL, and R. TRIVEDI, 1988b), in: Rapid Solidification Processing: Principles and Technologies R. Mehrabian and P. A. Parrish, eds., (Claitor's Publishing, Baton Rouge), p. 13.
BOETTINGER, W. J., L. A. BENDERSKY, R. J. SCHAEFER and F. S. BIANCANIELLO, 1988c, Metall. Trans. **19A**, 1101.
BOETTINGER, W. J., and M. J. AZIZ, 1989, Acta Metall. **37**, 3379.
BOLLING, G. F., 1971, in: Solidification (ASM, Metals Park, Oh.), p. 341.
BOWER, T. F., H. D. BRODY, and M. C. FLEMINGS, 1966, Trans. Met. Soc. AIME **236**, 624.
BOWER, T. F. and M. C. FLEMINGS, 1967, Trans. Met. Soc. AIME **239**, 1620.
BOWER, T. F., D. A. GRANGER and J. KEVERIAN, 1971, in: Solidification (ASM Metals Park, OH), p. 385.
BRAUN, R. J., and S. H. DAVIS, 1991, J. Cryst. Growth **112**, 670.
BRICE, J. C., 1973, in: The Growth of Crystals from Liquids (North Holland, Amsterdam), p. 120
BRIMACOMBE, J. K., 1993, Metall. Trans., **24B**, 917.
BRIMACOMBE, J. K., and I. V. SAMARASEKERA, 1990, in: Principles of Solidification and Materials Processing, T. 1, (Trans. Tech. Publication), p. 179.
BRODY, H. D., 1974, in: Solidification Technology, eds. J. J. Burke, M. C. Flemings and A. E. Quorum (Brook Hill Pub., Chesnut Hills, MA) p. 53.
BRODY, H. D. and FLEMINGS, M. C., 1966, Trans. Met. Soc. AIME **236**, 615.
BRODY, H. D., and S. A. DAVID, 1979, in: Solidification and Casting of Metals (The Metals Society, London) p. 144.
BROUGHTON, J. Q., A. BONISSENT, and F. F. ABRAHAM, 1981, J. Chem Phys. **74**, 4029.
BROUGHTON, J. Q., G. H. GILMER, and K. A. JACKSON, 1982, Phys. Rev. Lett. **49**, 1496.
BROWN, R. A., 1988, J. AiChE J., **34**, 881.
BROWN, S. G. R. and J. A. SPITTLE, 1989, Mat. Sc. Tech. **5**, 362.
BURDEN, M. H., D. J. HEBDITCH and J. D. HUNT, 1973, J. Cryst. Growth **20**, 121.
BURDEN, M. H. and J. D. HUNT, 1974a), J. Cryst. Growth **22**, 99.
BURDEN, M. H., and J. D. HUNT, 1974b), J. Cryst. Growth **22**, 109.
BURDEN, M. H., and J. D. HUNT, 1974c), J. Cryst. Growth **22** 328.
BURTON, J. A., R. C. PRIM and W. P. SCHLICHTER, 1953, J. Chem. Phys. **21**, 1987.
CAGINALP, G., 1986, Arch. Rational Mech. Anal. **92**, 205.
CAHN, J. W., 1960, Acta Metall. **8**, 554.
CAHN, J. W., 1967, in: Crystal Growth, ed. H. S. Peiser (Pergamon Press, Oxford) p. 681.
CAHN, J. W., 1979, Metall. Trans. **10A**, 119.
CAHN, J. W., W. B. HILLIG, and G. W. SEARS, 1964, Acta Metall. **12**, 1421.
CAHN, J. W., S. R. CORIELL and W. J. BOETTINGER, 1980, in: Laser and Electron Beam Processing of Materials, C. W. White and P. S. Peercy eds. (Academic Press, NY), p. 89.

CAHN, R.W., 1983, in: Physical Metallurgy, Ch. 28, 3er. ed., eds. R.W. Cahn and P. Haasen (North Holland), p. 1709.
CALVO, C., and H. BILONI, 1971, Z. Metallk. **62**, 664.
CAMEL, D. and J.J. FAVIER, 1984 a), J. Cryst. Growth **67**, 42.
CAMEL, D. and J.J. FAVIER, 1984 b), J. Cryst. Growth **67**, 57.
CAMPBELL, 1981, Int. Met. Rev. **26**, 71.
CAMPBELL, J., 1991a), Castings (Butterworth–Heinemann, London).
CAMPBELL, J., 1991 b), Mat. Sc. and Tech. **7**, 885.
CAMPBELL, J., 1991 c), Cast Metals **4**, 101
CAMPBELL, J. and I.D. OLLIFF, 1971, AFS Cast Metals Research J. (ASM Metals Park, OH) **May**, 55.
CANTOR, B.and R. DOHERTY, 1979, Acta Metall. **27**, 33.
CAROLI, B., C. CAROLI and B. ROULET, 1982, J. Physique **43**, 1767.
CARRAD, M., M. GREMAUD, M. ZIMMERMANN, and W. KURZ, 1992, Acta Metall. Mater. **40**, 983.
CARRUTHERS, J.R., 1976, Thermal Convection Instabilities Relevant to Crystal Growth from Liquids in: Preparation and Properties of Solid State Materials, vol. 2 (Marcel Decker, N.Y.)
CECH, R.E., 1956, Trans. Met. Soc. AIME **206**, 585.
CHADWICK, G.A., 1963, in Progress in Materials Science, **12**, (Pergamon Press, Oxford) edited by B. Chalmers, p. 97.
CHADWICK, G.A., 1965, Brit. J. Appl. Phys. **16**, 1095.
CHALMERS, B., 1963, J. Aust. Inst. Metals **8**, 255.
*CHALMERS, B., 1964, Principles of Solidification (Wiley, N.Y.).
CHALMERS, B., 1971, in: Solidification (American Society for Metals, ASM, Metals Park, OH) p. 295.
CHANG, Ch. J. and R.A. BROWN, 1983, J. Cryst. Growth **63**, 343.
CHEN, C.H., C.P. JU and J.M. RIGSBEE, 1988a), Mat. Sci. and Tech. **4**, 161.
CHEN, C.H., C.P. JU and J.M. RIGSBEE, 1988b), Mat. Sci. and Tech. **4**, 167.
CHEN, S.W., and Y.A. CHANG, 1992, Metall. Trans. **23A**, 1038.
*CHERNOV, A.A., 1984, Modern Crystallography III: Crystal Growth, (Springer–Verlag, Berlin).
CHEVEIGNE de, S., C. GUTHMANN, P. KUROSKI, E. VICENTE and H. BILONI, 1988, J. Cryst. Growth **92**, 616.
CHOPRA, M.A., M.E. GLICKSMAN, and N.B. SINGH, N.B., 1988, Metall. Trans **19A**, 3087.
CLAPHAM, L. and R.W. SMITH, 1988, J. Cryst. Growth **92**, 263.
CLYNE, T.W. and A. GARCÍA, 1980, Int. J. Heat and Mass Transfer **23**, 773.
CLYNE, T.W., 1980 a), J. Cryst. Growth **50**, 684.
CLYNE, T.W., 1980 b), J. Cryst. Growth **50**, 691.
CLYNE, T.W., 1984, Metall. Trans. **15B**, 369.
CLYNE, T.W. and A. GARCIA, 1981, J. Mat. Sci. **16**, 1643.
COCHRANE, R.F., D.M. HERLACH and B. FEUERBACHER, 1991, Mat. Sci. Eng. **A133**, 706.
*COLE, G.S., 1971, in: Solidification (ASM Metals Park, OH), p. 201.
COLE, G.S. and G.F. BOLLING, 1968, Trans. Met. Soc. AIME **242**, 153.
COLE, G.S. and G.F. BOLLING, 1969, in: Proc.16th. Sagamore Army Materials Res. Conf. Conference quoted by BOLLING [1971].
COLLIGAN, G.A., V.A. SUPRENANT and F.D. LEMKEY, 1961, J. Metals **13**, 691.
CORIELL, S.R., D.T.J. HURLE and R.F. SEKERKA, 1976, J. Cryst. Growth **32**, 1.
CORIELL, S.R. and R.F. SEKERKA, 1979, J. Cryst. Growth **46**, 479.
CORIELL, S.R., R.F. BOISVERT, R.G. REHM and R.F. SEKERKA, 1981, J. Cryst. Growth **54**, 167.
CORIELL, S.R. and D. TURNBULL, 1982, Acta Metall. **30**, 2135.
CORIELL, S.R. and R.F. SEKERKA, 1983, J. Cryst. Growth **61**, 499.
CORIELL, S.R., G.B. MCFADDEN and R.F. SEKERKA, 1985, Ann Rev. Mat. Sci **15**, 119.
CORIELL, S.R., G.B. MCFADDEN, P.W. VOORHEES and R.F. SEKERKA, 1987, J. Cryst. Growth **82**, 295.
CORIELL, S.R., and G.B. MCFADDEN, 1989, J. Cryst. Growth **94**, 513.
CORIELL, S.R., and G.B. MCFADDEN, 1990, in: Low Gravity Fluid Dynamics and Transport Phenomena, eds. J.N. Koster and R.L. Sani, vol.130 of Progress in Astronautics and Aeronautics AIAA, Washington D.C., p. 369.
CORIELL, S.R., G.B. MCFADDEN, and R.F. SEKERKA, 1990, J. Cryst. Growth **100**, 459.

*CORIELL, S.R. and G.B. MCFADDEN, 1993, in: Handbook of Crystal Growth ed. D.T.J. Hurle (Elsevier Science Publishers, Amsterdam) vol. 1b, p. 785.
CORIELL, S.R. and W.J. BOETTINGER, 1994, NIST, unpublished research.
CRAIG, D.B., M.J. NORNUNG and T.K. CLUHAN, 1988, Metals Handbook, 9th.ed., (ASM, Metals Park, OH) **15 "Casting"**, 629.
CRATCHLEY, D., 1965, Metall. Rev. **10**, (37), 79.
CROKER, M.N., R.S. FIDLER, and R.W. SMITH, 1973, Proc. Roy. Soc. London **A335**, 15.
CROSSLEY, P.A. and L.F. MONDOLFO, 1966, Modern Casting **49**, 89.
CURRERI, P.A. and D.M. STEFANESCU, 1988, Metals Handbook, 9th.ed., (ASM, Metals Park, OH) **15 "Casting"**, 147.
DANTZIG, J.A. and S.C. LU, 1985, Metall. Trans. **16B**, 195.
DANTZIG, J.A. and J.W. WIESE, 1985, Metall. Trans. **16B**, 203.
DANTZIG, J.A. and J.W. WIESE, 1986, Advanced Manufacturing Processes **1**, 437.
DAS, S. and A.J. PAUL, 1993, Metall. Trans. **24B**, 1073.
DAVID, S.A. and J.M. VITEK, 1989, Int. Met. Rev. **34**, 213.
DAVID, S.A., J.M. VITEK, M. RAPPAZ and L.A. BOATNER, 1990, Metall. Trans. **21A**, 1753.
DAVID, S.A. and J.M. VITEK, 1992, in: The Metal Science of Joining, eds. A.J. Cieslak, J.H. Perepezko, S. Kang and M.E. Glicksman, (TMS Pub., Warrendale, PA) p. 101.
DAVID, S.A., T. DEBROY and J.M. VITEK, 1994, MRS Bull. **xix**, N° 1, 29.
DAVIES, G.J. and J.G. GARLAND, 1975, Int. Met. Rev. **20**, 83.
DAYTE, V., and J.S. LANGER, 1981, Phys. Rev. B **24**, 4155.
DAYTE, V., R. MATHUR and J.S. LANGER, 1982, J. Stat. Phys. **29**, 1.
DERBY, B., and J.J. FAVIER, 1983, Acta Metall. **31**, 1123.
DEVAU, G. and D. TURNBULL, 1987, Acta Metall. **35**, 765.
DRAPER, C.W. and J.M. POATE, 1985, Int. Met. Rev. **30**, n° 2, 85.
DUWEZ, P., R.H. WILLENS and W. KLEMENT, 1960, J. Apply Phys. **31**, 1136.
EASTERLING, K.E., 1984, Mat. Sci. and Eng. **65**, 191.
ECKLER, K., R.F. COCHRAN, D.M. HERLACH, B. FEUERBACHER, and M. JURISCH, 1992, Phys. Rev. B **45**, 5019.
ELMER, J.W., M.J. AZIZ, L.E. TANNER, P.M. SMITH, and M.A. WALL, 1994, Acta Metall. Mater. **42**, 1065.
ELLIOT, R., 1964, Br. Foundryman **9**, 389.
ELLIOT, R., 1988, in: Cast Iron Technology (Butterworths, London)
EMLEY, E.F., 1976, Int. Met. Rev. **21**, 175.
ESHELMAN, M.A., V. SEETHARAMAN and R. TRIVEDI, 1988, Acta Metall. **36**, 1165.
ESHELMAN, M.A., and R. TRIVEDI, 1988, Scripta Metall. **22**, 893.
FAINSTEIN–PEDRAZA, D. and G.F. BOLLING, 1975, J. Cryst. Growth **28**, 311.
FAVIER, J.J., 1981a), Acta Metall. **29**, 197.
FAVIER, J.J., 1981b), Acta Metall. **29**, 205.
FAVIER, J.J., 1990, J. Cryst. Growth **99**, 18.
FAVIER, J.J. and A. ROUZAUD, 1983, J. Cryst. Growth **64**, 367.
FAVIER, J.J. and D. CAMEL, 1986, J. Cryst. Growth **79**, 50.
FAVIER, J.J., and L.O. WILSON, 1982, J. Cryst. Growth **58**, 103.
FECHT, H.J., and J.H. PEREPEZKO, 1989, Metall. Trans. **20A**, 785.
FELICELLI, S.D., J.C. HEINRICH and D.R. POIRIER, 1991, Metall. Trans. **22B**, 847.
FELLIU, S., L. LUIS, D. SIGUIN and J. ALVAREZ, 1962, Trans. AFS **70**, 145.
FEURER, U., and R. WUNDERLIN, 1977, DGM Fachber. (Oberusel, FRG). See also KURZ and FISHER [1989]., p. 257.
FISHER, D.J. and W. KURZ, 1979, in: Solidification and Casting of Metals (The Metals Soc., London), p. 57.
FISHER, D.J., and W. KURZ, 1980, Acta Metall. **28**, 777.
*FLEMINGS, M.C., 1974, Solidification Processing (McGraw Hill, New York).
FLEMINGS, M.C., 1976, Scand. J. Metall. **5**, 1.
FLEMINGS, M.C., 1991, Metall. Trans. **22A**, 957.
FLEMINGS, M.C. and G.E. NEREO, 1967, Trans. Met. Soc. AIME **239**, 1449.

FLEMINGS, M.C., D.R. POIRIER, R.V. BARONE, and H.D. BRODY, 1970, J. Iron and Steel Inst. **208**, 371.
*FLEMINGS, M.C. and R. MEHRABIAN, 1971, in: Solidification (ASM, Metals Park, OH) p. 311.
FLEMINGS, M.C. and Y. SHIOHARA, 1984, Mat. Sci. and Eng. **65**, 157.
FLOOD, S.C. and J.D. HUNT, 1987a), J. Cryst. Growth **82**, 543.
FLOOD, S.C. and J.D. HUNT, 1987b), J. Cryst. Growth **82**, 552.
FLOOD, S.C. and J.D. HUNT, 1988, Metals Handbook 9th.ed., (ASM, Metals Park, OH) **15 "Casting"**, p. 130.
FRANK, F.C., 1949, Disc. Farad. Soc. **5**, 48.
FREDRIKSSON. H., and M. HILLERT, 1972, Scand. J. Metall. **2**, 125.
FREDRIKSSON, H., M. HILLERT and N. LANGE, 1973, J. Inst. Metals **101**, 285.
FREDRIKSSON, H., and T. NYLEN, 1982, Metall. Sci. **16**, 283.
FRENKEL, J., 1932, Phys. Z. Sowjetunion **1**, 498.
GANESAN, S. and D.R. POIRIER, 1989, J. Cryst. Growth **97**, 851.
GANESAN, S. and D.R. POIRIER, 1990, Metall. Trans. **21B**, 173.
GARBELLINI, O., H. PALACIO and H. BILONI, 1990, Cast Metals **3**, 82.
GARCIA, A. and M. PRATES, 1978, Metall. Trans. **9B**, 449.
GARCIA, A., T.W. CLYNE and M. PRATES, 1979, Metall. Trans. **10B**, 85.
GARCIA, A. and T.W. CLYNE, 1983, in: Solidification Technology in the Foundry and Casthouse, ed. J.A. Charles (The Metals Society, London), p. 33.
GETSELEV, Z.N., 1971, J. Metals **23**, 38.
GILL, S.C. and W. KURZ, 1993, Acta Metall. Mater. **41**, 3563.
GIOVANOLA, B., and W. KURZ., 1990, Metall. Trans. **21A**, 260.
GLASSON, E.L. and E.F. EMLEY, 1968, in: The Solidification of Metals (Iron and Steel Inst., London) Public. 110, p. 1.
GLICKSMAN, M.E., 1965, Acta Metall. **13**, 1231.
GLICKSMAN, M.E., 1981, in: Aluminum Transformation Technology and Applications 1981, eds. C.A. Pampillo, H. Biloni, L. Mondolfo and F. Sacchi (ASM, Metals Park, OH), p. 347.
GLICKSMAN, M.E., R.J. SCHAEFER, and J.D. AYERS, 1976, Metall. Trans. **7A**, 1747.
GLICKSMAN, M.E., S.R. CORIELL and G.S. MCFADDEN, 1986, Ann. Rev. Fluid Mech. **18**, 307.
*GLICKSMAN, M.E., and S.P. MARSH, 1993, in: Handbook of Crystal Growth 1B: Fundamentals, Transport and Stability, D.T.J. Hurle, ed., (North-Holland, Amsterdam) p. 1075.
GOSH, A.K., 1990, in: Principles of Solidification and Materials Processing (Oxford and IBH Publication Co.) p. 585.
GRANGER, D.A. and R. ELLIOT, 1988, Metals Handbook, 9th. ed., (ASM, Metals Park, OH) **15 "Casting"**, p. 159.
GRANT, N.J., 1992, Metall. Trans. **23A**, 1083.
GREMAUD, M., W. KURZ, and R. TRIVEDI, 1987, unpublished work. See TRIVEDI and KURZ [1988].
GREMAUD, M., M. CARRAD and W. KURZ, 1991, Acta Metall. Mater. **39**, 1431.
GRUGEL, R.N., A. HELLAWELL, 1981, Metall. Trans. **12A**, 669.
GRUGEL, R.N., T.A. LOGRASSO, A. HELLAWELL, 1984, Metall. Trans. **15A**, 1003.
GULLIVER, G.H., 1922, Metallic Alloys, ed. Charles Griffin (London) p. 397.
GUNDUZ, M., and J.D. HUNT, 1985, Acta Metall. **33**, 1651.
HANNA, M.D., SHU-ZU LU and A. HELLAWELL, 1984, Metall. Trans. **15A**, 459.
HAO, S.W., Z.Q. ZHANG, J.Y. CHEN and P.C. LIU, 1987, AFS. Trans. **95**, 601.
HARDY, S.C., G.B. MCFADDEN, S.R. CORIELL, P.W. VOORHEES, and R.F. SEKERKA, 1991, J. Cryst. Growth **114**, 467.
HAYES, A. and J. CHIPMAN, 1938, Trans. Met. Soc. AIME **135**, 85.
HEIPLE, C.R., P. BURGARDT and J.R. ROPER, 1984, in: Modeling of Casting and Welding Processes, III. The Met. Soc. of AIME, Warrendale. Ed. J.A. Dantzing and J.T. Berry, p. 193.
HELLAWELL, A., 1970, Prog. Mater. Sci. **15**, 3.
HELLAWELL, A., 1979, in: Solidification and Casting of Metals (The Metals So., London) p. 161.
HELLAWELL, A., 1990, in: F. Weinberg International Symp. on Solidification Processing, ed. V.E. Lait and I.V. Samarasekera (Pergamon Press), p. 395.
HENZEL, J.G. Jr. and J. KEVERIAN, 1965, J. Metals **17**, 561.

*HERLACH, D. M., R. F. COCHRANE, I. EGRY, H. J. FECHT and A. L. GREER, 1993, Internat. Mat. Reviews **38**, n° 6, 273.
HILLERT, M., 1953, Acta Metall. **1**, 764.
HILLERT, M., 1957, Jernkontorets Ann. **141**, 757.
HILLERT, M., 1979, in: Solidification and Casting of Metals, The Metals Society, London, p. 81.
HILLERT, M. and V. V. SUBBARAO, 1968, in: Solidification of Metals (Iron and Steel Inst., London), Publication n° 110, p. 204.
HILLIG, W. D. and D. TURNBULL, 1956, J. Chem. Phys. **24**, 219.
HILLIG, W. D., 1966, Acta Met. **14**, 1868.
HILLS, A. W. D., S. L. MALHOTRA and M. R. MOORE, 1975, Metall. Trans. **6B**, 131.
HO, K. and R. D. PEHLKE, 1984, AFS Trans. **92**, 587.
HO, K. and R. D. PEHLKE, 1985, Metall. Trans. **16B**, 585.
HOAGLUND, D. E., M. E. AZIZ, S. R. STIFFLER, M. O. THOMSON, J. Y. TSAO and P. S. PEERCY, 1991, J. Cryst. Growth **109**, 107.
HOFFMEYER, M. K. and J. H. PEREPEZKO, 1988, Scripta Metall. **22**, 1143.
HOFFMEYER, M. K. and J. H. PEREPEZKO, 1989a) in: Light Metals 1989, Ed. P. G. Campbell, (TMS, Warrendale, PA), p. 913.
HOFFMEYER, M. K. and J. H. PEREPEZKO, 1989b) Script. Metall. **23**, 315.
HOFFMEYER, M. K. and J. H. PEREPEZKO, 1991, in: Light Metals 1991, Ed. E. L. Roy, (TMS, Warrendale, PA), p. 1105.
*HOGAN, L. M., R. W. KRAFT, and F. D. LEMKEY, 1971, in: Advances in Materials Research, Vol. 5, (Wiley, New York), edited by H. Herman, p. 83.
HOLLOMON, J. H., and D. TURNBULL, 1953, Progress in Met. Phys., vol. 4, (Interscience, New York), p. 333.
HORVAY, G., 1965, Int. J. Heat Mass Transfer **8**, 195.
HUANG, S. C. and M. E. GLICKSMAN, 1981, Acta Metall. **29**, 717.
HUANG, S. C., E. L. HALL, K. M. CHANG, and R. P. LAFORCE, 1986, Metall. Trans. **17A**, 1685.
HUANG, S. C. and E. L. HALL, 1989, Mater. Res. Soc. Symp. Proc. **133**, 373.
HUGHES, I. R. and H. JONES, 1976, J. Mater. Sci. **11**, 1781.
HUGHES, I. C. H., 1988, Metals Handbook, 9th. ed., (ASM, Metals Park, OH) **15 "Casting"**, 647.
HUNT, J. D., 1979, in: Solidification and Casting of Metals (Metals Society, London), p. 3.
HUNT, J. D., 1984, Mat. Sci. and Eng. **65**, 75.
HUNT, J. D., 1990, Acta Metall. Mater. **38**, 411.
HUNT, J. D., and K. A. JACKSON, 1966, Trans. Met. Soc. AIME **236**, 843.
HUNT, J. D., and K. A. JACKSON, 1967, Trans. Met. Soc. AIME **239**, 864.
HURLE, D. T. J., 1969, J. Cryst. Growth **5**, 162.
HURLE, D. T. J., 1972, J. Cryst. Growth **13/14**, 39.
HURLE, D. T. J., 1987, J. Cryst. Growth **85**, 1.
HURLE, D. T. J., E. JAKEMAN, 1968, J. Cryst. Growth **3–4**, 574.
INOUE, A., T. MASUMOTO, H. TOMIOKA and N. YANO, 1984, Int. J. Rapid Solidification **1**, 115.
ISHIHARA, K. N., M. MAEDA and P. H. SHINGU, 1985, Acta Metall. **33**, 2113.
IVANTSOV, G. P., 1947, Dokl. Akad. Nauk S.S.S.R. **58**, 567.
JACKSON, K. A., 1958, in: Liquid Metals and Solidification (ASM, Metals Park, OH) p. 174.
JACKSON, K. A., 1968, Trans. Met. Soc. AIME **242**, 1275.
JACKSON, K. A., 1971, in: Solidification (ASM, Metals Park, OH) p. 121.
JACKSON, K. A., 1974, J. Cryst. Growth **24/25**, 130.
*JACKSON, K. A. and J. D. HUNT, 1966, Tran. Met. Soc. AIME **236**, 1129.
JACKSON, K. A., J. D. HUNT, D. R. UHLMANN and T. P. SEWARD, 1966, Trans. Met. Soc. AIME **236**, 149.
JACKSON, K. A., D. R. UHLMANN, and J. D. HUNT, 1967, J. Cryst. Growth **1**, 1.
JACKSON, K. A., 1975, in: Treatise on Solid State Chemistry, Vol. 5, edited by N. B. Hannay, (Plenum, NY), p. 233.
JACKSON, K. A., G. H. GILMER and H. J. LEAMY, 1980, in: Laser and Electron Beam Processing of Materials, edited by C. W. White and P. S. Peercy, (Academic Press, NY), p. 104.
JACOBI, H., and K. SCHWERDTFEGER, 1976, Metall. Trans. **7A**, 811.

JANSEN, R. and R.R. SAHM, 1984, Mat. Sci. and Eng. **65**, 199.
JOHNSSON, M., L. BACKERUD and G.K. SIGWORTH, 1993, Metall. Trans. **24A**, 481.
JONES, B.L. and G.M. WESTON, 1970 a) J. Aust. Inst. Met. **15**, 189.
JONES, B.L. and M. WESTON, 1970 b), J. Mat. Sci. **5**, 843.
JONES, H. and W. KURZ, 1980, Metall. Trans. **11A**, 1265.
JONES, H., 1982, Rapid Solidification of Metals and Alloys. Monograph, n° 8, (The Institute of Metals, London).
JORDAN, R.M. and J.D. HUNT, 1971, J. Cryst. Growth **11**, 141.
JORDAN, R.M. and J.D. HUNT, 1972, Metall. Trans. **3**, 1385.
JUNZE, J., K.F. KOBAYASHI and P.H. SHINGU, 1984, Metall. Trans. **15A**, 307.
KAMIO, A., S. KUMAI, and H. TEZUKA, 1991, Mat. Sci. and Eng. **A146**, 105.
KARMA, A., 1987, Phys. Rev. Let. **59**, 71.
KATO, H. and J.R. CAHOON, 1985, Metall. Trans. **16A**, 579.
KATTAMIS, T.Z., 1970, Z. Metallk. **61**, 856.
KATTAMIS, T.Z., 1976, J. Cryst. Growth **34**, 215.
KATTAMIS, T.Z., and M.C. FLEMINGS, 1965, Trans. Met. Soc. AIME **233**, 992.
KATTAMIS, T.Z. and M.C. FLEMINGS, 1966, Trans. Met. Soc. AIME **236**, 1523.
KATTAMIS, T.Z. and M.C. FLEMINGS, 1967, Mod. Cast. **52**, 97.
KATTAMIS, T.Z., J.C. COUGLIN, and M.C. FLEMINGS, 1967, M.C., Trans. Met. Soc. AIME **239**, 1504.
KELLY, A. and G.J. DAVIES, 1965, Metall. Rev. **10** (37), 1.
KELLY, T.F., and J.B. VANDERSANDE, 1987, Intl. J. of Rapid Solidification **3**, 51.
KENNEY, M.P., J.A. COURTOIS, R.D. EVANS, G.M. FARRIOR, C.P. KYONKA and A.A. KOCH, 1988, Metals Handbook, 9th.ed., (ASM, Metals Park, OH) **15**, **"Casting"** 327.
KERR, H.W., and W.C. WINEGARD, 1967, in: Crystal Growth (suppl. to the Physics and Chemistry of Solids), H.S. Peiser, ed., (Pergamon, Oxford), p. 179.
KERR, H.W., J. CISSE, and G.F. BOLLING, 1974, Acta Metall. **22**, 677.
KERR, H.W. and J.C. VILLAFUERTE, 1992, in: The Metal Science of Joining, eds. H.J. Cieslak, J.H. Perepezko, S. Kang and M.E. Glicksman, (TMS Pub., Warrendale, PA), p. 11.
KIM, Y.J. and S. KOU, 1988, Metall. Trans. **19A**, 1849.
KIM, Y.-W., H.-M. LIN, and T.F. KELLY, 1988 a), Acta Metall. **36**, 2525.
KIM, Y.-W., H.-M. LIN, and T.F. KELLY, 1988 b), Acta Metall. **36**, 2537.
KIM, W.T. and B. CANTOR, 1991, J. Mat. Sci. **26**, 2868.
KIRKALDY, J.S. and W.V. YOUDELIS, 1958, Trans. Met. Soc. AIME **212**, 833.
KIRKWOOD, D.H., 1985, Mat. Sci. and Eng. **73**, L1.
KITTL, J.A., M.J. AZIZ, D.P. BRUNCO, and M.O. THOMPSON, 1994, Apply. Phys. Lett. **64**, 2359.
KOBAYASHI, S., 1988, J. Cryst. Growth **88**, 87.
KOBAYASHI, R., 1991, J. Jpn. Assoc. Cryst. Growth **18(2)**, 209 in Japanese.
KOBAYASHI, R., 1992, in: Pattern Formation in Complex Dissipative Systems, S. Kai, ed., (World Science, Singapore) p. 121.
KOBAYASHI, K. and L.M. HOGAN, 1978, Met. Forum **1**, 165.
KOBAYASHI, K. and P.H. SHINGU, 1988, J. Mat. Science **23**, 2157.
KOCH, C.C., 1988, Int. Mat. Rev. **33**, 201.
KOFLER, A., 1950, Z. Metallk. **41**, 221.
KOU, S., S.C. HSU and R. MEHRABIAN, 1981, Metall. Trans. **12B**, 33.
KUBO, K. and R.D. PEHLKE, 1985, Metall. Trans. **16B**, 359.
*KURZ, W. and D.J. FISHER, 1979, Int. Met. Rev. **24**, 177.
KURZ, W. and T.W. CLYNE, 1981, Metall. Trans. **12A**, 965.
KURZ, W. and D.J. FISHER, 1981, Acta Metall. **29**, 11.
KURZ, W., B. GIOVANOLA, and R. TRIVEDI, 1986, Acta Metall. **34**, 823.
KURZ, W., B. GIOVANOLA, and R. TRIVEDI, 1988, J. Cryst. Growth. **91**, 123.
*KURZ, W. and D.J. FISHER, 1989, Fundamentals of Solidification, 3rd.ed. (Trans. Tech. Publication, Switzerland).

KURZ, W. and R. TRIVEDI, 1989, in: Series M.D., vol. 14, Microstructural Development and Control in Materials Processing, ed. D.R. Durham and A. Saigai (ASM, Metals Park, OH), p. 47.
LANGER, J.S., 1980, Phys. Rev. Lett. **44**, 1023.
LANGER, J.S., and H. MUELLER–KRUMBHAAR, 1978, Acta Metall. **26**, 1681.
LANGER, J.S., and H. MUELLER–KRUMBHAAR, 1981, Acta Metall. **29**, 145.
LARSON, M.A., and J. GARSIDE, 1986, J. Cryst. Growth **76**, 88.
LAVERNIA, E.J., J.D. AYERS and T.S. SRIVATSAN, 1992, Int. Mat. Rev. **37**, n° 1, 1.
LEAMY, H.J., and K.A. JACKSON, 1971, J. Appl. Phys. **42**, 2121.
LEAMY, H.J., and G.H. GILMER, 1974, J. Cryst. Growth **24/25**, 499.
LEE, J.T.C. and R.A. BROWN, 1993, Phys. Rev. **B 47**, 4937.
LEVI, C.G. and R. MEHRABIAN, 1982, Metall. Trans. **13A**, 221.
LIPTON, J., A. GARCIA and W. HEINEMANN, 1982, Archiv. für des Einsenhüttenwessen **53**, 469.
LIPTON, J., M.E. GLICKSMAN, and W. KURZ, W., 1984, Mat. Sci. and Eng. **65**, 57.
LIPTON, J., W. KURZ and R. TRIVEDI, 1987, Acta Metall. **35**, 957.
LIVINGSTON, J. and H. CLINE, 1969, Trans. Met. Soc. AIME **245**, 351.
LU, S.Z. and A. HELLAWELL, 1985, J. Cryst. Growth **73**, 316.
LU, S.Z. and A. HELLAWELL, 1987, Metall. Trans. **18A**, 1721.
LU, S.Z. and A. HELLAWELL, 1988, in: Proc. Solidification Processing 1987. The Institute of Metals (London), p. 44.
LU, S.Z., and J.D. HUNT, 1992, J. Cryst. Growth **123**, 17.
LU, S.Z., J.D. HUNT, P. GILGIEN, and W. KURZ, 1994, Acta Metall. Mater. **42**, 1653.
MCCARTNEY, D.G., J.D. HUNT, and R.M. JORDAN, 1980a, Metall. Trans. **11A**, 1243.
MCCARTNEY, D.G., J.D. HUNT, and R.M. JORDAN, 1980b, Metall. Trans. **11A**, 1251.
MCCARTNEY, D.G., 1989, Int. Mat. Rev. **34**, 247.
MCLEOD, A.J., 1971, J. Aust. Int. Metals **16**, 124.
MCLEOD, A.J. and L.M. HOGAN, 1978, Metall. Trans. **9A**, 987.
MCDONALD, C.A., A.M. MALVEZZI, F. SPAEPEN, 1989, J. Appl. Phys. **65**, 129.
MAGNIN P., and W. KURZ, 1987, Acta Metall. **35**, 1119.
MAGNIN, P., J.T. MASON and R. TRIVEDI, 1991, Acta Metall. Mater. **39**, 469.
MAGNIN, P., and R. TRIVEDI, 1991, Acta Metall. Mater. **39**, 453.
MAHAPATRA, R.B., J.K. BRIMACOMBE, I.V. SAMARASEKERA, N. WALKER, E.A. PATERSON and J.D. YOUNG, 1991 a), Metall. Trans. **22B**, 861.
MAHAPATRA, R.B., J.K. BRIMACOMBE and I.V. SAMARASEKERA, 1991 b), Metall. Trans. **22B**, 875.
MAJOR, J.F. and J.W. RUTTER, 1989, Mat. Sci. and Tech. **5**, 645.
MARCANTONIO, J.A. and L.F. MONDOLFO, 1974, Metall. Trans. **5**, 1325.
MASUR, L.J. and M.C. FLEMINGS, 1982, Proc.4th. Int. Conf. on Rapidly Quenched Metals, Sendai, Japan, edited by T. Masumoto and K. Suzuki (Jap. Inst. of Metals, Sendai), 1557.
MATSUMIYA, T. and M.C. FLEMINGS, 1981, Metall. Trans. **12B**, 17.
MAXWELL, I. and A. HELLAWELL, 1975, Acta Metall. **23**, 229.
*MEHRABIAN, R., 1982, Int. Met. Rev. **27**, 185.
MEHRABIAN, R., N. KEANE and M.C. FLEMINGS, 1970, Metall. Trans. **1**, 1209.
MEHRABIAN, R., D.R. GEIGER and M.C. FLEMINGS, 1974, Metall. Trans. **5**, 785.
MERCHANT, G.J., and S.H. DAVIS, 1990, Acta Metall. Mater. **38**, 2683.
METZ, S.A. and M.C. FLEMINGS, 1969a), Trans. AFS **77**, 329.
METZ, S.A. and M.C. FLEMINGS, 1969b), Trans. AFS **77**, 453.
MEYER, G.H., 1981, Int. J. Heat Mass Transfer **24**, 778.
MIKEEV, L.V., and A.A. CHERNOV, 1991, J. Cryst. Growth **112**, 591.
MINAKAWA, S., V. SAMARASEKERA and F. WEINBERG, 1985, Metall. Trans. **16B**, 595.
*MINKOFF, I., 1983, The Physical Metallurgy of Cast Iron (Wiley, N.Y.).
MINKOFF, I., 1986, Solidification and Cast Structure (John Wiley & Sons, N.Y.).
MINKOFF, I., 1990, in: F. Weinberg Int. Symposium on Solidification Processing, ed. J.E. Lait and L.V. Samarasekera (Pergamon Press, N.Y.) p. 255.
MOHANTY, P.S., F.H. SAMUEL and J.E. GRUZLESKI, 1993, Metall. Trans. **24A**, 1845.

MOLLARD F., and M.C. FLEMINGS, 1967, Trans. Met. Soc. AIME **239**, 1534.
MONDOLFO, L., 1965, J. Austr. Inst. Metals **10**, 169.
MOORE, K.I., D.L. ZHANG, and B. CANTOR, 1990, Acta Metall. Mater. **38**, 1327.
MORALES, A., J.J. FISSOLO and H. BILONI, 1977, Z. Metallk. **68**, 180.
MORALES, A., M.E. GLICKSMAN and H. BILONI, 1979, in: Solidification and Casting of Metals (The Metals Society, London) p. 184.
MORANDO, R., H. BILONI, G.S. COLE and G.F. BOLLING, 1970, Metall. Trans. **1**, 1407.
MORRIS, L.R. and W.C. WINEGARD, 1969, J. Cryst. Growth **5**, 361.
MORROG, H., 1968a), J. Iron Steel Inst. **206**, 1.
MORROG, H., 1968b), in: The Solidification of Metals (Iron and Steel Institute, London) Publication n° 110, p. 238.
MORTENSEN, A., 1991a), Metall. Trans. **22A**, 569.
MORTENSEN, A., 1991b), in: *Proceedings of the 12th. RISØ International Symposium on Materials Science: Metal matrix composites processing. Microstructures and Properties*, Ed. H. Hansen, D.J. Jensen, T. Leffers, H. Liholt, T. Lorentzen, A.S. Pedersen, O. Pedersen and B. Ralph. RISØ Nat. Lab. Rolskilde, Denmark, p. 101.
MORTENSEN, A. and I. JIN, 1992, Int. Mat. Rev. **37**, n° 3, 101.
MULLINS, W.W. and R.F. SEKERKA, 1963, J. Appl. Phys. **34**, 323.
MULLINS, W.W. and R.F. SEKERKA, 1964, J. Appl. Phys. **35**, 444.
MURRAY, J.L., 1983a, Mat. Res. Soc. Symp. Proc. **19**, 249.
MURRAY, J.L., 1983b, Bull. Alloy Phase Diagrams **4**, 271.
MURRAY, B.T., S.R. CORIELL and G.B. MCFADDEN, 1991, J. Cryst. Growth **110**, 713.
NAKAGAWA, H., H. KATO, F. MATSUDA and T. SENDA, 1970, J. Japan Weld. Soc. **39**, 94.
NANDAPURKAR, P. and D.R. POIRIER, 1988, J. Cryst. Growth **92**, 88.
NARASHIMAN, M.C., 1980, U.S. Patent 4221257.
NARAYAN, J.J., 1982, J. Cryst. Growth **59**, 583.
NI, J. and C. BECKERMANN, 1991, Metall. Trans. **22B**, 349.
NIYAMA, E., 1977, J. Japan Foundrymen Soc. **49**, 26.
O'HARA, and W.A. TILLER, 1967, Trans. Met. Soc. AIME **239**, 497.
OHNAKA, I., 1986, Trans. ISIJ **26**, 1045.
OHNAKA, I., 1988, Metals Handbook 9th. ed., (ASM, Metals Park, OH) **15 "Casting"**, p. 136.
OHNAKA, I., 1991, in: Freezing and Melting Heat Transfer in Engineering, eds. K.C. Ching and H. Seki, Chapter 21: Solidification Analysis of Casting (Hemispher Pub.), p. 1.
OHNO, H., 1986, J. of Metals **38**, 14.
OHNO, H., 1970, J. Japan Inst. Metals **34**, 244.
OHNO, H., T. MOTEGI and H. SODA, 1971, The Iron and Steel Inst.of Japan **11**, 18.
OKAMOTO, T.K., K. KISHITAKE, and I. BESSHO, 1975, J. Cryst. Growth **29**, 131.
OKAMOTO, T.K., and K. KISHITAKE, 1975, J. Cryst. Growth **29**, 137.
OLDFIELD, W., 1973, Mat. Sci. and Eng. **11**, 211.
OSTROWSKI, A. and E.W. LANGER, 1979, in: Solidification and Casting of Metals, (The Metals Society, London), p. 139.
OXTOBY, D.W., and A.D.J. HAYMET, 1982, J. Chem. Phys. **76**, 6262.
PALACIO, H., M. SOLARI and H. BILONI, 1985, J. Cryst. Growth **73**, 369. See also H. BILONI [1983].
PATON, B., 1959, Electroslag Welding (Foreing Language Publishing House, Moscow).
PAWLOWSKI, L. and P. FAUCHAIS, 1992, Int. Mat. Rev. **37**, 271.
PEHLKE, R.D., 1988, Metals Handbook, 9th. Ed., (ASM, Metals Park, OH) **15 – "Casting"**, p. 308.
PEREPEZKO, J.H., 1984, Mat. Sci. and Eng. **65**, 125.
PEREPEZKO, J.H., 1988, in: Metals Handbook, (ASM, Metals Park, OH) **15 – "Casting"**, p. 101.
PEREPEZKO, J.H., 1992, in: Thermal Analysis in Metallurgy, ed. by R.D. Shull and A. Joshi, (TMS, Warrendale, PA) p. 121.
*PEREPEZKO, J.H., 1994, Mat. Sci. and Eng. **A178**, 105. See also I.E. ANDERSON, Ph. D. Thesis, University of Wisconsin, Madison WI, 1983.

PEREPEZKO, J. H. and I. E. ANDERSON, 1980, in: Synthesis and Properties of Metastable Phases, edited by E. S. Machlin and T. S. Rowland, (TMS-AIME, Warrendale, PA), p. 31.
PEREPEZKO, J. H. and S. E. LEBEAU, 1982, in: Aluminum Transformation Technology and Applications 1981, eds. C. A. Pampillo, H. Biloni, L. Mondolfo and F. Sacchi (ASM, Metals Park, OH) p. 309.
PEREPEZKO, J. H. and W. J. BOETTINGER, 1983, Mat. Res. Soc. Symp. Proc. **19**, 223.
PEREZ, T., M. SOLARI and H. BILONI, 1981, Int. Inst. Weld. DOC11–541–81.
PETEVES, S. D. and G. J. ABBASCHIAN, 1986, J. Cryst. Growth **79**, 775.
PFANN, W. G., 1952, Trans. Met. Soc. AIME **194**, 747.
PFANN, W. G., 1966, Zone Melting, 2nd.ed. (Wiley, New York).
PIMPUTKAR, M. and S. OSTRACH, 1981, J. Cryst. Growth **55**, 614.
PIRES, O. S., M. PRATES and H. BILONI, 1974, Z. Metallk. **65**, 143.
PIWONKA, T. S. and M. C. FLEMINGS, 1966, Trans. TMS-AIME **236**, 1157.
PIWONKA, T. S., 1988, in: Metals Handbook, 9th. ed., (ASM, Metals Park, OH) **15 "Casting"**, p. 319.
PLASKETT, T. S. and W. C. WINEGARD, 1959, Trans. ASM **51**, 222.
POIRIER, D. R., 1987, Metall. Trans. **18B**, 245.
POIRIER, D. R., K. YEUM and A. L. MAPPLES, 1987, Metall. Trans. **18A**, 1979.
POND, R. B., 1958, U.S. Patent 2, 825, 198, Metallic Filaments and Method of Making Same.
POWELL, G. L. F., 1965, J. Aust. Inst. Met. **10**, 223.
POWELL, G. L. F., 1980, Metals Forum **3**, 37.
POWELL, G. L. F. and L. M. HOGAN, 1968, Trans. Met. Soc. AIME **242**, 2133.
POWELL, G. L. F. and L. M. HOGAN, 1969, Trans. Met. Soc. AIME **245**, 407.
PRATES, M. and H. BILONI, 1972, Metall. Trans. **3**, 1501.
PRESCOTT, P. J., F. P. INCROPERA and W. D. BENNON, 1991, Int. J. Heat Mass Transf. **34**, 2351.
QIYANG, L., L. QING CHUN and L. QIFU, 1991, Act. Metall. Mater. **39**, 2497.
*RAPPAZ, M., 1989, Int. Mat. Rev. **34**, 93.
RAPPAZ, M., and D. M. STEFANESCU, 1988, Metals Handbook, 9th.ed., (ASM, Metals Park, OH) **15 "Casting"**, p. 883.
RAPPAZ, M., S. A. DAVID, J. M. VITEK and L. A. BOATNER, 1989, Metall. Trans. **20A**, 1125.
RAPPAZ, M., S. A. DAVID., J. M. VITEK, L. A. BOATNER, 1990, Metall. Trans. **21A**, 1767.
RAPPAZ, M. and Ch. A. GANDIN, 1993, Acta Metall. Mater. **41**, 345.
RAPPAZ, M. and Ch. A. GANDIN, 1994, Mat. Research Bull. **xix**, n°1, 20.
RICHMOND, J. J., J. H. PEREPEZKO, S. E. LEBEAU and K. P. COOPER, 1983, in: Rapid Solidification Processing: Principles and Technologies III, edited by R. Mehrabian, (NBS, Washington, DC), p. 90.
RIDDER, S. D., S. KOU and R. MEHRABIAN, 1981, Metall. Trans. **12B**, 435.
RIPOSAN, T., M. CHISAMERA, L. SOFRONI and V. BRABIE, 1985, in: Physical Metallurgy of Cast Iron, ed. H. Fredricksson and M. Hillert (North Holland, N.Y.) p. 131.
RODWAY, G. H. and J. D. JUNT, 1989, J. Cryst. Growth **97**, 680.
RODWAY, G. H. and J. D. HUNT, 1991, J. Cryst. Growth **112**, 554.
ROHATGI, P., 1988, Metals Handbook, 9th. ed., (ASM, Metals Park, OH) **15 "Casting"**, p. 840.
ROSENTHAL, D., 1941, Welding J. **20**, 220-s.
ROSS, A. B. De and L. F. MONDOLFO, 1980, in: Aluminum Transformation Technology and Applications, eds. C. A. Pampillo, H. Biloni and D. E. Embury (ASM, Metals Park, OH) p. 81.
ROVIGLIONE, A. and H. D. HERMIDA, 1994, Materials Characterization **32**, 127.
ROVIGLIONE, A. and H. BILONI, 1994, Fifth International Symposium on the Physical Metallurgy of Cast Iron (SCI-S). To be published in Key Engineering Materials (Trans. Tech. Publications, London).
SADOCHA, J. P. and GRUZLESKI, 1975, in: Metallurgy of Cast Iron (Georgi Pub. Co, St. Saphorin, Switzerland) p. 443.
SATO, A. and R. MEHRABIAN, 1976, Metall. Trans. **7B**, 443.
SATO, T. and G. OHIRA, 1977, J. Cryst. Growth **40**, 78.
SATO, A., Y. OHSAWA and G. ARAGANE, 1989, Mat. Trans. JIM **30**, 55.
SATO, A., Y. OHSAWA and G. ARAGANE, 1991, Mat. Trans. JIM **32**, 77.
SATO, A., Y. OHSAWA and G. ARAGANE, 1992, Mat. Trans. JIM **33**, 66.
SAVAGE, W. F., C. D. LUNDIN and A. H. ARONSON, 1965, Welding J. **40**, 175-s.

SAVAGE, W.F. and E.S. SZEKERES, 1967, Welding J. **46**, 94-s.
SCHAEFER, R.J. and M.E. GLICKSMAN, 1970, Metall. Trans. **1**, 1973.
SCHAEFER, R.J. and S.R. CORIELL, 1984, Metall. Trans. **A15**, 2109.
SCHEIL, E., 1942, Z. Metallk. **34**, 70.
SCHWARZ, M., A. KARMA, K. ECKLER and D.M. HERLACH, 1994, Phys. Rev. Lett. **73**, 1380.
SEETHARAMAN, V., and R. TRIVEDI, 1988, Metall. Trans. **19A**, 2955.
SEKERKA, R.F., 1967, in: Crystal. Growth, ed. H.S. Peiser (Pergamon Press, Oxford) p. 691.
SEKERKA, R.F., 1986, Am. Assoc. Cryst. Growth Newslett. **16**, 2.
SHANGGUAN, D., S. AHUJA and D.M. STEFANESCU, 1992, Metall. Trans. **23A**, 669.
SHARMA, D.G.R. and KRISHMAN, 1991, AFS Trans. **99**, 429.
SHARP, R.M., and M.C. FLEMINGS, 1973, Metall. Trans. **4**, 997.
SHARP, R.M., and M.C. FLEMINGS, 1974, Metall. Trans. **4**, 823.
SHERCLIFF, H.R., O.R. NYHR and S.T.J. TOTTA, 1994, Mat. Research Bull **xix**, n°1, 25 .
SIKORA, J.A., G.L. RIVERA and H. BILONI, 1990, in: Proceedings of the F. Weinberg Symposium on Solidification Processing, eds. J.E. Lait and L.V. Samarasekera (Pergamon Press, N.Y.) p. 255.
SINGER, A.R.E., 1970, Met. Mater. **4**, 246.
SINGER, A.R.E., 1972, J. Inst. Metals **100**, 185.
SKALAND, T., O. GRONG and T. GRONG, 1993, Metall. Trans. **24A**, 2321.
SMITH, P.M. and M.J. AZIZ, 1994, Acta Metall. Mater. **42**, 3515.
SMITH, R.W., 1968, in: The Solidification of Metals (Iron and Steel Inst., London) Pub. 110, p. 224.
SOLARI, M., and H. BILONI, 1980, J. Cryst. Growth **49**, 451.
SOMBOONSUK, K., J.T. MASON, and R. TRIVEDI, 1984, Metall. Trans. **15A**, 967.
SOUTHIN, R.T., 1967, Trans. Met. Soc. AIME **236**, 220.
SOUTHIN, R.T. and G.M. WESTON, 1973, J. Aust. Inst. Met. **18**, 74.
SOUTHIN, R.T. and G.M. WESTON, 1974, J. Aust. Inst. Met. **19**, 93.
SOUTHIN, R.T. and G.A. CHADWICK, 1978, Acta Metall. **26**, 223.
SPAEPEN, F., 1975, Acta Metall. **23**, 729.
SPAEPEN, F., 1994, in: Solid State Physics, edited by H. Ehrenreich and D. Turnbull **47**, (Academic Press, San Diego) p. 1.
SPAEPEN, F. and R.B. MEYER, 1976, Scripta Metall. **10**, 257.
SPENCER, D.B. 1971, Ph. D. Thesis. Massachusetts Institute of Technology, Cambridge, MA. Quoted by M.C. Flemings 1991.
SPENCER D.B., R. MEHRABIAN and M.C. FLEMINGS, 1972, Metall. Trans. **3**, 1925.
STEEN, H.A.H., and A. HELLAWELL, 1975, Acta Metall. **23**, 529.
*STEFANESCU, D.M., 1988, Metals Handbook, 9th.ed., (ASM, Metals Park, OH) **15 "Casting"**, p. 168.
STEFANESCU, D.M., R. HUMMER and E. NECHTELBERGER, 1988, Metals Handbook, 9th. ed., (ASM, Metals Park, OH) **15 "Casting"**, p. 667.
STEFANESCU, D.M. and B.K. DHINDAW, 1988, Metals Handbook 9th.ed., (ASM, Metals Park, OH) **15 "Casting"**, p. 142.
STEFANESCU, D.M., G. UPADHYA and D. BANDYOPADHYAY, 1990, Metall. Trans. **21A**, 997.
STRANGE, E.H., 1911, U.S. Patent 993904.
SUBRAMANIAN, S.V., D.A.R. KAY and G.R. PURDY, 1985, in: Physical Metallurgy of Cast Irons, eds. H. Fredriksson and M. Hillert (North Holland, N.Y.), p. 47.
SUNDQUIST, B.E. and L.F. MONDOLFO, 1961, Trans. Met. Soc. AIME **221**, 157.
SURYANARAYANA, C., F.H. ROSS and R.G. ROWE, 1991, Int. Mat. Rev. **36**, n° 3, 85.
TADA, K. and H. OHNO, 1992, Keikinzoku **42**, 321. (In Japanese).
TAMMANN, G., and A.A. BOTSCHWAR, 1926, Z. Anorg. Chem. **157**, 27.
TARSHIS, C.A., J.L. WALKER and J.W. RUTTER, 1971, Met. Trans. **2**, 2589.
TASSA, M. and J.D. HUNT, 1976, J. Cryst. Growth **34**, 38.
TAYLOR, C.R., 1975, Metall. Trans. **6B**, 359.
TEMKIN, D.E., 1964, Crystallization Processes (Tranl. by Consultants Bureau, New York, 1966) p. 15.
TEMKIN, D.E., 1969, Sov. Phys. Crystallogr. **14**, 344.

THEVOS, Ph., J. L. DESBIOLLES, and M. RAPPAZ, 1989, Metall. Trans. **20A**, 311. See also M. RAPPAZ, 1989, Int. Mat. Rev. **34**, 93.
THOMPSON, C. V., A. L. GREER and F. SPAEPEN, 1983, Acta Metall. **31**, 1883.
THOMPSON, C. V. and F. SPAEPEN, 1983, Acta Metall. **31**, 2021.
THORTON, P. H., 1968, in: Techniques of Metals Research, Ed. R. F. Bunshah (Interscience, New York), vol.1, part 2, p. 1069.
TILLER, W. A., 1958, in: Liquid Metals and Solidification (ASM, Metals Park, OH) p. 276.
TILLER, W., 1970, Solidification, in: Physical Metallurgy, 2nd edition, ed. R. W. Cahn, (North-Holland, Amsterdam), p. 403.
TILLER, W. A., K. A. JACKSON, J. W. RUTTER and B. CHALMERS, 1953, Acta Metall. **1**, 453.
TILLER, W. A., and J. W. RUTTER, 1956, Can. J. Phys. **34**, 96.
TITCHENER, A. P. and J. A. SPITTLE, 1975, Acta Metall. **23**, 497.
TOLOUI, B. and A. HELLAWELL, 1976, Acta Metall. **24** 565.
TRAJAN, P. K., 1988, in: Metals Handbook, 9th. ed., (ASM, Metals Park, OH) **15 "Casting"**, p. 88.
TRIVEDI, R. and K. SOMBOONSUK, 1984, Mat. Sci. and Eng. **65**, 65.
TRIVEDI, R, P. MAGNIN, and W. KURZ, 1987, Acta Metall. **35**, 971.
TRIVEDI, R., and W. KURZ, 1988, in Solidification Processing of Eutectic Alloys, edited by D. M. Stefanescu, G. J. Abbaschian and R. J. Bayuzick, (The Metallurgical Society, Warrendale, PA), p. 3.
TRIVEDI R., and W. KURZ, 1994, Int. Mat. Rev. **39**, 49.
TRIVEDI, R., 1995, Met. Trans., **26A,** 1583.
TURNBULL, D., 1962, J. Phys. Chem. **66**, 609.
TURNBULL, D. and R. E. CECH, 1950, J. Appl. Phys. **21**, 804.
TURNBULL, D. and B. G. BAGLEY, 1975, in: Treatise on Solid State Chemistry, vol. 5, edited by N. B. Hannay, (Plenum, NY), p. 513.
UNGAR, L. H. and R. A. BROWN, 1985, Phys. Rev. B **31**, 5931.
VERHOEVEN, J. D., and E. D. GIBSON, 1978, J. Mat. Sci **13**, 1576.
VERHOEVEN, J. D., W. N. GILL, J. A. PUSZYNSKI and R. M. GINDE, 1988, J. Cryst. Growth **89**, 189.
VERHOEVEN, J. D., W. N. GILL, J. A. PUSZYNSKI and R. M. GINDE, 1989, J. Cryst. Growth **97**, 254.
VISKANTA, R., 1990, ISME Int. J. (Series II) **33**, 409.
VITEK, J. M. and S. A. DAVID, 1992, in: The Metal Science of Joining, eds. H. J. Cieslak, J. H. Perepezko, S. Kang and M. E. Glicksman (TMS Pub., Warrendale, PA) p. 115.
VIVES, Ch. and R. RICOU, 1985, Metall. Trans. **16B**, 377.
VOLLER, V. R., and S. SUNDARRAJ, 1993, in: Modeling of Casting, Welding and Advanced Solidification Processes V, T. S. Piwonka, V. Voller, and L. Katgerman eds., (TMS, Warrendale, PA), p. 251.
VOLMER, M. I., and M. MARDER, 1931, Z. Phys. Chem. **A154**, 97.
VOORHEES, P. W., 1990, Metall. Trans. **21A**, 27.
WALKER, J. L., 1959, in: The Physical Chemistry of Process Metallurgy, part 2, ed. G. S. St. Pierre (Interscience, New York), p. 845.
WALKER, J. L., 1964, cited in: Principles of Solidification, ed. B. Chalmers, Chap. 4, (Wiley, New York) p. 122.
WALTON, D. and B. CHALMERS, 1959, Trans. Met. Soc. AIME **188**, 136.
WANG, C. Y. and C. BECKERMANN, 1993, Mat. Sci. and Eng. **A171**, 199.
WANG, Y. H. and S. KOU, 1987, in: Advances in Welding Science and Technology, ed. S. A. David, (ASM, Metals Park, OH.), p. 65.
WANG, Y. H., Y. J. KIM and S. KOU, 1988, J. Cryst. Growth **91**, 50.
WARREN, J. A., and W. J. BOETTINGER, 1995, Acta Metall. et Mater. **43,** 689.
WEI, C. and J. T. BERRY, 1980, Int. J. Heat and Mass Transfer **25**, 590.
WEINBERG, F., 1975, Metall. Trans. **6A**, 1971.
WEINBERG, F., 1979 a), in: Solidification and Casting of Metals (The Metals Society, London) p. 235.
WEINBERG, F., 1979 b), Metals Technology **February**, 48.
WEINBERG, F. and E. TEGHTSOONIAN, 1972, Metall. Trans. **3**, 93.
WETTERFALL, S. E., H. FREDRICKSSON, H. and M. HILLERT, 1972, J. Iron Steel Inst. **210**, 323.
WHEELER, A. A., W. J. BOETTINGER, and G. B. MCFADDEN, 1992, Phys. Rev A **45**, 7424.

WHEELER, A. A., B. T. MURRAY, and R. J. SCHAEFER, 1993a, Physica D **66**, 243.
WHEELER, A. A., W. J. BOETTINGER, and G. B. MCFADDEN, 1993b, Phys. Rev E **47**, 1893.
WHITE, C. W., D. M. ZEHNER, S. U. CAMPISANO and A. G. CULLIS, 1983, in: Surface Modification and Alloying by Lasers, Ion, and Electron Beams, edited by J. M. Poate, G. Foti and D. C. Jacobson (Plenum Press, NY), p. 81.
WHITE, G. and D. W. OLSON, 1990, in: The New Materials Society. Challenges and Opportunities, (Bureau of Mines, U.S. Dept. of the Interior.) Quoted by MORTENSEN and JIM [1992].
WIESE, J. W. and J. A. DANTZIG, 1988, Applied Mathematical Modelling **12**, 213.
WILLNECKER, R., D. M. HERLACH and B. FEUERBACHER, 1989, in: Proc.7th. Europ. Symp. on "Materials and Fluid Sciences under Microgravity", Oxford, ESA SP-295, p. 193.
WILLNECKER, R., D. M. HERLACH, and R. FEUERBACHER, 1990, Apply Phys. Lett. **56**, 324.
WILSON, H. A., 1900, Phil Mag. **50**, 238.
WILSON, L. O., 1978, J. Cryst. Growth **44**, 371.
WILSON, L. O., 1980, J. Cryst.l Growth **48**, 363.
WINEGARD, W. and B. CHALMERS, 1954, Trans. Quart. ASM **46**, 1214.
WOLLKIND, D. and L. SEGAL, 1970, Phil. Trans. Roy. Soc. London **268**, 351.
WU, Y., T. J. PICONNE, Y. SHIOHARA, and M. C. FLEMINGS, 1987, Metall. Trans. **18A**, 915.
YOON, W., PAIK, J. S., LACOURT, D., and PEREPEZKO, 1986, J. H., J. Appl. Phys. **60**, 3489.
YOUNG, K. P., and D. H. KIRKWOOD, 1975, Metall. Trans. **6A**, 197.
ZACHARIA, T., A. H. ERASLA, and D. K. AIDUN, 1988, Weld. J. **67**, 18-s.
ZACHARIA, T., S. A. DAVID, J. M. VITEK, 1992, in: The Metal Science of Joining, eds. H. J. Cieslak, J. H. Perepezko, S. Kang and M. E. Glicksman, (TMS Pub., Warrendale, PA), p. 257.
ZENER, C., 1946, Trans Met. Soc. AIME **167**, 550.
ZHU, J. D. and I. OHNAKA, 1991, Modelling of Casting, Welding and Advanced Solidification Processes, eds. M. Rappaz, M. R. Ozgü and K. W. Mahin, (TMS Pub., Warrendale, PA), p. 435.
ZHU, P. and R. W. SMITH, 1992 a), Acta Metall. Mater. **40**, 683.
ZHU, P. and R. W. SMITH, 1992 b) Acta Metall. Mater. **40**, 3369.
ZIMMERMANN, M., A. KARMA, and M. CARRARD, 1990, Phys. Rev. B **42**, 833.
ZIV, I. and F. WEINBERG, 1989, Metall. Trans. **20B**, 731.

Further reading

The publications marked with an asterisk in the above list of references may be consulted.

CHAPTER 9

MICROSTRUCTURE

H. GLEITER

Forschungszentrum Karlsruhe, GmbH
D-76021 Karlsruhe, Germany

R. W. Cahn and P. Haasen†, eds.
Physical Metallurgy; fourth, revised and enhanced edition

1. Definition and outline

The *microstructure* of crystalline materials is defined by the type, structure, number, shape and topological arrangement of phases and/or lattice defects which are in most cases not part of the thermodynamic equilibrium structure.

In the first part (paragraph two) of this chapter, the different types of lattice defects involved in the formation of microstructure (elements of microstructure) will be discussed. As far as the arrangement, shape and crystal structure of phases are concerned, we refer to chs. 1, 4, 8, 15–17, and 28. The third and fourth paragraph of this chapter will be devoted to the characterization and to the present understanding of the development of microstructures.

2. Elements of microstructure

2.1. Point defects, dislocations and stacking faults

Point defects, point-defect clusters, dislocations and stacking faults are important elements of the microstructure of most materials. The atomistic structure and properties of these defects are discussed in chs. 18 and 20.

2.2. Grain boundaries

Control of the grain size is one of the most widely used means of influencing the properties of materials. Consequently, intense efforts have been directed in recent years towards a better understanding of grain boundaries. The progress achieved is documented in several comprehensive reviews (BALLUFFI [1980], AUST [1981], GLEITER [1982], SUTTON and BALLUFFI [1987], SUTTON [1990], FINNIS and RÜHLE [1991], WOLF and YIP [1992], SUTTON and BALLUFFI [1995]).

The complex nature of interatomic forces and relaxations at interfaces has motivated the development of simple, mostly crystallographic, criteria for predicting the structure, the energy and other physical properties of interfaces. Some of these criteria and the underlying physical concepts of the atomic structure of grain boundaries will be briefly discussed in the following sections.

2.2.1. Crystallography

2.2.1.1. Coincidence site lattice. The coincidence site lattice (CSL) has proved a useful concept in the crystallography of interfaces and in the description of dislocations in interfaces. It is defined as follows (fig. 1). Two crystal lattices A and B which meet at an interface are imagined to be extended through each other in both directions. Crystal A or B is then translated so that a lattice point in A coincides with one in B. This point which is labelled O is designated as the origin of coordinates. Now it is possible that no other lattice points of A and B coincide, in which case O is the only common lattice point. However, for many orientations of the two crystals there will be other coincidences. These coinciding lattice points form a regular lattice which is known as the